ESTIMATING DELIVERABILITY IN MULTI-LAYERED GAS RESERVOIRS USING ARTIFICIAL INTELLIGENCE

BY

MALIK KHALID AL-ARFAJ

A Thesis Presented to the

DEANSHIP OF GRADUATE STUDIES

KING FAHD UNIVERSITY OF PETROLEUM & MINERALS

DHAHRAN, SAUDI ARABIA

In Partial Fulfillment of the
Requirements for the Degree of

MASTER OF SCIENCE

In

PETROLEUM ENGINEERING

JULY, 2012

KING FAHD UNIVERSITY OF PETROLEUM & MINERALS
DHAHRAN, SAUDI ARABIA

DEANSHIP OF GRADUATE STUDIES

This thesis written by **Malik Khalid Al-Arfaj** under the direction of his thesis advisor and approved by his thesis committee, has been presented to and accepted by the Dean of Graduate Studies, in partial fulfillment of the requirements for the degree of **MASTER OF SCIENCE IN PETROLEUM ENGINEERING**.

Thesis Committee

Thesis Advisor
Dr. Abdulazeez Abdulraheem

Member
Dr. Abdulaziz Al-Majed

Member
Dr. Enamul Hossain

Department Chairman
Dr. Abdulaziz Al-Majed

Dean of Graduate Studies
Dr. Salam Zummo

DEANSHIP OF GRADUATE STUDIES

21/12/12

Date

DEDICATION

To my parents.

To my wife.

ACKNOWLEDGEMENT

I would like to offer my sincere gratitude to my thesis committee: Dr. Abdulraheem, Dr. Al-Majed, and Dr. Hossain for providing support, guidance and technical advice throughout my thesis. I would also like to thank Majed Kanfar for his help with the PLTs. My gratitude and appreciation goes to all those who helped me with their knowledge, advice, and support during this research.

Table of Contents

LIST OF TABLES

LIST OF FIGURES

ABSTRACT

Full Name of Student: Malik Khalid Al-Arfaj

Title of Study: Estimating Deliverability in Multi-Layered Gas Reservoirs Using Artificial Intelligence

Major Field: Petroleum Engineering

Date of Degree: 30 May 2012

In this research, an artificial intelligence (AI) model has been created to estimate the production rate of each layer in a multi-layered gas reservoir using static properties such as those obtained from well logging, in addition to dynamic properties such as pressure. This approach will be helpful in several reservoir engineering applications, such as understanding layers' depletion, or targeting specific layers for workover. It could also be used for PLT analysis where the measured PLT values are compared to the expected values and a variance analysis could be performed.

Data were collected from more than 100 wells in a certain reservoir spanning over four fields. They were combined in related input variables and fed to the AI model for learning purposes. To compare different AI methods, the data were fed to 5 methods, namely ANFIS, MLP, RBF, SVM, and GRNN, and results were optimized for each method.

Between the tested AI methods, SVM and GRNN performed best as shown by a low mean absolute percentage error and a very high correlation coefficient. This research shows promising use for AI methods in estimating production rate from each layer in a multi-layered gas reservoir.

ملخص الرسالة

الاسم: مالك خالد العرفج

عنوان الرسالة: تقدير إنتاجية الطبقات في مكامن الغاز متعددة الطبقات باستخدام أساليب الذكاء الاصطناعي

التخصص: هندسة البترول

تاريخ التخرج: 30 مايو 2102

في هذا البحث ، تم إنشاء نموذج باستخدام أدوات الذكاء الاصطناعي لتقدير كمية الإنتاج من كل طبقة في مكمن غاز متعدد الطبقات باستخدام الخصائص الثابتة مثل تلك المستخرجة من قياسات الآبار ، بالإضافة إلى الخصائص الحيوية مثل الضغط. تساعد هذه الطريقة في العديد من تطبيقات هندسة المكامن ، مثل فهم آلية نضوب الطبقات ، أو استهداف طبقات معينة عند صيانة الآبار. يمكن أيضًا استخدام نتائج النموذج لتحليل نتائج اختبار إنتاج البئر ، حيث تتم مقارنة النتائج التي تم قياسها بالنتائج المتوقعة وتحليل الفارق.

تم جمع البيانات من أكثر من 100 بئر في أحد المكامن التي تمتد على مدى أربعة حقول ، وقد تم جمع المتغيرات في مجموعة متغيرات إدخال ، وتمت تغذيتها إلى أدوات الذكاء الاصطناعي من أجل التعليم ، وقد تم تمرين الأدوات لاستخراج النتائج المثلى من كل أداة.

بين الطرق المجربة ، حازت الشبكات العصبية الانحدارية العامة وآلة المتجه الداعم على الأداء الأفضل كما يتضح من حصولها على أقل متوسط لنسبة الخطأ المطلق بالإضافة إلى ترابط خطي عال جدًا. هذا البحث يبين الاستخدام الواعد لأساليب الذكاء الاصطناعي لتقدير إنتاج الطبقات في مكامن الغاز متعددة الطبقات.

Chapter 1:

INTRODUCTION

This chapter presents the research problem, the objectives, the motivation behind the research, and the approach. In addition, few definitions and tools relevant to this research are presented.

1.1. PROBLEM STATEMENT

Estimating the deliverability of gas reservoirs is complicated by the non-Darcy flow. This complication compounds when one tries to estimate the flow of each layer in a multi-layered reservoir. In this research, artificial intelligence (AI) methods are used to correlate between production contribution, measured by using production logging tools, from each layer in a multi-layered gas well and the well and reservoir properties. The results obtained from different AI method are compared against each other and the best one is recommended for field application.

1.2. OBJECTIVE

The objective of this research was to estimate the production ratio from each flow zone in a gas well using readily available data from well logs and well tests within an acceptable accuracy range and using practical methods. The ultimate goal of this research is to create a model that can estimate the production ratio of each layer in a well creating what could be considered as a “virtual PLT curve”.

1.3. MOTIVATION

The ability to estimate the contribution of each layer in a well could help in a multitude of applications. It could be used in diagnosing the well after a PLT test to compare the measured and estimated values and analyzing the differences. It could also be used in advanced underbalanced workover operations where the layers with the highest contribution could be targeted.

1.4. APPROACH

The approach consisted of the following steps:

- Gather relevant data from well logs, PVT tests, and well tests in a tabular form that can be processed by the AI Software to create an AI model using these data.
- Include the results of flow equations given by Darcy and to help guide the artificial model.
- Use several artificial intelligence methods and recommend the method with the highest accuracy.

AI models were built using the aforementioned inputs and some of them are combined together in the form of different variables which are discussed later. Several AI methods have been tested such as ANN, GRNN, RBF, SVM and ANFIS.

Two different data sets were used: The first one consisted of the input data in their original formats and the other one had the normalized inputs. The results of each data set were compared against each other and analyzed for their performance.

1.5. WELL LOGGING

Well logging is an essential tool for understanding the well and the reservoir. There is hardly any well drilled today without well logging. Well logs are used to obtain several important pieces of information such as the formation porosity, hydrocarbon saturation, and water saturation. Some measures are obtained directly such as caliper log, gamma ray, neutron porosity, density, and resistivity and some others are estimated using indirect measurements such as water saturation and permeability [Schlumberger, 1989].

1.5.1 POROSITY

Porosity is defined as the pore volume divided by the bulk volume of the formation. It is the fraction of the total volume of the rock not occupied with the rock material but rather by pores or voids. It can vary widely for different kinds of formations. Whereas evaporates show practically zero porosity, consolidated sands usually range between 10 to 15%, and unconsolidated sands could reach 30% or more.

Rock porosity is usually obtained using three tools, the density log, the sonic log, and/or the neutron log [Schlumberger, 1989].

Porosity in clastic sediments is usually affected by the uniformity of grain size, the degree of cementation or consolidation, the amount of compaction during and after deposition, and the method of packing [Tiab et al., 2004].

1.5.1.1 Sonic Logs

Sonic logs consist of transmitters that emit pulse sounds and receivers that pick up the reflective sound waves. If the lithology is known, porosity can be determined using the velocity of the waves. Figure 1-1 shows a schematic of a sonic log [Schlumberger, 1989].

In the presence of secondary porosity, caused by vuggs and fractures, sonic logs models yield apparent porosity which reflects only the primary or intergranular porosity. Then secondary porosity can be obtained by comparing the results of sonic logs interpretation to the total porosity obtained from neuron or density logs [Bassiouni, 1994].

1.5.1.2 Density Logs

Density logs are used to help in porosity determination. They are also used for gas detection, determination of hydrocarbon density, minerals identification in evaporate deposits, and evaluation of complex lithologies and shaly sands. The principle of density logs is based on a radioactive source and a detector. After colliding with electrons in the formation, the decaying gamma ray reaches the detector. The number of collisions is directly related to the number of electrons in the formation which are related to the true bulk density. The true bulk density is dependent on the rock matrix density, the formation porosity, and the density of the fluids in the pores. Interpretation of complex matrix lithologies can be simplified using the combination of formation sonic, density, and neutron logs. [Alger et al., 1963]. Figure 1-2 shows a schematic of a density log.

1.5.1.3 Neutron logs

The neutron log is used in identifying the liquid-filled porosity. It can also be used in identifying gas-bearing zones by comparing it to other porosity logs. It works by emitting neutrons from a radioactive source. The velocity and energy of neutrons are influenced by the concentration of the hydrogen in the zone. This is captured by a detector in the sonde Porosity values measure by the neutron logging tool must be corrected if the formation lithology is different from the one the tool has been calibrated with [Khan et al., 1989]. Figure 1-3 shows a schematic diagram of a neutron log.

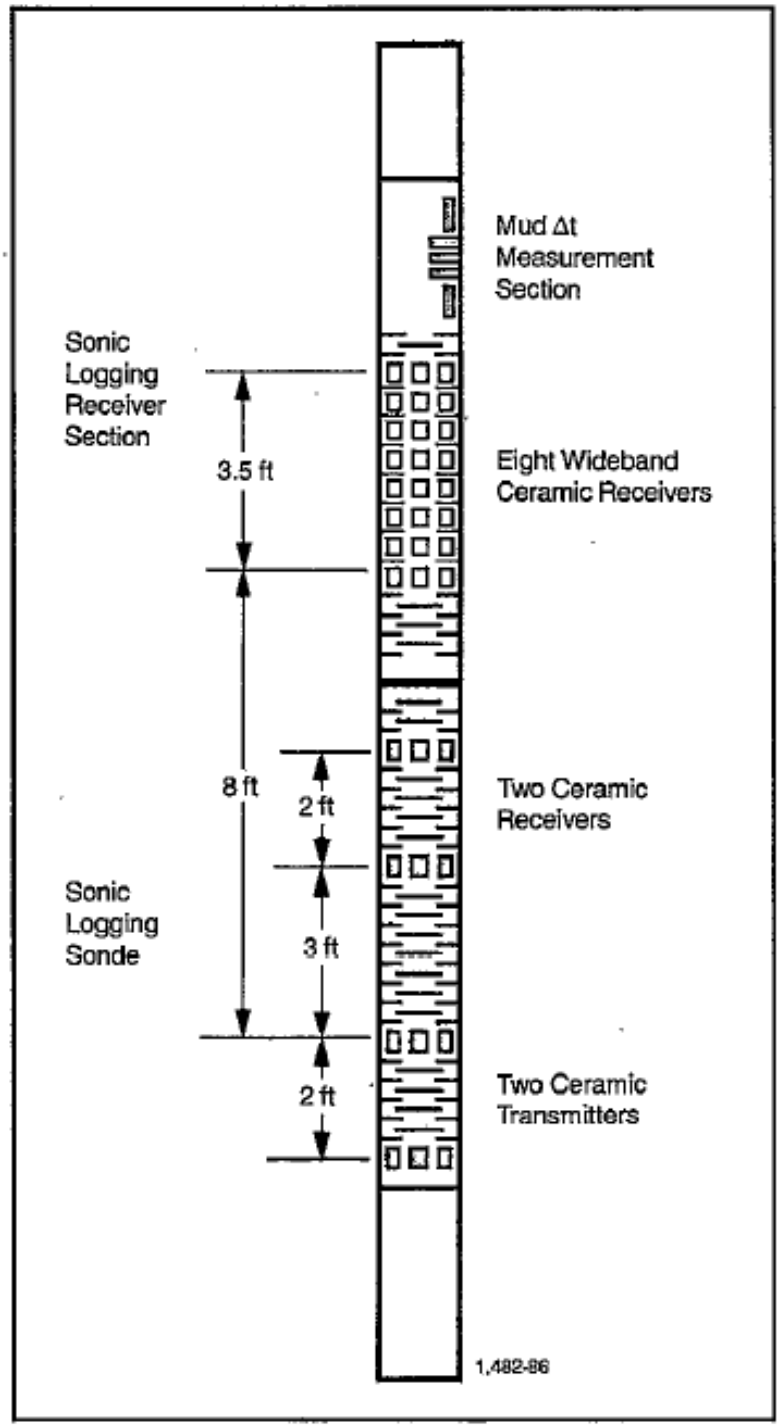

Figure 1-1: Multipurpose sonic sonde configuration [Schlumberger, 1989].

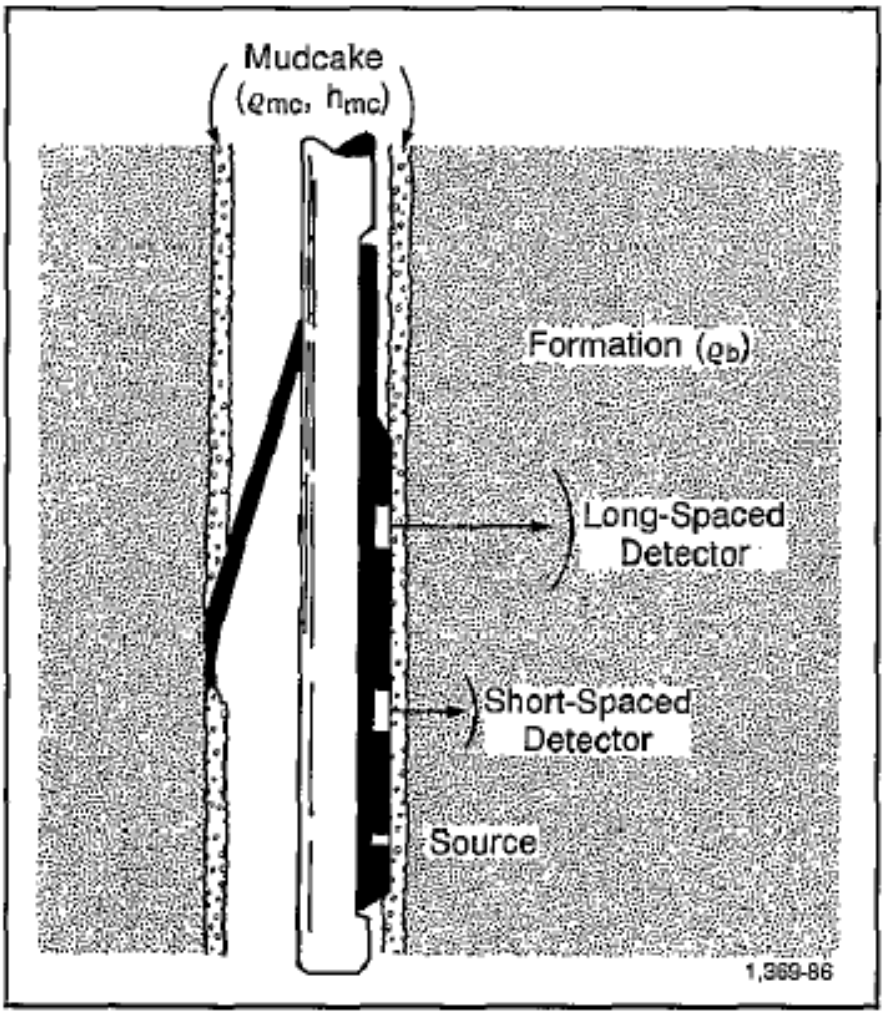

Figure 1-2: Schematic drawing of the dual spacing Formation Density Logging Device (FDC) [Schlumberger, 1989].

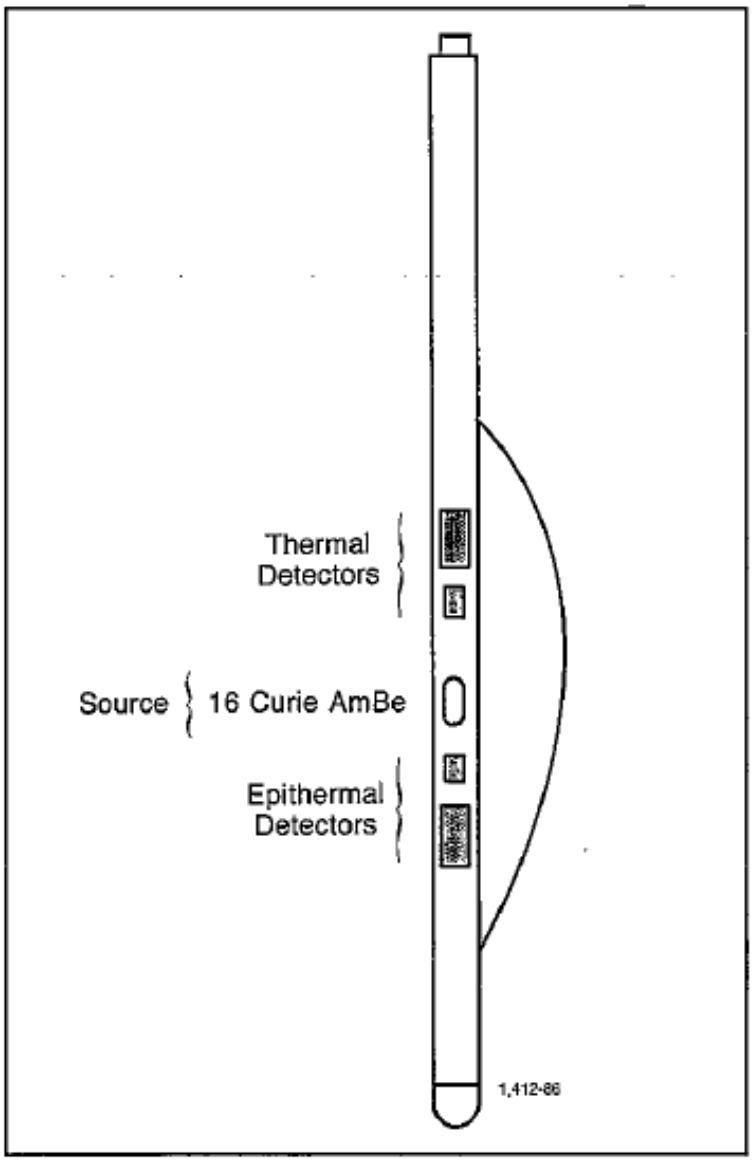

Figure 1-3: Density Neutron Log tool configuration [Schlumberger, 1989].

1.5.2 *SATURATION*

One of the most important parameters for reservoir engineers is the fluid saturation. It is the fraction of the pore volume that is occupied by a fluid. The pores are always filled with fluids and thus the fluids saturations (oil, gas, water, etc.) should always amount to 100%. Water saturation is usually determined using a combination of resistivity logs and empirical correlations. Saturation can be expressed as either a percentage ofr a fraction. However, it is always used as a fraction in equations. Estimation of fluids saturation can be done using direct methods in the laboratory or indirect methods such as well logs [Craft et al, 1991].

1.5.3 *PERMEABILITY*

It is a measure of how easy it is for fluids to flow through a formation. Darcy is the unit of permeability, but since it is large, millidarcy (mD) is used more often. In order for rocks to be permeable, they have to have some interconnected pores, fractures or capillaries. Permeability is usually measured in the laboratory by using extracted cores. It is then correlated with lithology, porosity, and other formation properties. Henry Darcy was the first to give a quantitative definition for permeability in his empirical relationship [Lyons et al., 2005].

1.6. PRODUCTION LOGGING

1.6.1 INTRODUCTION

Production logging is a set of tools and techniques used to evaluate the well or the reservoir performance. It is also used to evaluate the flow distribution in a well into or out of the reservoir and to generate a well flow profile which shows what comes from where. It provides detailed information about the behavior of the fluids in the well while it is producing. It has been traditionally employed for reservoir surveillance or well diagnosis and is a crucial tool for well evaluation.

Like most logging methods, production logs rely on indirect measurement to obtain the flow distribution. Thus, production log interpretation requires a thorough understanding of the fluid movements in the wellbore and their effect on the logging measurements [Hill, 1990].

1.6.2 PRODUCTION LOGGING TOOLS (PLT)

The primary logging tools used in quantifying and measuring the flow profile usually consists of a thermometer, gradiomanometer, capacitor, and a fullbore-spinner flowmeter. The tool set could also include a continuous flowmeter, packer flowmeter, manometer, caliper, water holdup meter, and a radioactive tracer [Schlumberger, 1973].

1.6.2.1 Thermometer

It is used to measure the wellbore fluid temperature under static (shut-in) and/or dynamic (flowing) conditions. It also helps in casing annulus flow detection.

1.6.2.2 Gradiomanometer

It is used for calculating the mean density of the wellbore fluids by measuring the difference in pressure over two feet of the wellbore. It could be affected by the friction and kinetic components or the hole deviation.

1.6.2.3 Fullbore-Spinner Flowmeter

The fluid velocity in a wellbore is measured with a spinner velocimeter and is correlated to volumetric flow rate. It can measure very low velocities in single-phase flow. However, it requires higher flow rates to give useful measurements in a multi-phase flow.

1.6.2.4 Continuous Flowmeter

The continuous flowmeter is used to measure the fluid velocity with a spinner velocimeter and the fluid velocity is correlated to volumetric flow rate. It is particularly useful in single-phase flow regimes such as high-flow-rate gas wells, high-flow-rate oil wells, or waterfloods.

1.6.2.5 Manometer

The manometer is used to measure the wellbore fluid pressure and it helps in fluid conversion. The productivity index in oil wells or the open-flow-potential in gas wells can be determined using this tool.

1.6.2.6 Caliper

The caliper is used for measuring the hole or the casing diameter, breakouts, or washouts. It can be also used to determine hole obstructions.

1.6.2.7 Water holdup meter

The water holdup meter is used to directly measure the water holdup in flow regimes where water is the continuous phase.

1.6.2.8 Radioactive-Tracer Survey

Radioactive-Tracer Survey tool is used to determine the fluid velocity in single-phase flow regimes. It helps in detecting fluid movements outside the casing or tubing [Schlumberger, 1973].

1.7. WELL TESTING

Reservoir Engineers use information obtained by well testing such as flow and pressure to understand the in-situ reservoir conditions. This information is vital for optimizing wells production and achieving the best reservoir production performance [Chaudhry, 2003].

Deliverability tests are used to determine the Inflow Performance Relationship (IPR) which in turn describes the relationship between the production rate at the surface and the bottomhole flowing pressure. Using and the current bottomhole flowing pressure, and the current average reservoir pressure, one can estimate this well's productivity and its deliverability potential.

There are several methods to perform deliverability tests. One is the flow-after-flow test which is accomplished by producing the well at three different successive stabilized rates with no shut-in periods in between the tests. The tests are followed by a long shut-in period to establish the average reservoir pressure. To shorten the time taken by the tests, the isochronal and the modified isochronal tests were developed. The isochronal test is consists of a series of single point tests that are performed by alternating between production at a stabilized sandface rate and shut-in for buildup. The modified isochronal test is done in a similar manner but the flow periods have the same duration [Lee et al., 1996].

1.8. PVT AND FLUID PROPERTIES

PVT analysis is required to understand the reservoir fluid behavior and properties. Usually, samples are collected from test separators and recombined to imitate the reservoir conditions. Afterwards, a series of tests are applied on the samples to understand the fluid composition, properties and phase behavior. While some properties are determined in the laboratory, others are estimated using empirical correlations. Gas specific gravity is usually one of the main factors in natural gas empirical correlations [Danesh, 1998].

1.8.1 Z-FACTOR

The gas compressibility factor, known as the z-factor, is a measure of the behavior deviation of real gas from the ideal gas law. It is the ratio of the gas volume at a given pressure and temperature conditions to the ideal gas volume at the same conditions [Danesh, 1998].

$$Z = \frac{V_{actual}}{V_{ideal}} \tag{1-1}$$

In this research we are using the correlation proposed by Dranchuk and Abou-Kassem [Dranchuck et al., 1975].

$$Z = 1 + \left(A_1 + \frac{A_2}{{}_pT_r} + \frac{A_3}{{}_pT_r^3} + \frac{A_4}{{}_pT_r^4} + \frac{A_5}{{}_pT_r^5}\right)\rho_r + \left(A_6 + \frac{A_7}{{}_pT_r} + \frac{A_8}{{}_pT_r^2}\right)\rho_r^2 - A_9\left(\frac{A_7}{{}_pT_r} + \frac{A_8}{{}_pT_r^2}\right)\rho_r^5 +$$

$$A_{10}(1 + A_{11}\rho_r^2)\left(\frac{\rho_r^2}{{}_pT_r^3}\right)\exp(-A_{11}\rho_r^2) \tag{1-2}$$

Where ρ_r the pseudo reduced density, is defined as,

$$\rho_r = 0.27[\frac{{}_pp_r}{Z_p\ {}_pT_r}] \tag{1-3}$$

and the constants are given as,

$$A_1 = 0.3265 \quad A_2 = -1.0700 \quad A_3 = -0.5339 \quad A_4 = 0.01569 \quad A_5 = -0.05165$$

$$A_6 = 0.5475 \quad A_7 = -0.7361 \quad A_8 = 0.1844 \quad A_9 = 0.1056 \quad A_{10} = 0.6134$$

$$A_{11} = -0.7210$$

The data used in this study falls within the valid range which is the following:

$$1 < {}_pT_r \leq 3 \text{ and } 0.2 \leq {}_pP_r < 30$$

$$0.7 < {}_pT_r \leq 1 \text{ and } {}_pP_r < 1$$

Where ${}_pT_r$ and ${}_pP_r$ are the pseudo-reduced temperature and pressure respectively.

1.8.2 VISCOSITY

In general, as the pressure increases, the gas viscosity increases. On the other hand, as the temperature increases, the viscosity decreases. However, at high pressures the gas behavior becomes similar to liquid behavior.

In this research, we are using the following viscosity correlation proposed by Lee et al. [Lee et al., 1966]:

$$\mu_g = 10^{-4} a \exp\left(b\,(\rho_g/62.43)^c\right) \tag{1-4}$$

Where

$$a = \frac{(9.379+0.0160MW)T^{1.5}}{209.2+19.26MW+T} \tag{1-5}$$

$$b = 3.448 + .01009MW + \frac{986.4}{T} \tag{1-6}$$

$$c = 2.4 - 0.2b \tag{1-7}$$

and

$$MW = 28.96443 \cdot \text{SG} \tag{1-8}$$

Where MW is the molecular weight and SG is the specific gravity.

This correlation is valid for 100 < pressure (psi) < 8000 and 100 <Temperature (^{o}F) < 340. All of the data used in this study fall within this range.

Chapter 2:

LITERATURE REVIEW

In this chapter, methods for estimating well deliverability presented in the literature are discussed. The discussion is focused on methods used to estimate gas well deliverability.

2.1. WELL DELIVERABILITY

All well deliverability equations describe the relationship between the well production rate and the drawdown pressure, i.e. the difference between the reservoir pressure and the flowing bottomhole pressure. Presenting the production rate as a function of the drawdown pressure helps in comparing wells as well as in estimating the production rate under various conditions. This is also known as the "inflow performance relationship" or IPR [Economides et al., 1994].

2.1.1 GAS WELL DELIVERABILITY

In a single-layered gas reservoir (Figure 2-1), the gas well deliverability can be approximated using a pseudo-steady state relationship developed from Darcy's law [Economides et al., 1994]:

$$\bar{p}^2 - p_{wf}^2 = \frac{1424 q \mu Z T}{kh}\left[\ln\left(0.472\frac{r_e}{r_w}\right) + s\right] \tag{2-1}$$

Which can be rearranged as:

$$q = \frac{kh}{1424\mu ZT\left(\ln\left(0.472\frac{r_e}{r_w}\right)+s\right)}\left(\bar{p}^2 - p_{wf}^2\right) \tag{2-2}$$

The gas rate is in MSCF/d and the properties μ and Z are average properties between $\bar{p}$ and p_{wf}.

Since this approximation assumes Darcy flow in the reservoir, it is acceptable for low gas flow rate only. It is commonly presented as:

$$q = C(\bar{p}^2 - p_{wf}^2) \tag{2-3}$$

Where C is defined as:

$$C = \frac{kh}{1424\mu ZT\left(\ln\left(0.472\frac{r_e}{r_w}\right)+s\right)} \tag{2-4}$$

For larger gas flow rates, where non-Darcy flow is dominant (Figure 2-2), we use the solution of the Forchheimer equation [Economides et al., 1994] for gas flow through porous media and get:

$$q = \frac{kh\left(\bar{p}^2-p_{wf}^2\right)}{1424\bar{\mu}\,\bar{z}\,T\,[\ln(r_d/r_w)+s+Dq\,]} \tag{2-5}$$

This equation can be rearranged as:

$$\bar{p}^2 - p_{wf}^2 = \frac{1424\bar{\mu}\,\bar{z}\,T}{kh}\left(\ln\frac{0.472r_e}{r_w}+s\right)q + \frac{1424\bar{\mu}\,\bar{z}\,TD}{kh}q^2$$

Or in different terms:

$$\bar{p}^2 - p_{wf}^2 = a\,q + b\,q^2 \tag{2-6}$$

Where

$$a = \frac{1424\bar{\mu}\,\bar{z}\,T}{kh}\left(\ln\frac{0.472r_e}{r_w}+s\right) \tag{2-7}$$

and

$$b = \frac{1424\bar{\mu}\,\bar{z}\,TD}{kh} \tag{2-8}$$

The Dq term refer to the turbulence skin effect which could be quite high for some high rate wells. Several authors proposed approximations for the non-Darcy coefficient (D). One is the following empirical correlation:

$$D = \frac{6\times10^{-5}\gamma k_S^{-0.1} h}{\mu r_w h_{perf}^2} \tag{2-9}$$

2.1.2 *Well Deliverability in a Multi-Layered Gas Reservoir*

In a multi-layered reservoir (Figure 2-3), we use the principle of superposition [Juell et al., 2011]:

$$q = \sum_{l=1}^{N} q_l \tag{2-10}$$

Where q is the total well rate and q_l is the rate of each layer.

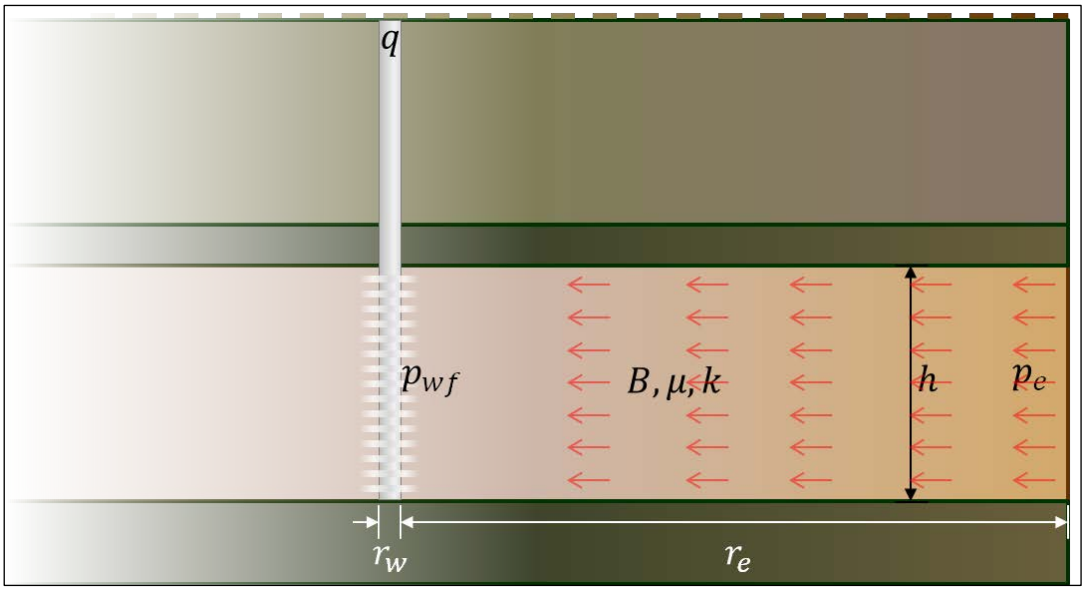

Figure 2-1: Flow in a gas reservoir.

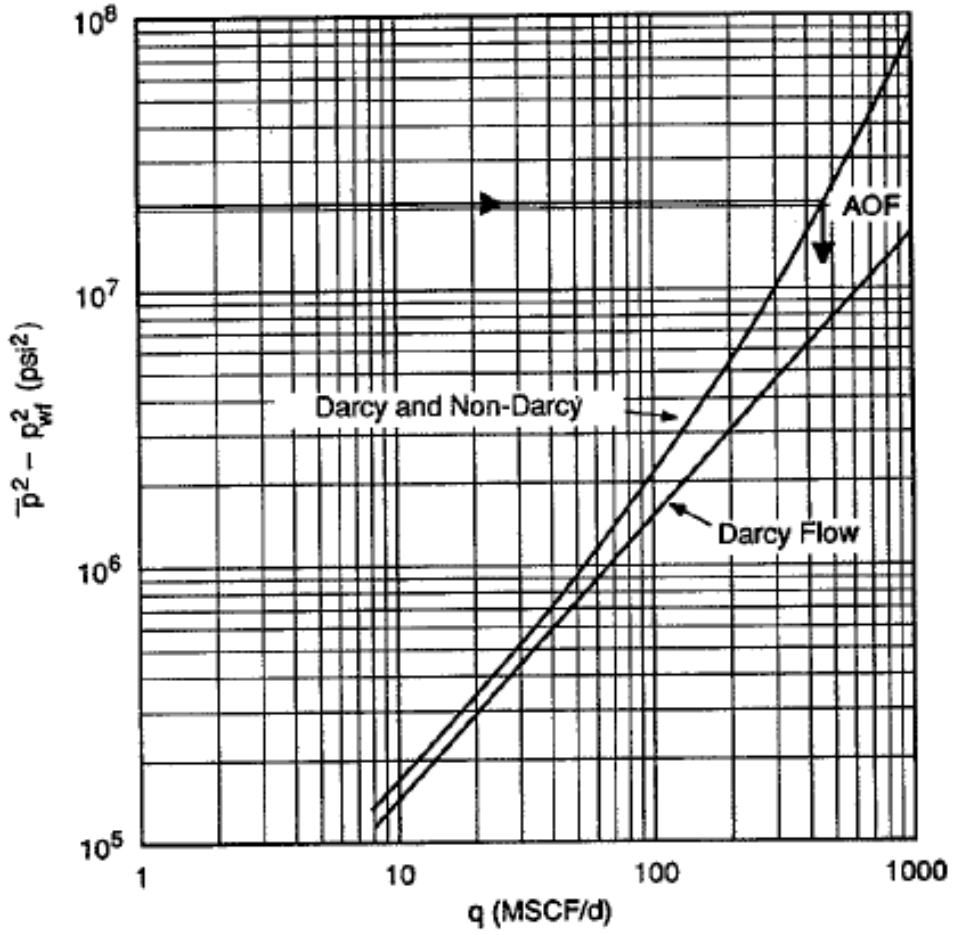

Figure 2-2: Difference between Darcy and Non-Darcy Flow [Ecnomides, 1994].

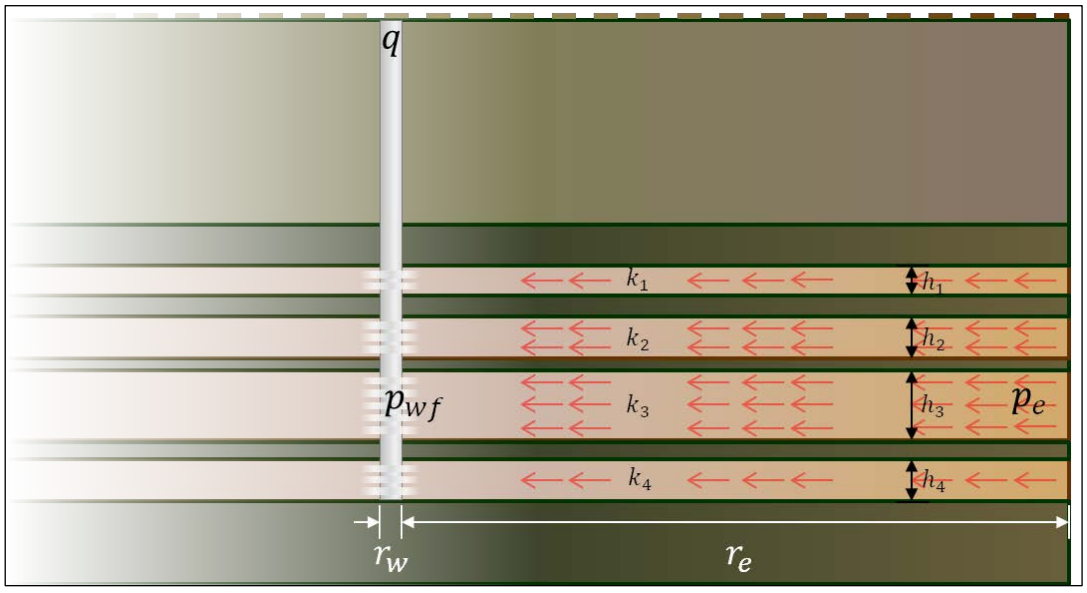

Figure 2-3: Flow in a multi-layer gas reservoir.

Chapter 3:

ARTIFICIAL INTELLIGENCE

This chapter covers Artificial Intelligence (AI) and describes the methods that are used in this research, namely, Multilayer Perception Networks (MLP), Probabilistic Neural Networks (PNN) and General Regression Neural Networks (GRNN), Radial Basic Functions (RBF), Support Vector Machine (SVM), and Adaptive Neuro-Fuzzy Inference System (ANFIS).

3.1. INTRODUCTION

AI is defined as "the subfield of computer science concerned with the use of computers in tasks that are normally considered to require knowledge, perception, reasoning, learning, understanding and similar cognitive abilities" [Duda, 1981]. It uses soft computing techniques to provide better results than the conventional solutions. It includes, amongst many things, perceptrons, problem solving, language, conscious, and unconscious processes.

3.2. USE OF AI IN PETROLEUM ENGINEERING

AI has become increasingly popular in the last two decades in the petroleum industry. It has been extensively used and many SPE papers show successful usages of AI methods to solve petroleum engineering problems [Mohaghegh, 2005].

AI applications in the petroleum industry includes lithofacies identification, PVT properties estimation, production optimization, reserve estimation, history matching, Measuring while Drilling (MWD) data analysis, drill bit diagnosis, hydraulic fracture

analysis, bottomhole pressure prediction, well test analysis, critical gas flow rate prediction, and gas-lift optimization [Saputelli et al.,2002 and Al-Dhufairi, 2011].

3.3. ARTIFICIAL INTELLIGENCE METHODS

3.3.1 ANN

There are several types of Artificial Neural Networks (ANN). The most common ones are Multilayer Perception Networks (MLP), Probabilistic Neural Networks (PNN) and General Regression Neural Networks (GRNN), and Radial Basic Functions (RBF), We will briefly discuss each of these types.

3.3.1.1 MLP

It is the most common type of ANN. Usually when the term ANN is used without qualification, it refers to MLP. It has been used extensively in the literature. Uses include global optimization in history matching [Silva et. al., 2006], reservoir characterization [Anifowose, 2011] modeling viscosity and wax deposition [Oladiipo et al., 2009], predicting relative permeability [Al-Fattah et al., 2009], modeling miscible displacements in heterogeneous reservoirs [Gharbi, 2003], predicting well inflow performance in solution gas reservoirs [Alrumah et al., 2005], estimating dewpoint pressure in gas condensate reservoirs [Akbari et al., 2007], and predicting casing collapse occurrence [Salehi et al., 2007].

An MLP Network usually consists of a single input layer, a single or multiple hidden layers, and a single output layer. Each layer consists of at least one neuron. For each predictor or input variable, there is a neuron in the input layer. Similarly, for each target or output variable there is a neuron in the output layer.

For optimum results, the input variables should be normalized so that each variable falls in the range between -1 and 1. The input layer feeds each input variable to all of the neurons in the next hidden layer. Moreover, the bias, which is a constant equals to 1, is also fed to all of the neurons in each hidden layer. After getting multiplied by a weight, the bias is added to the sum which is fed to the neuron.

Once received by the hidden layer, the values from the input layer get multiplied by a weight. Then all of the weighted received values are added together and fed to the transfer function in the neuron. The outputs from each of the neurons in the hidden layer are fed to the next hidden layer or to the output if that was the last hidden layer.

The process gets repeated until the values are received by the output layer. Once received by the output layer, the values from each hidden layer neuron get once again multiplied by a weight and added together to be fed to a transfer value which outputs the results of the network. If any normalization was done on the input layer, the output variables are transformed back to the same order of the input variables using the inverse of the normalization functions.

Most problems can be solved using one hidden layer. Only data with discontinuities require two hidden layers. Adding a layer won't usually improve the model, rather it may introduce the risk of converging to a local minimum. Theoretically, there is no reason to build a model with more than two hidden layers.

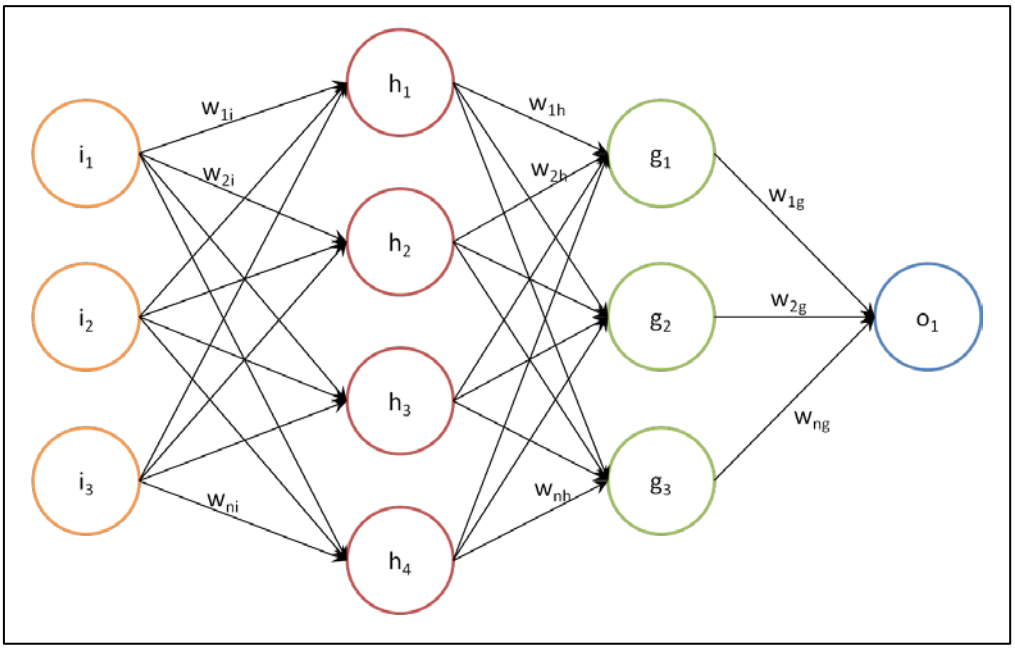

Figure 3-1: Typical MLP neural network.

Figure 3-1 shows a basic diagram of a fully connected 4-layer feed forward perception neural network. The difference between the feed forward and the back propagation networks is that in the feed forward networks, the values can only move from the input to the hidden layer and from the hidden layer to the next one and so on with no values fed back to earlier layers, while in the back propagation, networks allow the values to be fed backward [Beale et al., 2010].

3.3.1.2 PNN/GRNN

The probabilistic neural networks (PNN) and the general regression neural networks (GRNN) are very similar to each other with one very important difference: PNN is designed for categorical outputs whereas GRNN is designed for continuous outputs. Training a PNN or a GRNN is usually much faster than training an MLP Network. They are also usually more accurate and relatively insensitive to outliers. However, PNN or GRNN models require much more memory than MLP for storing the model.

There are several examples in the literature of using GRNN. These include uncertainty quantification [Mohamed et al., 2009], modeling the CVD behavior of retrograde-gas condensate reservoirs [Elsharkawy et al., 1998], predicting heavy oil molar composition [Al-Sirri et al., 2011], and predicting sanding [Kanj et al., 1999].

The basic idea of PNN/GRNN models is that the target variable is probably very close to the value of other variables that have very similar predictor or input variables.

There are always 4 layers in PNN and GRNN. For each predictor or input variable, there is one neuron. For PNN, there are N-1 neurons for N number of categories. The input is normalized by subtracting the median and dividing by the interquartile range. Subsequently the data is fed to all of the neurons in the hidden layer.

There is one neuron in the hidden layer for each case in the input data. The neuron in the hidden layer stores both the values of input variable for that specific case and the target value. The hidden neuron calculates the Euclidean distance between the center of the neuron and the test case. After that, using the sigma variables it applies the RBF kernel function using the sigma values. Then the data is fed to the neurons in the pattern/summation layer.

For PNN network the third layer contains one pattern neuron for each of the categories of the target or output layer. The weighted value that came from the hidden layer is fed only to the pattern neuron that is related to the category of the hidden neuron. The values of each class are added by the representative neuron.

On the other hand, the GRNN network has only 2 neurons in the summation layer. They are called the denominator summation unit and the numerator summation unit. The weight values coming from each of the hidden layers are summed in the denominator summation unit while the numerator summation unit sums the weights multiplied by the actual target (output) value of each hidden neuron.

The fourth and final layer is the decision layer. For PNN networks, the decision layer looks at the values of the weighted votes for each target category in the pattern layer and uses the largest accumulation to predict the target category (the output). For the GRNN networks, in the division layer, the value which accumulated in the numerator summation unit is divided by the value accumulated in the denominator summation unit and the result is used to predict the target value [Sherrod, 2008].

Figure 3-2 shows a basic diagram of a typical PNN/GRNN type neural network.

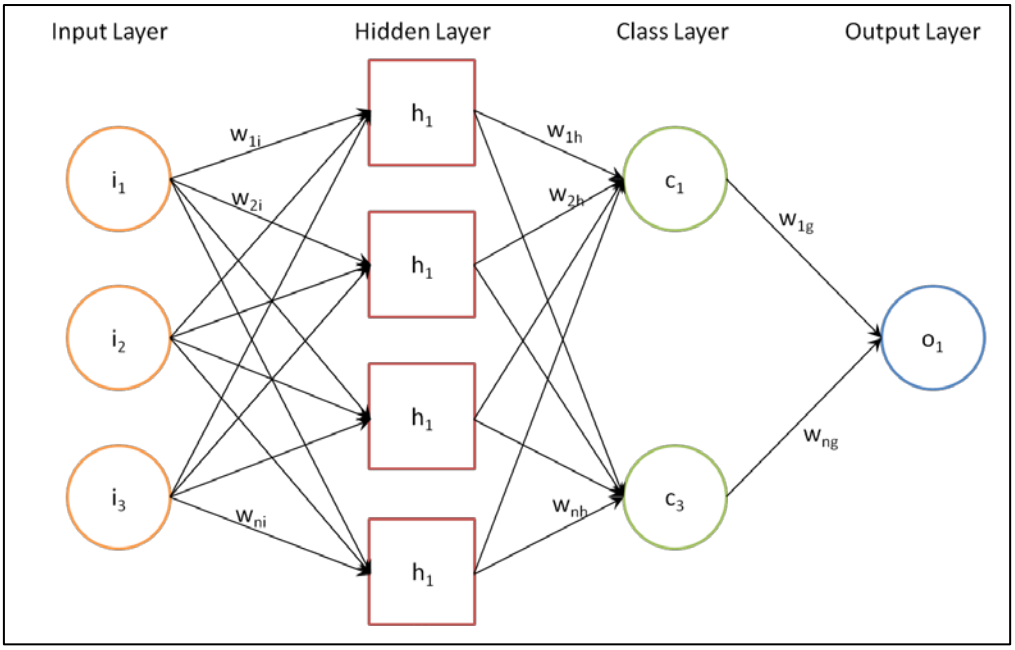

Figure 3-2: Typical PNN/GRNN type neural network.

3.3.1.3 RBF

Radial Basis Function Neural Networks (RBF) are very similar to GRNN networks with one main difference which is that while GRNN have one neuron for each input data point, RBF have a number of neurons which is most of the time much less than the number of input data points. It is recommended to use GRNN for small to medium-sized data sets as they will deliver more accurate results than RBF. However, RBF is more suited for large and very large data sets since GRNN is almost not practical for larger data sets.

RBF is not new to the petroleum industry; uses in the literature include predicting log properties from seismic attributes [Russel et al., 2003], predicting and managing bit wear [Gidh, 2012], determining structure parameters [Kaftan et al., 2009], optimizing CO_2 sequestration in coalbed methane reservoirs [Mohammadpoor, 2012], reservoir properties prediction [Lei et al., 2011], and well log data inversion [Huang et al., 2011].

The basic idea of RBF models is, like PNN/GRNN, that the target variable is probably very close to the value of other variables that have very similar predictor (input) variables. What RBF networks do is that they place at least one RBF neuron in the space which is described by the input variables. The dimensions of this space have the same number as those of predictor variables. The neuron being evaluated calculates the Euclidean distance between the center of the neuron and the center of each neuron in that space. An RBF function (usually Gaussian) is applied to each distance to estimate the weight based on the influence of each neuron. The further away a neuron is, the less influence it has on target neuron. The predicted value is best estimated by multiplying the weight of the connection by the output value of the RBF function.

RBF networks have three layers, input, a hidden layer which contains an RBF function usually Gaussian, and an output layer. The input is normalized by subtracting the

median and dividing by the interquartile range. Subsequently the data is fed to all of the neurons in the hidden layer.

The number of neurons in the hidden layer is variable and is determined by the training process. The neuron in the hidden layer stores both the values of input variable for that specific case and the target value. The hidden neuron calculates the Euclidean distance between the center of the neuron and the test case. After that, using the sigma variables it applies the RBF kernel function using the sigma values. Then the data is fed to the neurons in the summation layer.

The last layer is the summation layer. It gets the output of the hidden layer multiplied by a specific weight that is specific for that neuron (Figure 3-3). It then sums all of the incoming values to get the output [Sherrod, 2008].

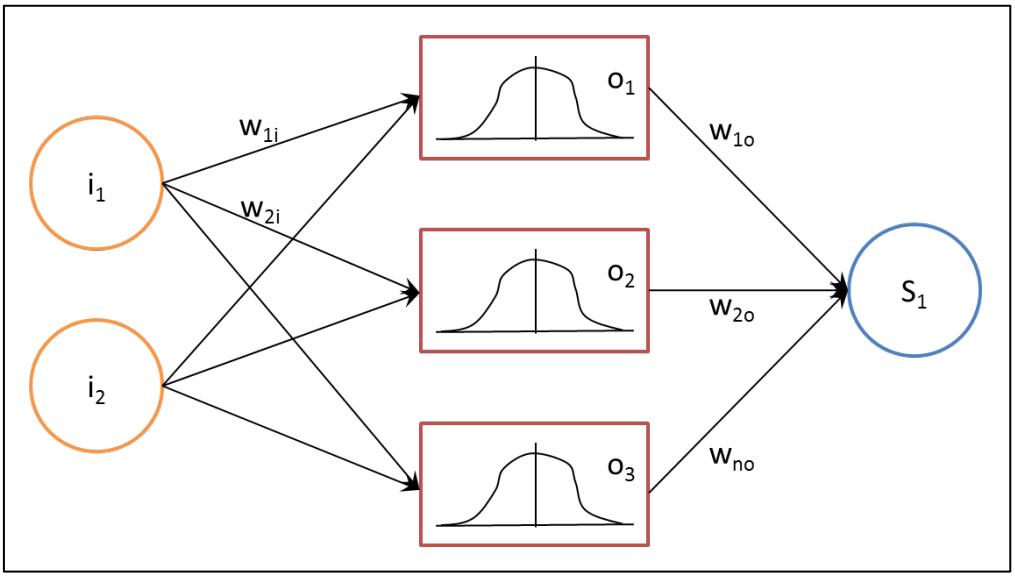

Figure 3-3: Typical Radial Basis Function Neural Network.

3.3.2 SVM

Support vector machine (SVM) model classifies data by creating an N-dimensional hyperplane which separates the data optimally. It has been used extensively in the literature; uses include predicting permeability from well log data and core measurements [Nazari, et al., 2011], predicting oil and gas reservoir properties [Anifowose et al., 2011], predicting porosity and permeability [Anifowose et al., 2010], estimating well cost [Bhuddharaju et al., 2007], selecting seismic attributes for hydrocarbon reservoir prediction [Chang-Kai et al., 2010], and permeability prediction in a heterogeneous reservoir [Al-Anazi et al., 2010].

In SVM, the predictor variable is called an attribute. When it is transformed to define the hyperplane, it is called a feature. The set of features that describes one case of predictor values is called a vector.

Ultimately, the goal of support vector machine is to find an optimal hyperplane where one category of the target variables is on one side, and another category is on the other. SVM uses kernel functions such as linear, polynomial, sigmoid, and radial based functions [Sherrod, 2008].

Figure 3-4 shows a linear hyperplane in a typical 2D problem which was not optimum while Figure 3-5 shows a better and more optimum solution using a hyperbolic function.

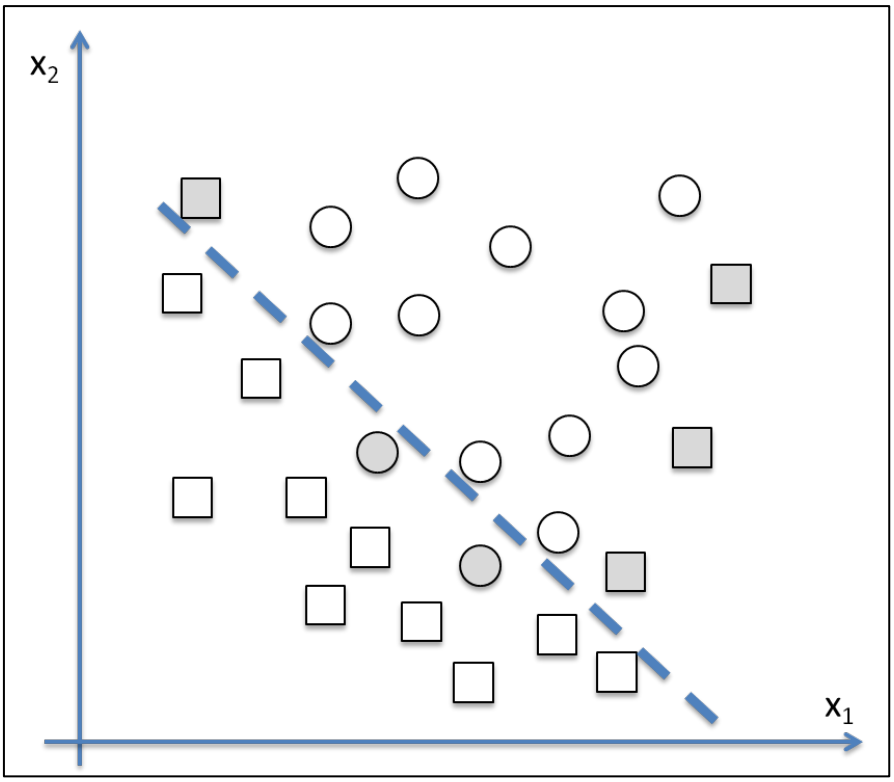

Figure 3-4: SVM using a linear separation boundary.

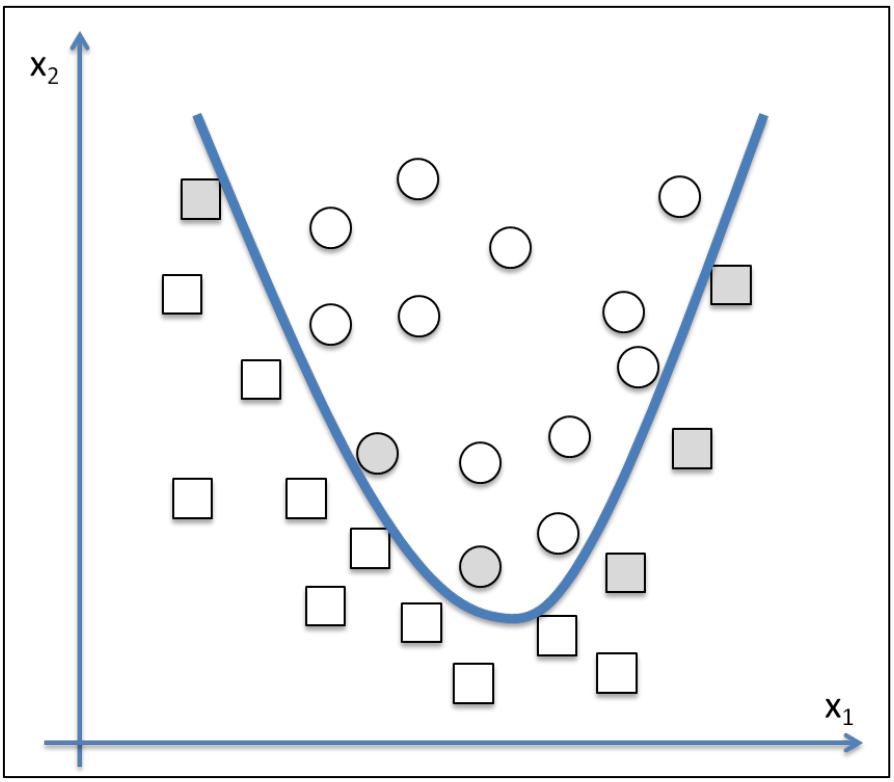

Figure 3-5: SVM using a nonlinear separation boundary.

3.3.3 ANFIS

The adaptive neuro-fuzzy inference system uses a set of data inputs/outputs to construct a fuzzy inference system (FIS) in which the membership functions are tuned using a back propagation function with or without combination with a least square type of method. This procedure allows the fuzzy inference system to learn from the data they are trying to model [Al-Shammari, 2012].

The network-type structure of ANFIS is similar to that of a neural network that maps the inputs through input membership functions and associated parameters. Then using the output parameters it tries to change the parameters associated with the membership functions through the learning process [Natick, 2010].

Chapter 4:

DATA ACQUISITION, ORGANIZATION, AND ANALYSIS

In this chapter, extraction of the data sets from different sources, and their organization combination and analysis is discussed.

4.1. PRODUCTION LOGS

After a production log test is performed, the engineer receives the data from the field and starts working on the analysis. These days, the engineers use state-of-the-art software to help them perform a more accurate analysis.

After the analysis is carried out, the well performance is compared to other wells for quality assurance and diagnostic. The test is finally archived in the PLT database.

For the purposes of this research, a program was created to pull the relevant data (Production Rate, Static Pressure, Flowing Pressure, and Flowing Temperature) from each flow zone from the archived files to produce a table that can be used as input for the AI tools.

4.2. WELL LOGS

Well logging tools are usually run after finishing well drilling or while drilling. The raw data is sent to the reservoir description engineer for analysis. A lot of information can be obtained using general correlations or correlations specific to a certain reservoir.

For the purposes of this research, a program was created to get the average properties of porosity, permeability, and water saturation from the archives of analyzed logs and match them with each flow zone that was picked from the PLT test results.

4.3. PVT DATA

Samples are taken from the wells for PVT analysis. The PVT lab issues a report on the composition and the PVT properties of the sample. Those PVT reports were used to estimate the gas viscosity and z-factor. A sample PVT report is included in Appendix-C.

4.4. WELL TESTING

Well test analysis results were used to estimate the well skin and to quality check the estimated reservoir pressures.

4.5. DATA COMBINING AND ORGANIZATION

It is generally a good idea to include physical relationships or correlations in the input of the AI model. It helps in guiding the model in the training phase. After examining the solution of Darcy's equation for flow in porous media:

$$q = C(\bar{p}^2 - p_{wf}^2) \tag{4-1}$$

and the solution of Forchheimer equation as well:

$$\bar{p}^2 - p_{wf}^2 = a\,q + b\,q^2 \tag{4-2}$$

One can observe that the gas rate is directly related to the difference of the squared pressures, so $d(p^2)$ is as an input:

$$d(p^2) = \bar{p}^2 - p_{wf}^2 \tag{4-3}$$

The constants used in these equations (C, a, and b) are also used as inputs:

$$C = \frac{kh}{1424\mu ZT\left(\ln\left(0.472\frac{r_e}{r_w}\right)+s\right)} \tag{4-4}$$

$$a = \frac{1424\bar{\mu}\,\bar{z}\,T}{kh}\left(\ln\frac{0.472r_e}{r_w} + s\right) \quad (4\text{-}5)$$

$$b = \frac{1424\bar{\mu}\,\bar{z}\,TD}{kh} \quad (4\text{-}6)$$

Moreover, to account for the effects of turbulent flow, the non-Darcy flow coefficient is also used as another input:

$$D = \frac{6\times10^{-5}\gamma k_S^{-0.1}h}{\mu r_w h_{perf}^2} \quad (4\text{-}7)$$

And finally since the permeability is a key difference between the wells in this study, it was also included as an input.

In summary, the model consisted of six inputs [a, b, C, D, d(p^2), and permeability] and one output [q_{layer}].

The raw data are presented in Appendix 1.

4.6. Data Analysis

Statistical analysis (Table 4-1 to 4-3, and Appendix-B) was performed on the input data to eliminate any anomalies and to learn the limits of the AI model. Histograms were also constructed to analyze the distribution of the data (Appendix-2-2).

These tables show the range covered by the data used in this study. Most importantly, it shows the reservoir pressure varies from 2298 psi to 6960 psi, while the flowing pressure varies from 1665 psi up to 6630 psi. It also shows that the porosity varies from 3.74% up to 23.03% and the permeability from as low as 0.1034 d to as high as 99.69 md. The gas flow rates cover a wide range from only 104 MSCF all the way to25385 MSCF.

Table 4-1: Statistical Analysis of Input Data – Part I

Property	Reservoir Pressure psi	Perforation Thickness ft	Flowing Temperature °F	Flowing Pressure psi
Minimum	2298	2.60	238.40	1665
Maximum	6960	61.70	292.03	6630
Mean	5334	14.79	256.47	4650
Median	5340	10.90	254.43	4708
Standard Deviation	1036	10.03	9.14	1154
Coefficient of Correlation	0.0040	0.2523	0.0500	-0.0296

Table 4-2: Statistical Analysis of Input Data – Part II

Property	Diameter ft	Flow Zone Thickness ft	Water Saturation Fraction	Porosity Fraction
Minimum	3.650	5.25	0.0454	0.0374
Maximum	9.020	66.50	0.4752	0.2303
Mean	5.361	18.37	0.2452	0.1067
Median	6.004	14.00	0.2321	0.1072
Standard Deviation	1.029	11.96	0.0809	0.0302
Coefficient of Correlation	0.1116	0.2484	-0.1265	0.2478

Table 4-3: Statistical Analysis of Input Data – Part III

Property	Permeability mD	Gas Specific Gravity Ratio	Skin	Gas Flow Rate MSCF
Minimum	0.1035	0.6333	-5.90	104
Maximum	99.69	0.6724	-1.59	25385
Mean	12.78	0.6480	-4.72	3349
Median	6.86	0.6490	-4.70	2023
Standard Deviation	15.90	0.0115	0.69	3700
Coefficient of Correlation	0.6323	0.0171	0.0062	1.0000

Chapter 5:

RESULTS AND CONCLUSIONS

In this chapter, the results of this research are presented and discussed. Finally, conclusions and recommendations are given.

Hundreds of runs were performed using different AI methods. In all runs a 70:30 training to testing and validation ratio was used. Below, the results of the best runs of each method are presented. Between the tested AI methods, SVM and GRNN performed best with a low mean absolute percentage error and a very high correlation coefficient. This work shows promising use for AI methods in estimating production rate from each layer in a multi-layered gas reservoir.

Overall, the normalized set has shown better performance and a major improvement in the cases of MLP and SVM. Figure 5-1 shows the mean absolute error of the model in MSCF. It shows that the normalized SVM model has peroformed best with a mean absolute error of 77 MSCF. Figure 5-2 shows the mean absolute percentage error of the different AI methods used in this study. Once again, the normalized SVM model has performed best with a mean absolute percentage error of 2.25%.

Figure 5-3 shows the coefficient of correlation between the model results and the measured data. All of the models had a high coefficient of correlation. However, the highest were the normalized GRNN and SVM sets.

Figure 5-4 compares the mean absolute error of empirical methods vs. AI methods. It shows that the AI methods are performing better. This is probably because the models are built using this data set whereas the empirical correlations are derived from general flow equations and not specifically tailor-made for this data set. Next, Figure 5-5

compares the mean absolute percentage error of empirical methods vs. AI methods. Similar observations can be made to those of Figure 5-4. Finally, Figure 5-6 compares the correlation coeficcient of empirical methods vs. AI methods where again the AI methods outperform the emperical methods.

Figures 5-7 and 5-8 show a more detailed comparison between the normalized SVM and GRNN AI models versus Darcy Empirical Equation. They show that both the estimation error and the absolute percentage error of the Darcy Equation are more dispersed than those of the AI methods. Similar observations are made from Figures 5-9 and Figure 5-105-10 which compare the results of Forchheimer empirical equation with the results of the same AI methods.

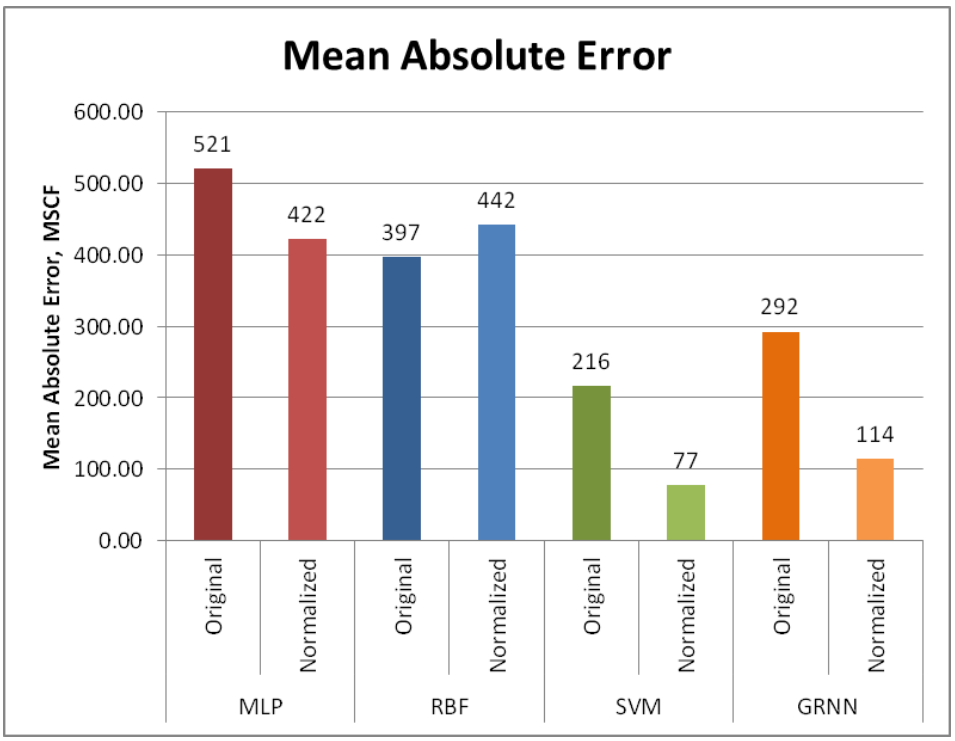

Figure 5-1: Mean absolute error of different AI methods.

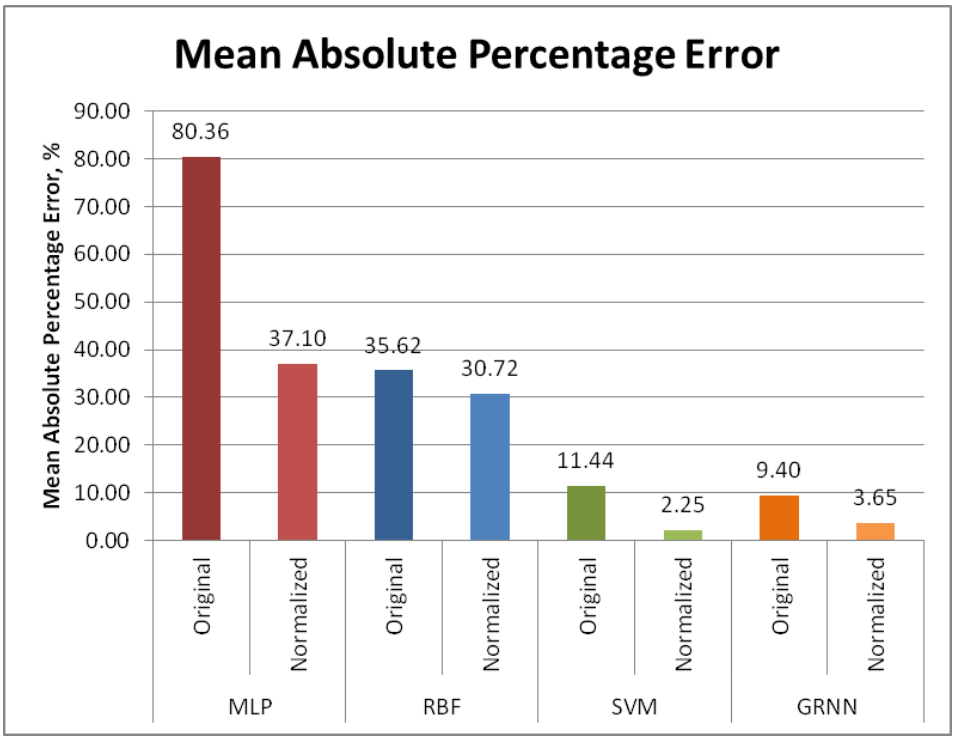

Figure 5-2: Mean absolute percentage error of different AI methods.

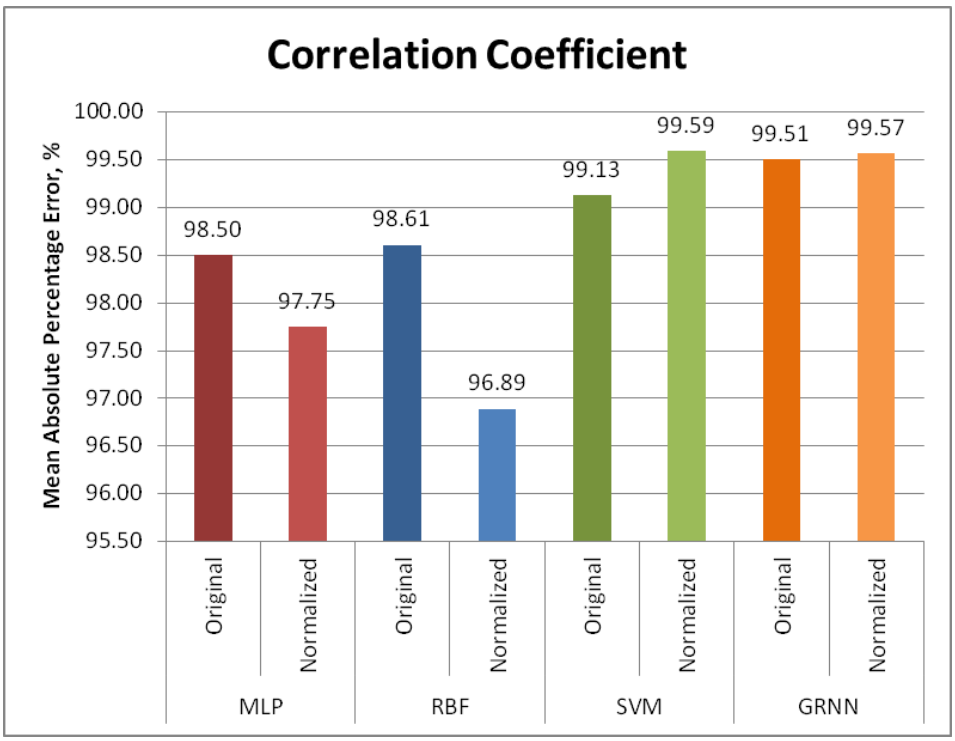

Figure 5-3: Correlation coefficient of different AI methods.

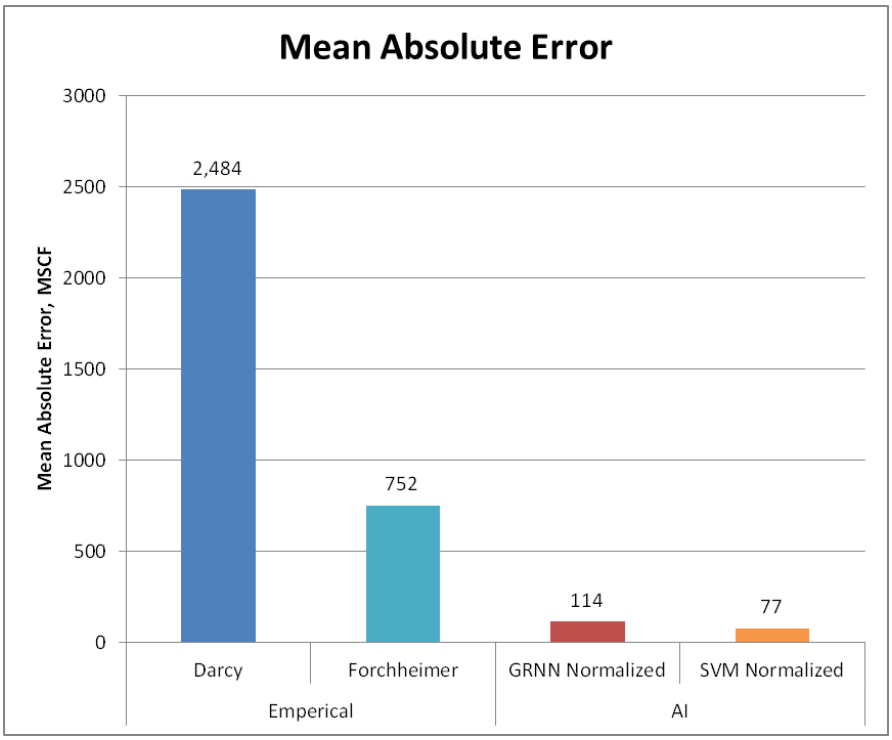

Figure 5-4: Mean absolute error of empirical methods vs. AI methods.

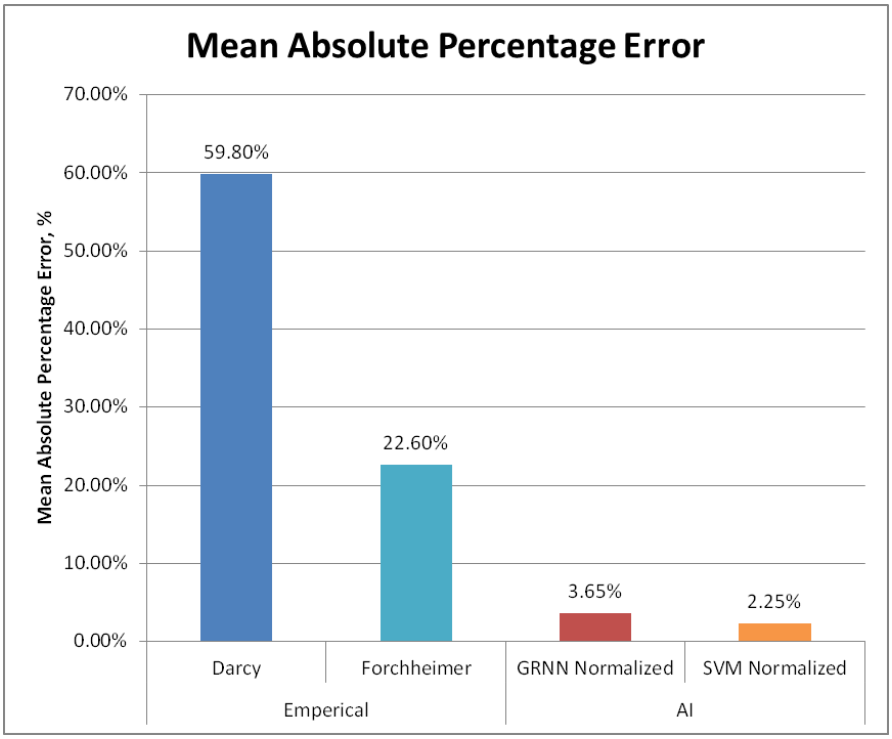

Figure 5-5: mean absolute percentage error of empirical ,ethods vs. AI methods.

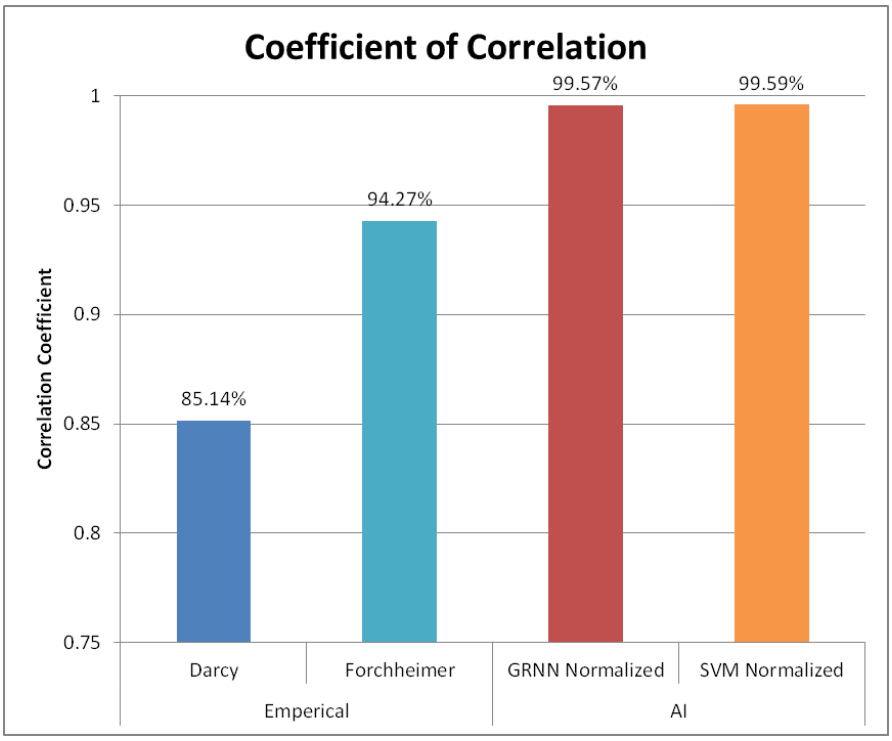

Figure 5-6: Correlation coefficient of empirical methods vs. AI methods.

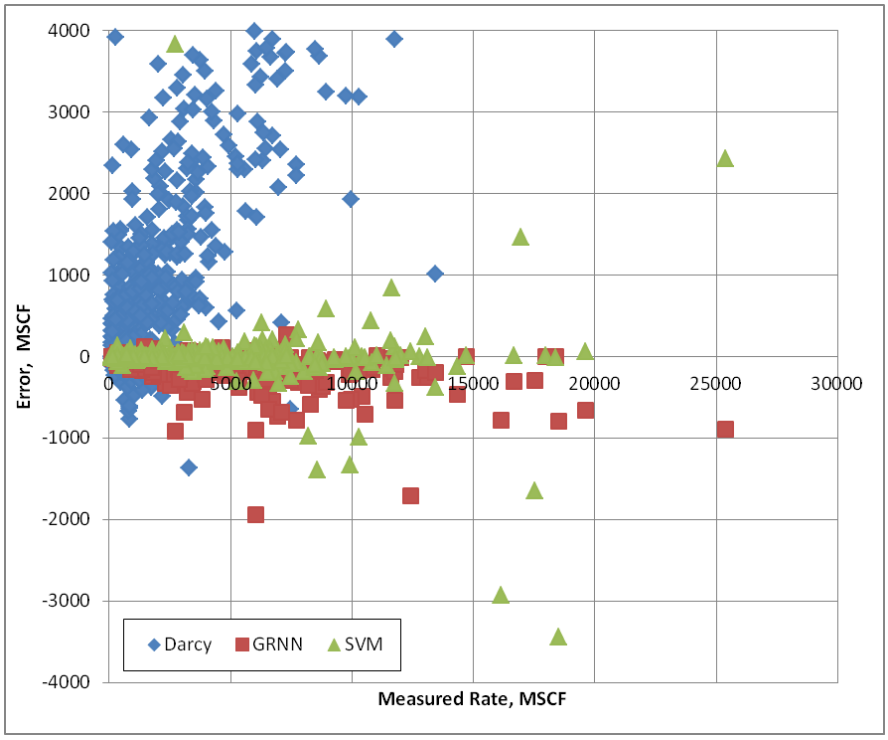

Figure 5-7: Estimation error of Darcy empirical equation vs. normalized GRNN and SVM.

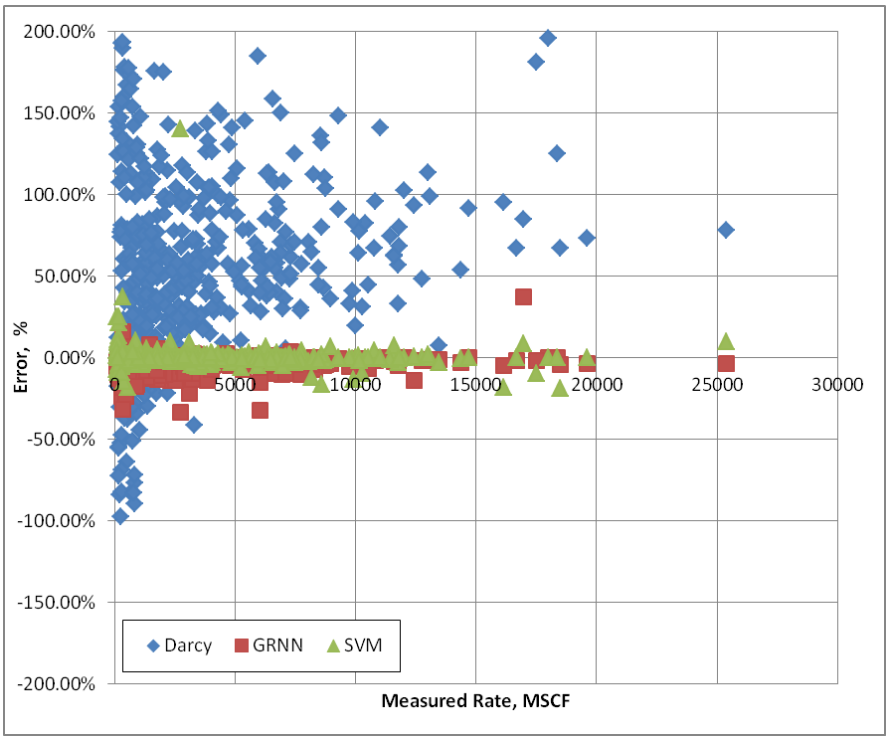

Figure 5-8: Estimation percentage error of Darcy empirical equation vs. normalized GRNN and SVM.

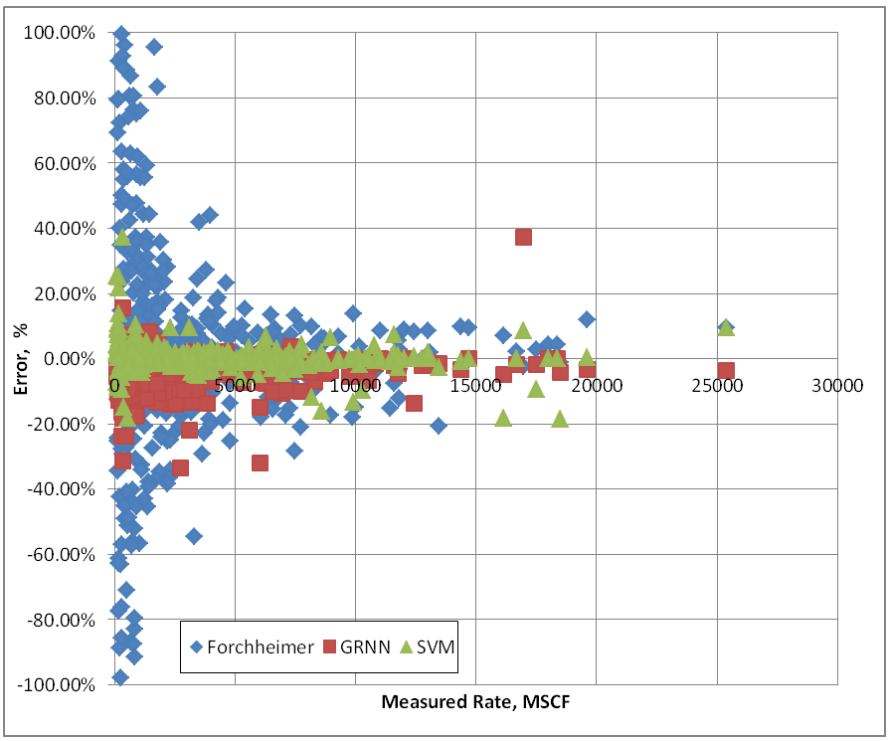

Figure 5-9: Estimation error of Forchheimer empirical equation vs. normalized GRNN and SVM.

Figure 5-10: Estimation percentage error of Forchheimer empirical equation vs. normalized GRNN and SVM.

5.1. ANFIS

All ANFIS runs didn't meet the either of the requirements set in this research (80% accuracy or 80% correlation coefficient) and thus, the results will not be presented.

5.2. MLP

Figures 5-11 and 5-12 show the crossplot between the measured rate and the rate estimated by the MLP model for both the original and the normalized data sets. They show a good linear correlation between the two beyond 3000 MSCF. Figure 5-12 shows that the normalized set has more dispersion than the non-normalized set overall but less dispersion at low rates.

Figures 5-13 and 5-14 show the model error for both the original and the normalized data sets respectively. We could observe that the non-normalized MLP model results are less dispersed around the x-axis which indicates departure from the desired value. The figures also show a higher error in the model as the rate increases. Figures 5-15 and 5-16, show the percentage error between the models results and the measured values. They also show more dispersion in the normalized data set results. The error patterns showing up in these plots signifies that these models are not optimum.

Table 5-1 shows summary statistics of the MLP model for both the original and the normalized data sets.

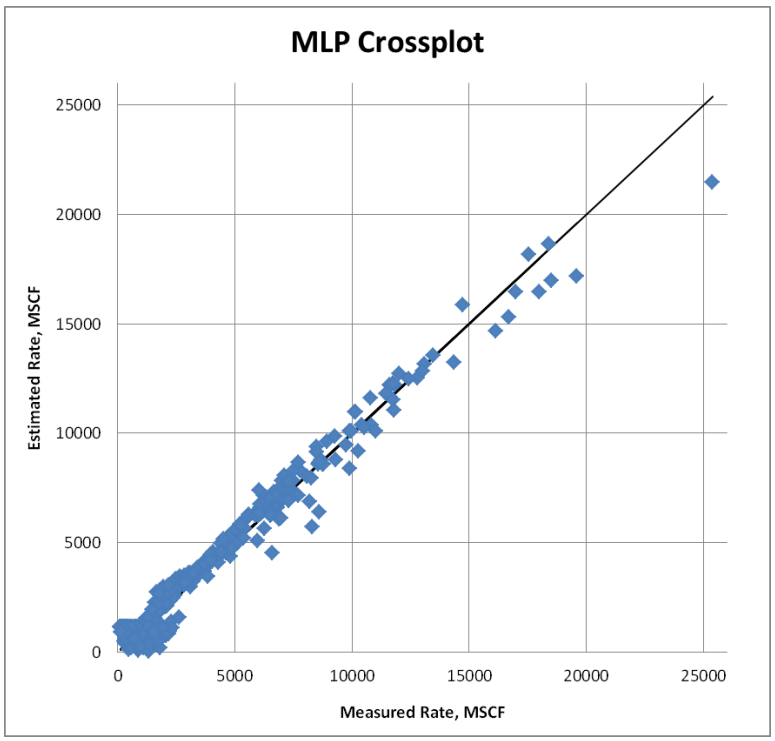

Figure 5-11: Crossplot of the measured and estimated rates using the MLP AI method and the original data set.

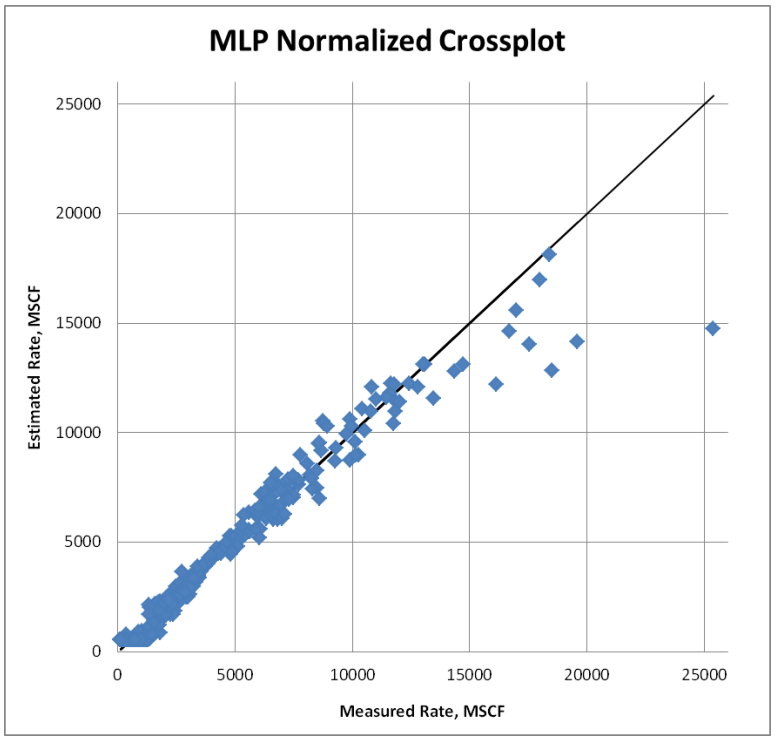

Figure 5-12: Crossplot of the measured and estimated rates using the MLP AI method and the normalized data set.

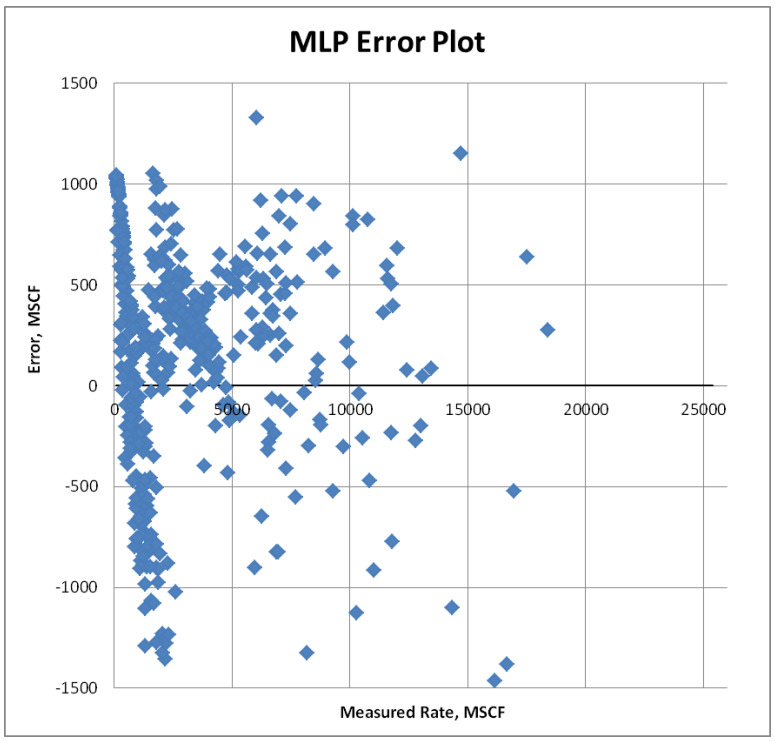

Figure 5-13: The estimation error using the MLP AI method and the original data set.

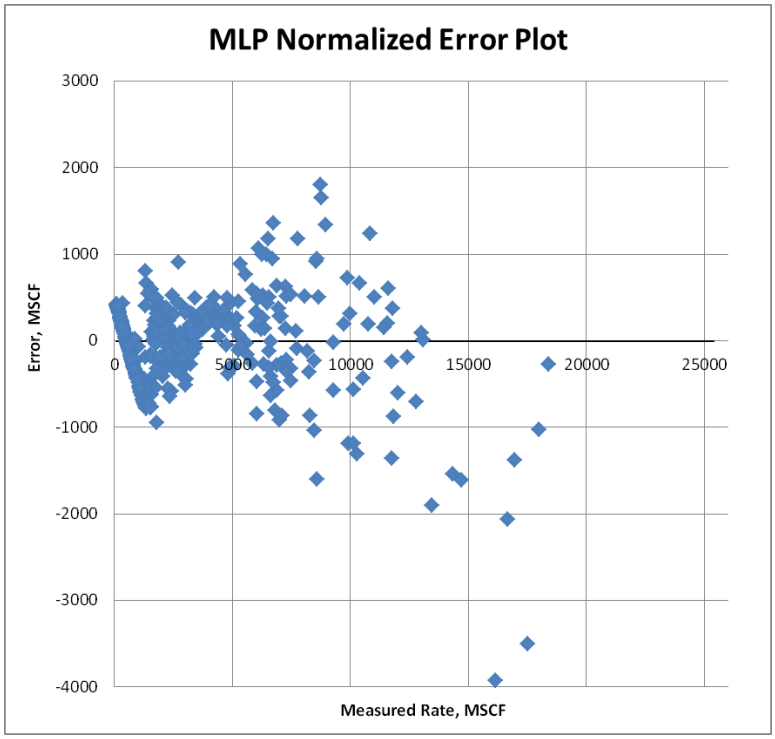

Figure 5-14: The estimation error using the MLP AI method and the normalized data set.

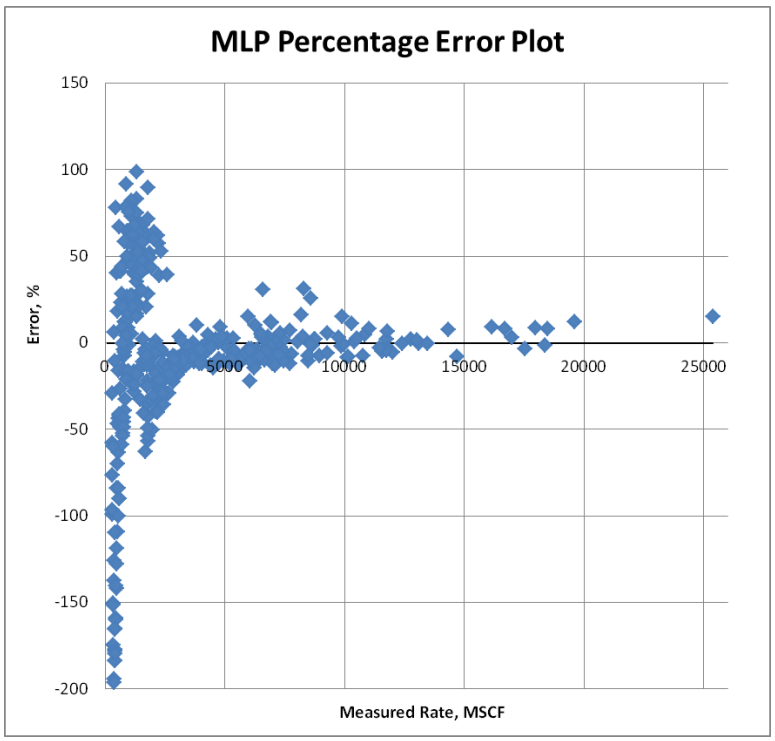

Figure 5-15: The estimation percentage error using the MLP AI method and the original data set.

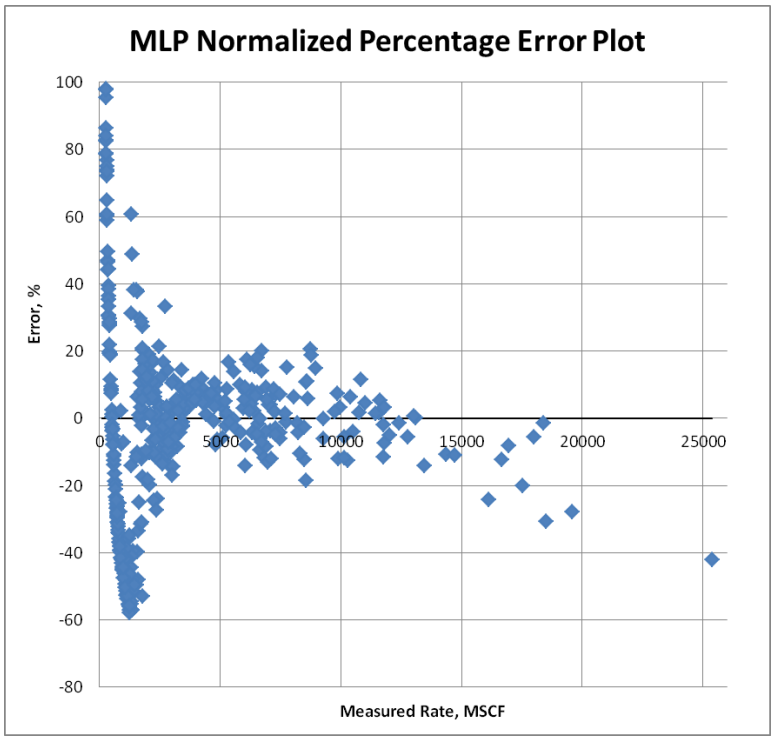

Figure 5-16: The estimation percentage error using the MLP AI method and the normalized data set.

Table 5-1: MLP Model Results

Method	MLP	
Set	Original	Normalized
Mean Absolute Error, MSCF	521.09	421.68
Mean Absolute Percentage Error, %	80.36	37.10
Correlation Coefficient, %	98.50	97.75

5.3. RBF

Figures 5-17 and 5-18 show the crossplot between the measured rate and the rate estimated by the RBF model for the original set and the normalized set respectively. They show a good linear correlation between the two. Figure 5-18 shows that the normalized set has less dispersion than the non-normalized set in figure 5-17 at lower rates.

Figures 5-19 and 5-20 show the model error for both the non-normalized and the normalized sets respectively. It is observed that the non-normalized model results are more dispersed at lower rates around the x-axis which indicates departure from the desired value. The figures also show a higher error in the model as the rate increases. However, as indicated by Figures 5-21 and 5-22, the percentage error decreases as the rate increases signifying that the model accuracy increases as the rate increases. Figures 5-21 and 5-22 also show less dispersion in the normalized data set results.

Table 5-2 shows summary statistics of the RBF model for both the original and the normalized data sets.

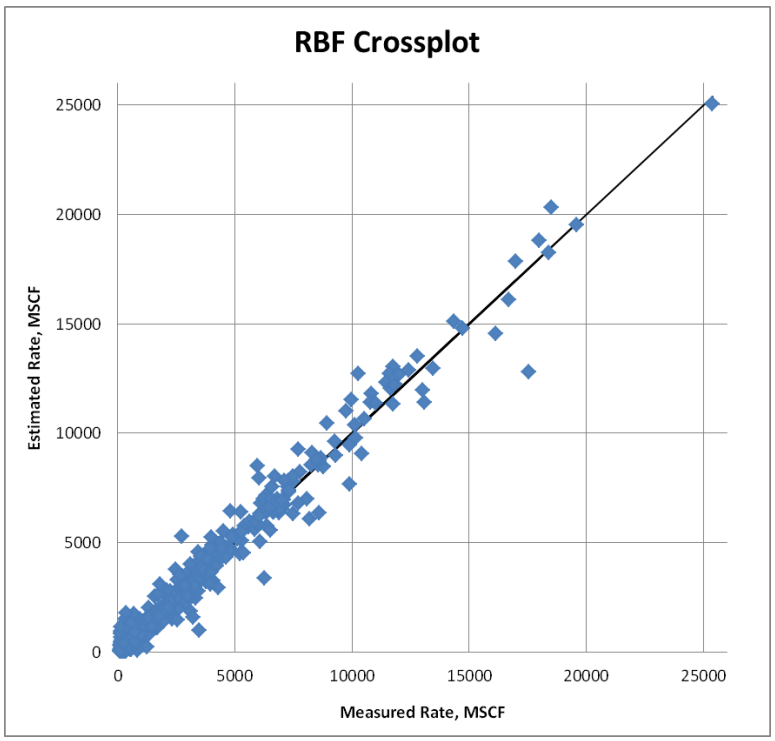

Figure 5-17: Crossplot of the measured and estimated rates using the RBF AI method and the original data set.

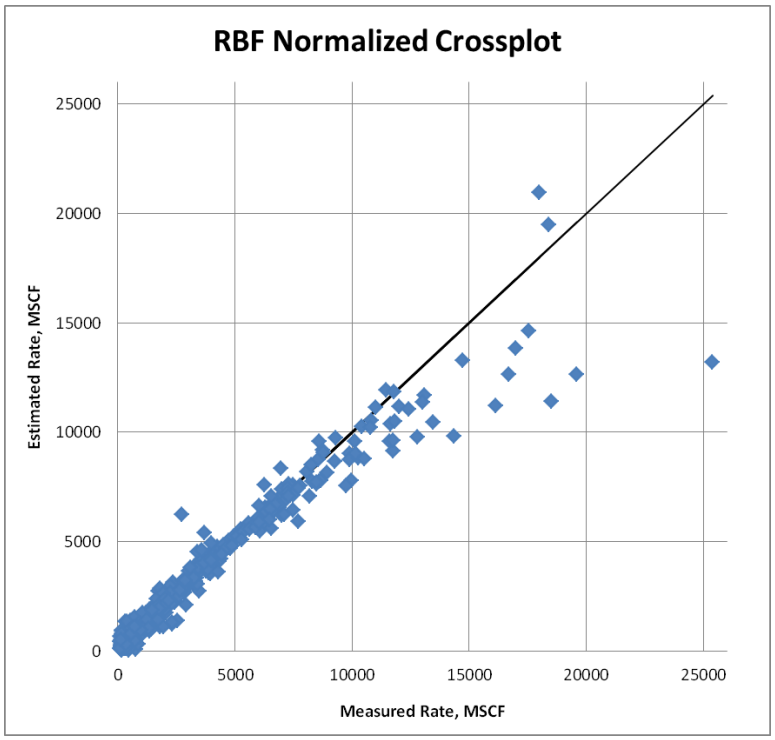

Figure 5-18: Crossplot of the measured and estimated rates using the RBF AI Method and the normalized data set.

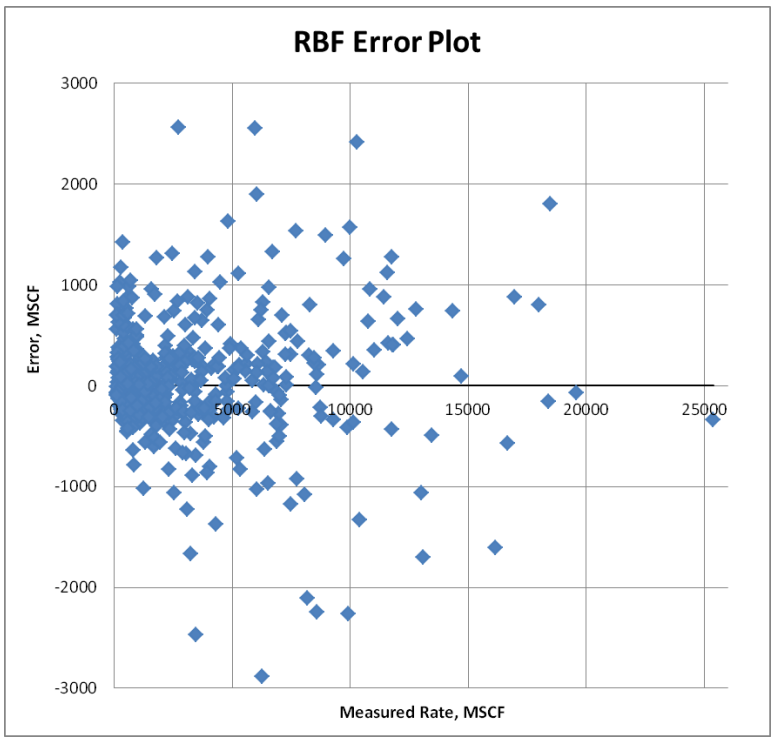

Figure 5-19: The estimation error using the RBF AI method and the original data set.

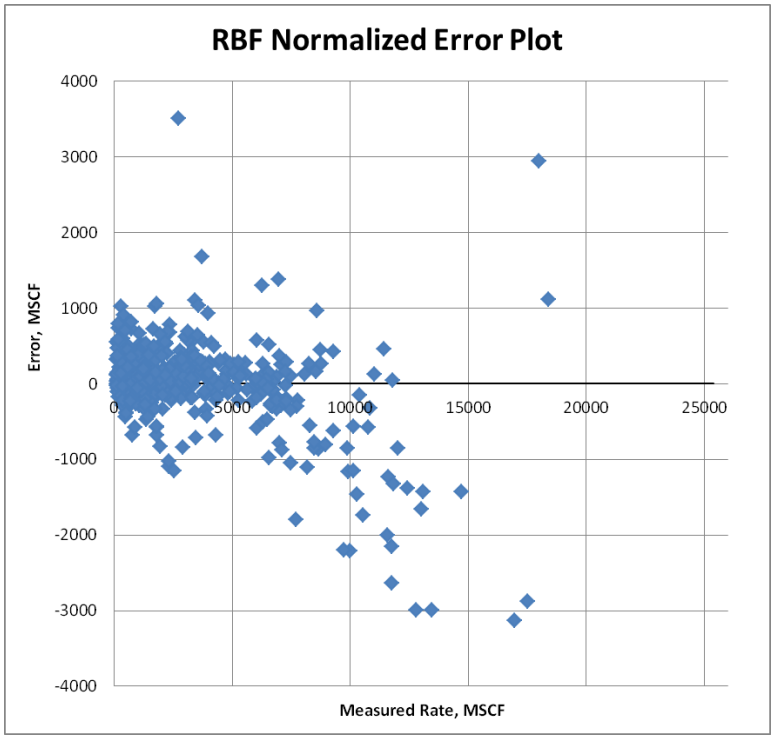

Figure 5-20: The estimation error using the RBF AI method and the normalized data set.

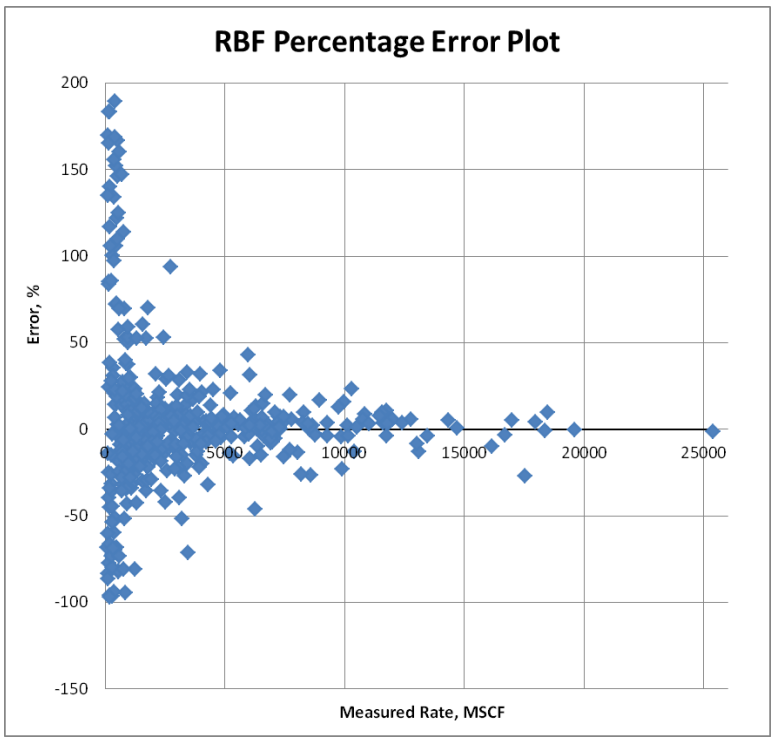

Figure 5-21: The estimation percentage error using the RBF AI method and the original data set.

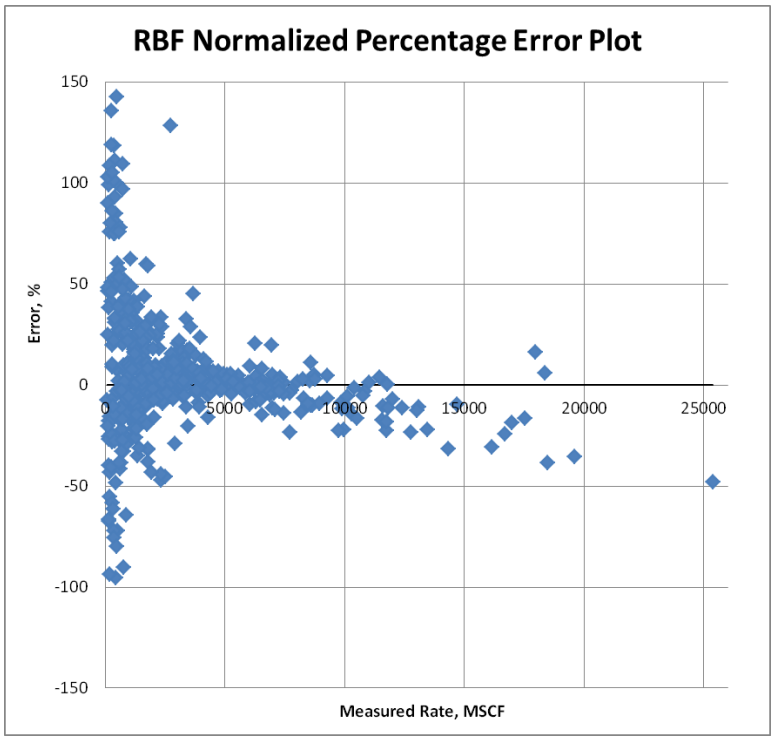

Figure 5-22: The estimation percentage error using the RBF AI method and the normalized data set.

Table 5-2: RBF Model Results

Method	RBF	
Set	Original	Normalized
Mean Absolute Error, MSCF	396.84	442.01
Mean Absolute Percentage Error, %	35.62	30.72
Correlation Coefficient, %	98.61	96.89

5.4. SVM

Figures 5-23 and 5-24 show the crossplot between the measured rate and the rate estimated by the SVM model for bothe the original data set and the normalized date set respectively. They show a good linear correlation between the two. Figure 5-24 shows that the normalized set has less dispersion than the non-normalized set. Similar observation is noted with the the GRNN method described later, which indicates the benefits of normalizing the data prior to training the model.

Figures 5-25 and 5-26 show the model error for both the non-normalized and the normalized sets respectively. We could observe that the non-normalized model results are more dispersed around the x-axis which indicates departure from the desired value. The figures also show a higher error in the model as the rate increases. However, as indicated by Figures 5-27 and 5-28, the percentage error decreases as the rate increases signifying that the model accuracy increases as the rate increases. Figures 5-27 and 5-28, also show less dispersion in the normalized data set results.

Table 5-3 shows summary statistics of the SVM model for both the original and the normalized data sets.

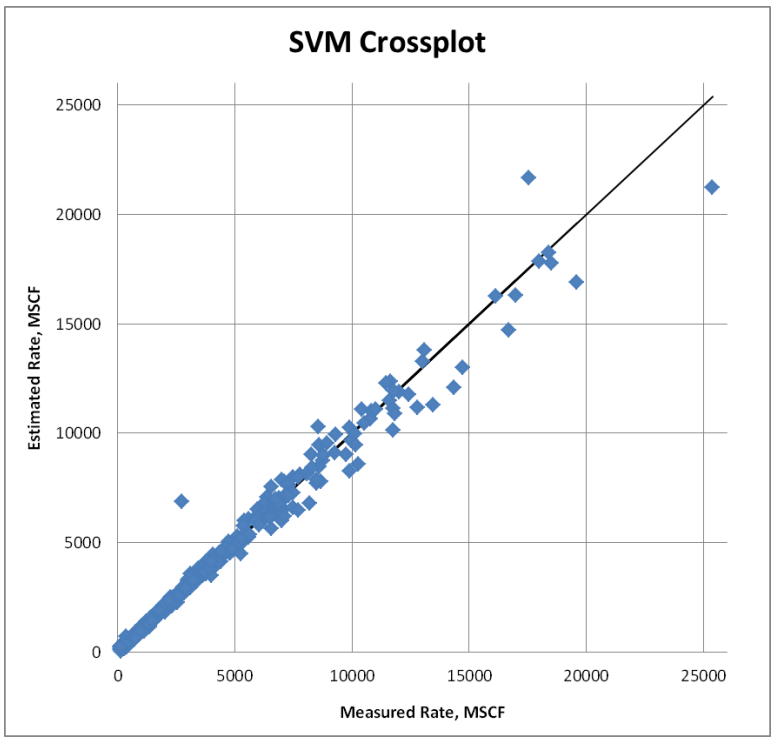

Figure 5-23: Crossplot of the measured and estimated rates using the SVM AI method and the original data set.

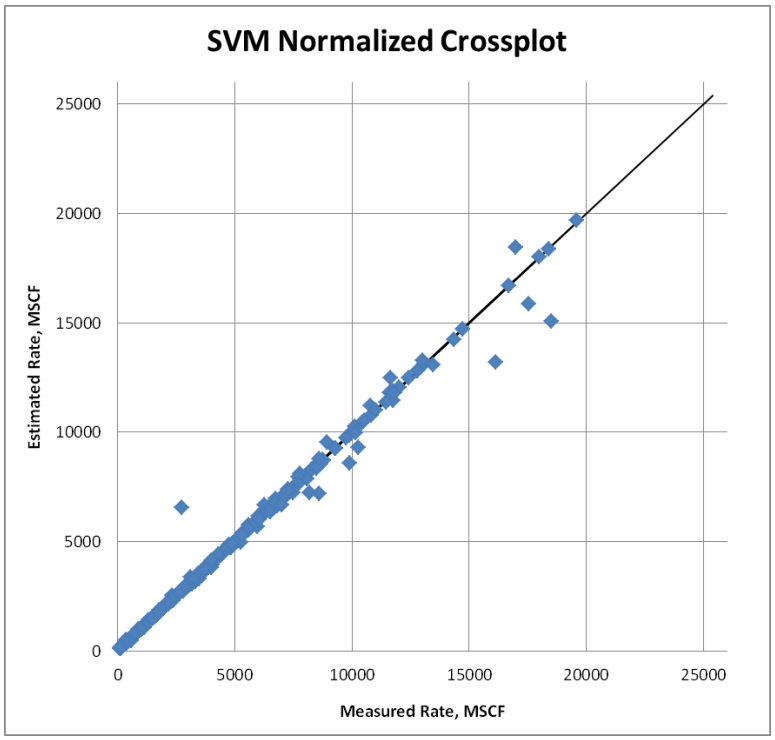

Figure 5-24: Crossplot of the measured and estimated rates using the SVM AI method and the normalized data set.

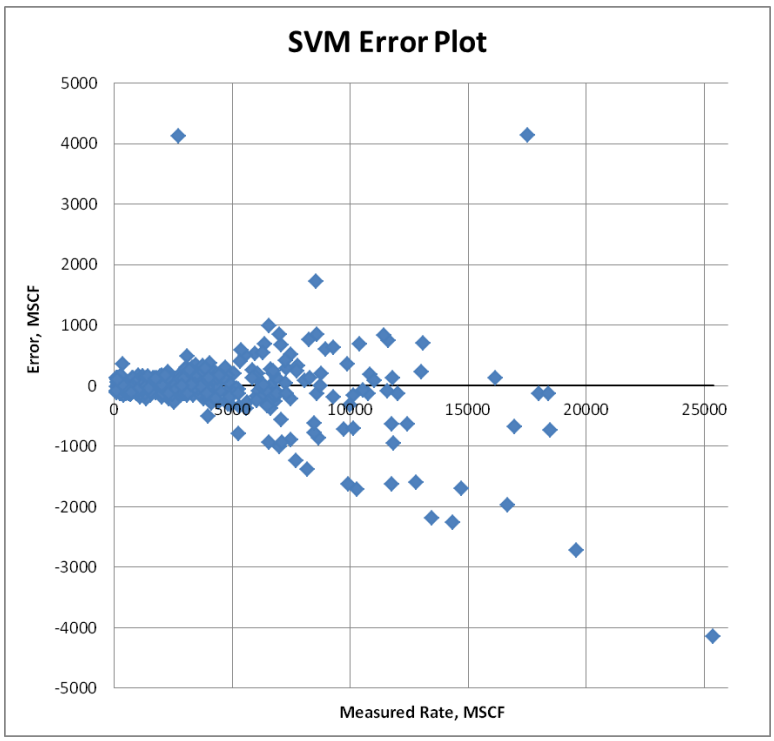

Figure 5-25: The estimation error using the SVM AI Method and the original data set.

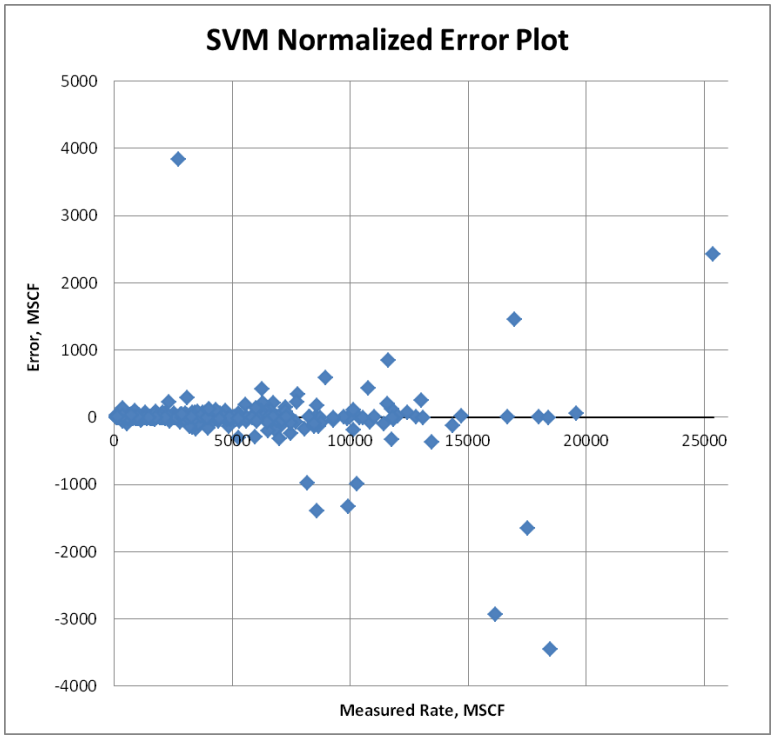

Figure 5-26: The estimation error using the SVM AI method and the normalized data set.

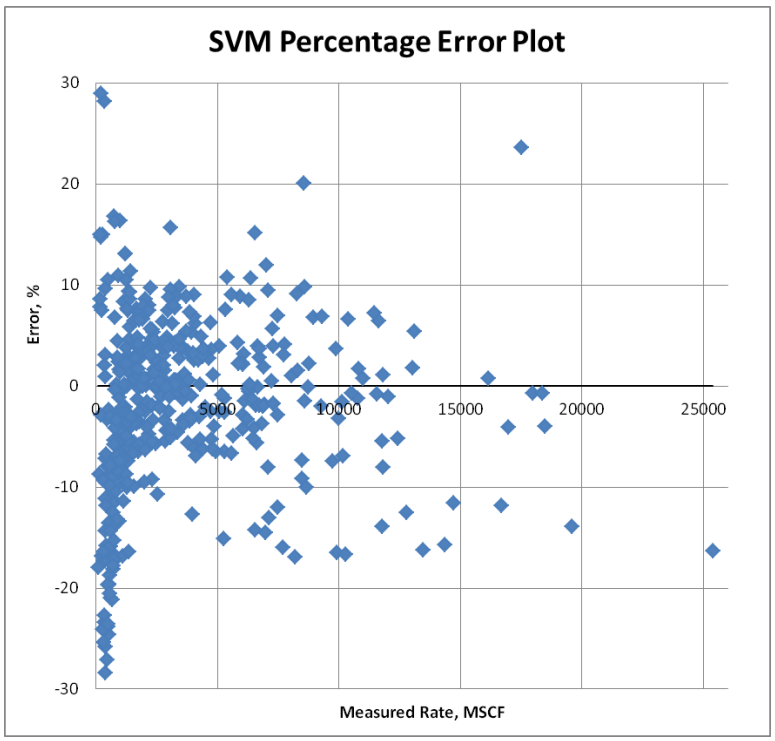

Figure 5-27: The estimation percentage error using the SVM AI Method and the original data set.

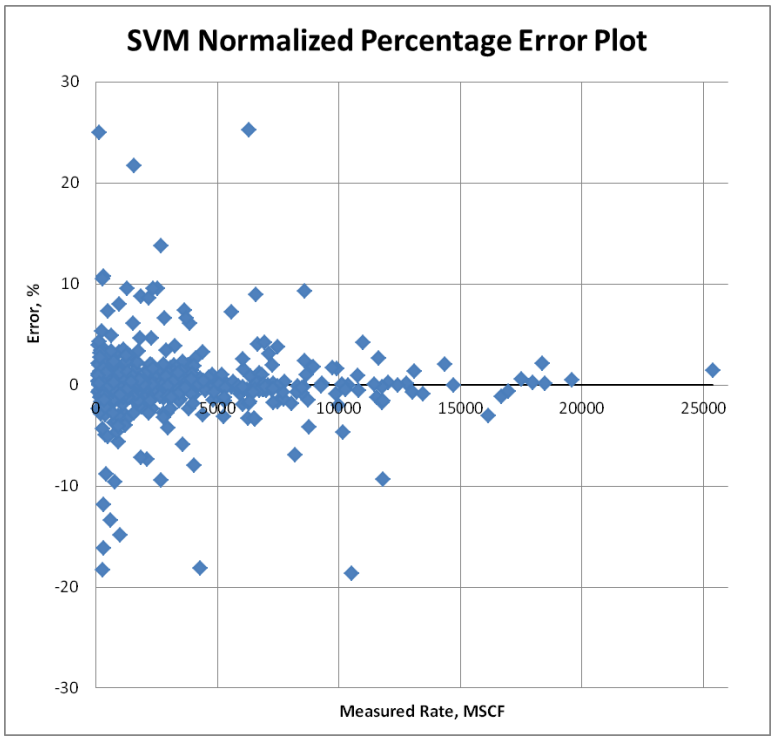

Figure 5-28: The estimation percentage error using the SVM AI method and the normalized data set.

Table 5-3: SVM Model Results

Method	SVM	
Set	Original	Normalized
Mean Absolute Error, MSCF	216.14	77.38
Mean Absolute Percentage Error, %	11.44	2.25
Correlation Coefficient, %	99.13	99.59

5.5. GRNN

Figures 5-29 and 5-30 show the crossplot between the measured rate and the rate estimated by the GRNN model. They show a good linear correlation between the two. Figure 5-30 shows that the normalized set has less dispersion than the non-normalized set. Similar observation is noted with the SVM method, which indicates the benefits of normalizing the data prior to training the model.

Figures 5-31 and 5-32 show the model error for both the non-normalized and the normalized sets respectively. We can observe that the non-normalized model results are more dispersed around the x-axis which indicates departure from the desired value. The figures also show a higher error in the model as the rate increases. However, as indicated by Figures 5-33 and 5-34, the percentage error decreases as the rate increases signifying that the model accuracy increases as the rate increases. Figures 5-33 and 5-34 also show less dispersion in the normalized data set results.

These figures also show that the GRNN model tends to underestimate the layer production rate.

Table 5-4 shows summary statistics of the GRNN model for both the original and the normalized data sets.

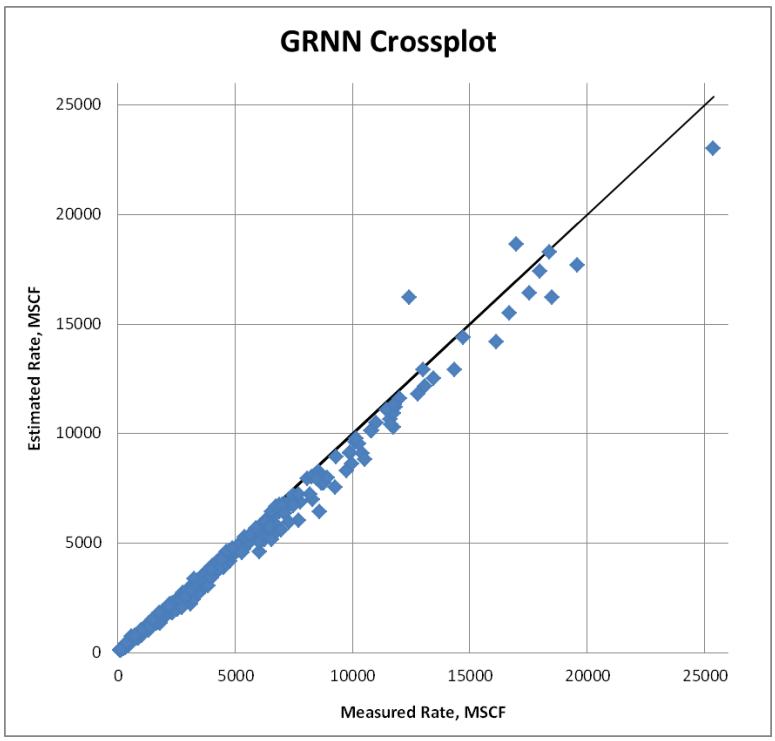

Figure 5-29: Crossplot of the measured and estimated rates using the GRNN AI method and the original data set.

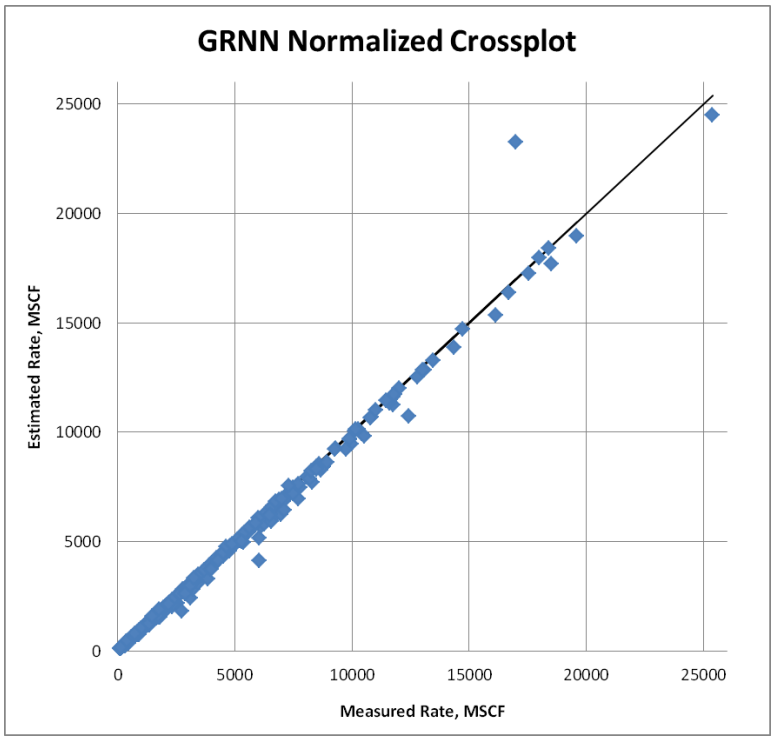

Figure 5-30: Crossplot of the measured and estimated rates using the GRNN AI method and the normalized data set.

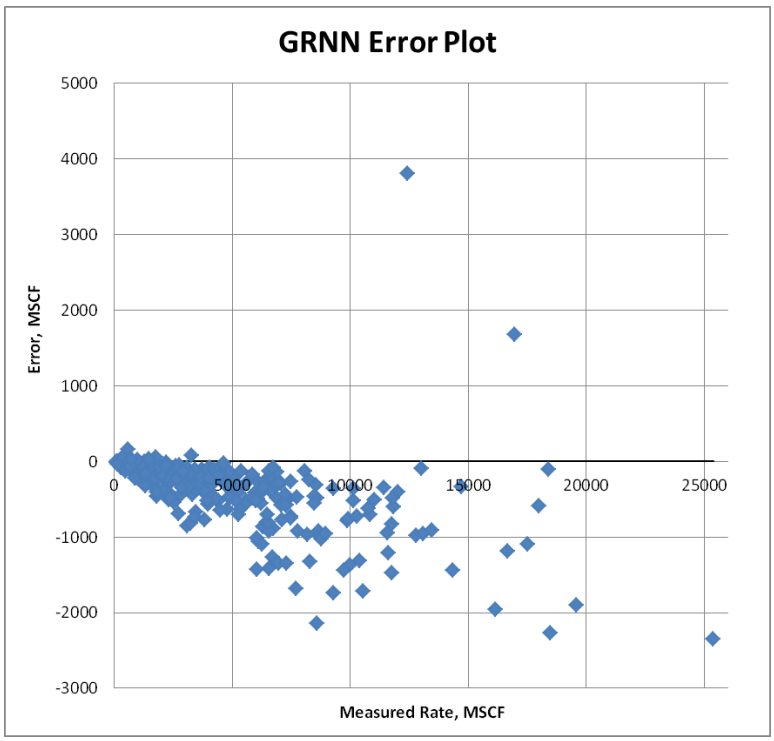

Figure 5-31: The estimation error using the GRNN AI method and the original data set.

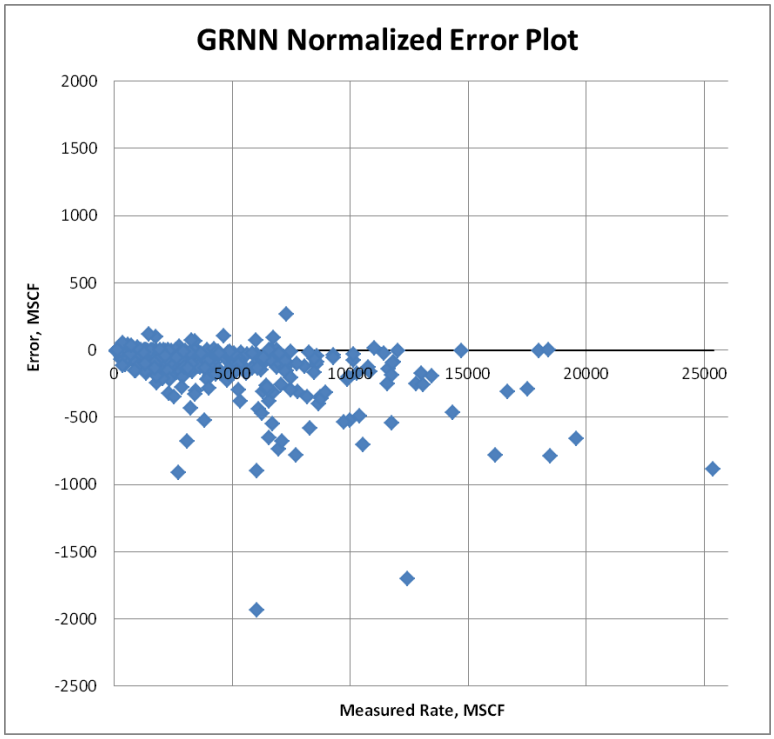

Figure 5-32: The estimation error using the GRNN AI method and the normalized data set.

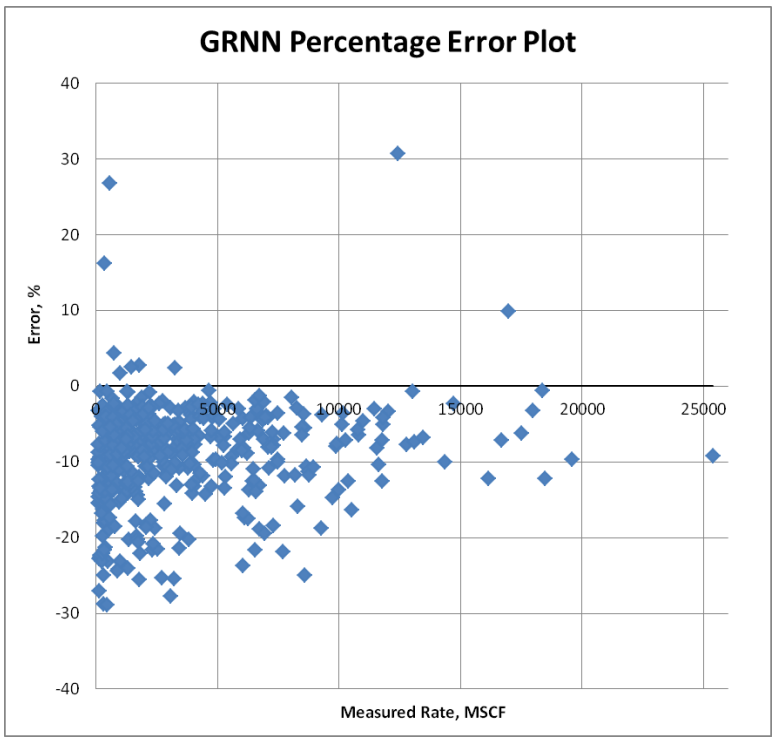

Figure 5-33: The estimation percentage rrror using the GRNN AI method and the original data set.

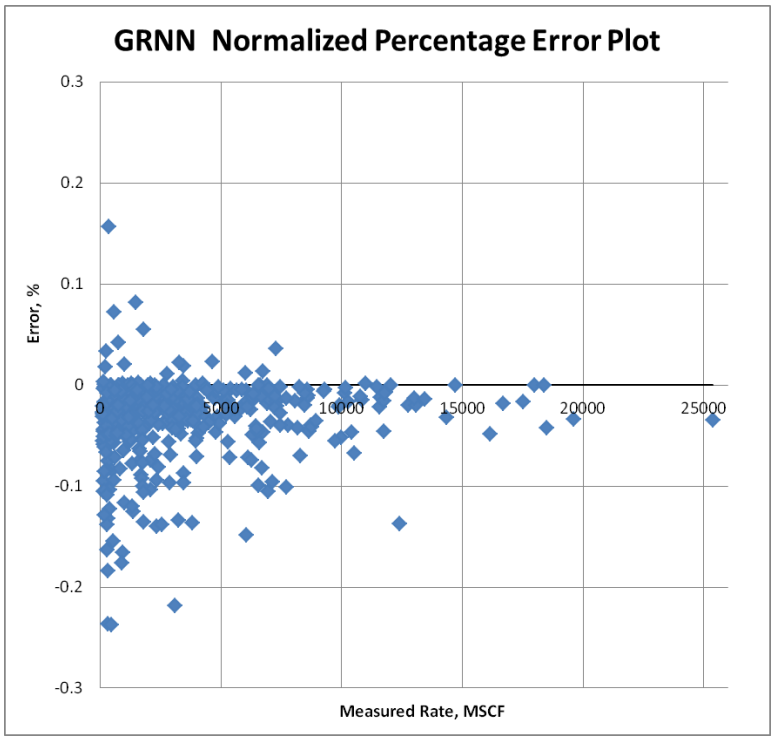

Figure 5-34: The estimation percentage error using the GRNN AI method and the normalized data set.

Table 5-4: GRNN Model Results

Method	GRNN	
Set	Original	Normalized
Mean Absolute Error, MSCF	292.19	113.82
Mean Absolute Percentage Error, %	9.40	3.65
Correlation Coefficient, %	99.51	99.57

Overall, it is clear that normalized data sets performed better than the non-normalized data set. Furthermore, the Support Vector Machine model has performed better than the General Regression Neural Networks model as shown by the lower mean absolute error and mean absolute percentage error as well as the higher correlation coefficient. Moreover, the crossplot the normalized SVM model shows less dispersion which means less overall error. It should be noted that the accuracy of both models are limited to the range of the training data. If need to use the model outside the training range arises, the model should be re-trained with new data points that widen the range.

5.6. CONCLUSIONS

From the discussions and the results presented in this study, the following conclusions can be drawn:

- GRNN and SVM methods show promising results for estimating production rate from each layer in a multi-layered gas reservoir as shown by the plots and the statistics.
- AI methods performed better than empirical approaches in this case since it adapted themselves to the data sets.
- Normalizing the input data sets has led to the improvement in the results, drastically in some cases such as SVM and GRNN.

- Combining data inputs and/or using the results of empirical formulas as inputs helps in guiding the artificial model to the desired results as demonstrated in this research.

5.7. RECOMMENDATIONS

- The accuracy of the model can be improved by quality checking and adding new data samples that covers wider ranges and different combinations.
- The developed model shouldn't be used outside the range of the training data. If need arises, it should be re-trained with new data points that widen the range.

APPENDICES

APPENDIX A: DATA

Table A-1: Collected Data

#	Reservoir Pressure	Perforation Thickness	Flowing Temperature	Flowing Pressure	Reservoir Thickness	Water Saturation	Porosity	Permeability	Gas Rate
	psi	ft	°F	psi	ft	fraction	fraction	mD	MSCF
1	2298	20	281.5	1665	23	0.204	0.099	9.77	4000
2	2368	30	264.6	2222	31	0.086	0.104	0.28	6046
3	2378	20	264.4	2229	21	0.085	0.084	7.95	358
4	2476	40	256.3	2346	41	0.083	0.104	8.70	2732
5	2930	9.6	254.4	2336	15	0.274	0.135	3.71	2915
6	2931	9.7	254.1	2337	11	0.127	0.184	24.30	1309
7	2932	15.7	254.0	2338	17	0.196	0.114	3.18	5350
8	2934	13.9	253.9	2340	20	0.210	0.119	1.98	1742
9	2940	10	251.0	2352	14	0.260	0.086	1.16	179
10	2970	10	259.0	2634	16	0.241	0.106	1.85	890
11	2973	13	259.9	2637	14	0.210	0.072	4.30	290
12	2974	15	261.2	2639	35	0.383	0.079	0.96	320
13	2979	4	261.7	2645	8	0.456	0.097	1.71	3830
14	2989	34	251.9	2642	35	0.240	0.092	22.54	312
15	2993	16	252.1	2645	17	0.234	0.108	2.05	291
16	2999	29	252.0	2648	36	0.302	0.057	2.03	913
17	3043	11	252.9	2785	33	0.327	0.083	23.19	303
18	3043	11	252.7	2677	33	0.327	0.083	94.20	515
19	3045	10	253.3	2786	16	0.221	0.112	1.27	461
20	3049	6	253.2	2681	8	0.179	0.139	2.46	2326
21	3050	13	253.4	2790	17	0.190	0.124	1.96	3090
22	3050	7	253.2	2682	11	0.185	0.122	3.12	2534
23	3060	11	253.8	2797	17	0.216	0.145	32.78	8581
24	3118	8	257.2	1913	9	0.153	0.064	27.95	1334
25	3127	10	254.0	1915	11	0.224	0.068	12.86	166
26	3195	10	254.8	2014	18	0.210	0.075	1.54	688
27	3195	10	254.4	1934	18	0.210	0.075	25.76	1285
28	3206	12.6	255.1	2018	17	0.123	0.117	15.89	8060
29	3207	16.9	254.9	1937	21	0.115	0.119	0.33	13026
30	3220	6	261.7	2031	21	0.217	0.063	2.94	1885
31	3220	6	262.4	1951	21	0.217	0.063	3.13	2221
32	3303	5	267.2	2469	6	0.440	0.055	25.71	1566
33	3304	8	267.2	2472	9	0.327	0.105	7.38	557

Table A-2: Collected Data—cont.

#	Reservoir Pressure	Perforation Thickness	Flowing Temperature	Flowing Pressure	Reservoir Thickness	Water Saturation	Porosity	Permeability	Gas Rate
34	psi	ft	°F	psi	ft	fraction	fraction	mD	MSCF
35	3314	48	267.3	2478	49	0.426	0.046	15.05	149
36	3351	11	268.0	2503	12	0.251	0.096	42.25	3646
37	3353	10	251.9	2956	11	0.216	0.091	0.12	397
38	3355	16	268.5	2526	20	0.457	0.054	11.31	187
39	3355	9.1	252.1	2958	9	0.428	0.053	9.35	6954
40	3356	4.2	252.8	2962	5	0.171	0.110	4.53	161
41	3357	8	268.8	2528	10	0.181	0.096	32.10	3871
42	3360	9.9	273.1	2533	11	0.448	0.069	9.57	1695
43	3530	5	263.6	2348	6	0.440	0.055	9.79	111
44	3530	5	263.7	2280	6	0.440	0.055	29.49	295
45	3531	8	263.6	2348	9	0.327	0.105	2.37	440
46	3531	8	263.9	2280	9	0.327	0.105	7.51	867
47	3580	4.9	264.5	2321	6	0.340	0.055	89.91	4037
48	3586	6.3	264.1	2326	8	0.165	0.102	2.49	4744
49	3586	6.7	263.5	2400	9	0.181	0.096	23.22	3089
50	3796	30	254.4	3143	31	0.234	0.078	0.74	6469
51	3796	30	255.0	3227	31	0.234	0.078	2.49	5288
52	3850	10	253.7	2795	14	0.212	0.109	17.70	3938
53	3851	10	253.8	2798	14	0.212	0.109	22.40	1091
54	3853	10	253.1	2798	11	0.183	0.124	2.62	1317
55	3854	10	253.3	2801	11	0.183	0.124	53.45	442
56	3859	10	254.1	3087	14	0.212	0.109	7.47	1137
57	3860	16	256.8	3187	18	0.168	0.125	9.77	2984
58	3860	16	257.0	3270	18	0.168	0.125	8.77	713
59	3870	44	256.4	3190	45	0.256	0.086	1.64	3121
60	3870	44	256.9	3274	45	0.256	0.086	2.33	3953
61	3880	30	255.9	3200	43	0.180	0.062	0.13	7469
62	3915	13	253.0	2826	19	0.145	0.164	9.89	7006
63	3916	13	253.1	2842	19	0.145	0.164	6.48	6388
64	3920	14	253.8	2828	26	0.205	0.120	13.05	8567
65	3921	14	253.8	2846	18	0.127	0.135	2.47	7095
66	3925	13	253.4	3141	19	0.145	0.164	6.23	4066
67	3929	6	254.2	3146	10	0.138	0.137	16.72	3364
68	3930	8	254.5	3147	18	0.232	0.118	2.50	804
69	3930	61.7	254.4	2847	63	0.360	0.074	17.80	1204
70	3930	4	256.2	2836	38	0.282	0.061	2.48	3704
71	3942	33	250.5	3537	34	0.270	0.093	19.18	803
72	3945	10	250.8	3544	11	0.184	0.116	7.24	6268

Table A-3: Collected Data—cont.

#	Reservoir Pressure	Perforation Thickness	Flowing Temperature	Flowing Pressure	Reservoir Thickness	Water Saturation	Porosity	Permeability	Gas Rate
	psi	ft	°F	psi	ft	fraction	fraction	mD	MSCF
73	4420	10.1	256.9	2989	10	0.260	0.050	4.38	5397
74	4426	5.2	258.1	2995	6	0.220	0.108	0.89	4416
75	4427	4.8	258.9	2996	6	0.217	0.126	3.34	748
76	4548	10	259.9	4059	13	0.165	0.143	29.72	6532
77	4553	30	259.9	4062	51	0.322	0.111	6.02	16143
78	4560	8.9	260.7	4072	25	0.235	0.098	3.49	4294
79	4630	10	252.3	4344	12	0.062	0.112	11.29	2070
80	4631	10	252.3	4346	11	0.068	0.092	20.70	1770
81	4632	3.8	252.4	4348	6	0.124	0.117	1.37	1810
82	4634	17	252.4	4349	18	0.136	0.130	4.03	580
83	4640	9.9	252.0	4359	11	0.045	0.056	0.84	1340
84	4722	20	254.7	4163	24	0.232	0.124	14.06	3447
85	4722	20	254.9	4168	24	0.232	0.124	13.65	3065
86	4775	13.9	248.8	4025	15	0.202	0.126	1.99	1188
87	4778	19.2	248.8	4027	21	0.188	0.108	8.58	8481
88	4780	10.8	249.0	4029	13	0.181	0.135	5.31	2650
89	4781	6.3	249.0	4030	8	0.224	0.103	14.85	1073
90	4782	10	256.2	4220	11	0.259	0.127	15.04	378
91	4782	10	256.2	4223	11	0.259	0.127	17.22	260
92	4783	9.8	248.9	4031	14	0.329	0.100	8.16	1243
93	4786	22	256.2	4222	23	0.226	0.097	12.25	4064
94	4786	22	256.3	4225	23	0.226	0.097	1.63	3006
95	4790	5.6	238.4	3524	7	0.337	0.116	33.40	1240
96	4790	30	256.4	4225	30	0.157	0.118	0.26	11624
97	4790	30	256.5	4228	30	0.157	0.118	106.03	8946
98	4793	8.1	239.3	3526	10	0.350	0.129	8.16	6648
99	4793	9.5	239.2	4268	12	0.321	0.134	0.81	2173
100	4795	9.5	239.8	4270	24	0.278	0.093	13.22	485
101	4795	10.9	239.7	3527	26	0.273	0.099	24.72	2189
102	4795	19	238.6	3646	34	0.299	0.104	57.15	6063
103	4797	20	257.2	4232	20	0.155	0.097	1.53	5581
104	4797	20	257.3	4235	20	0.155	0.097	8.49	3739
105	4800	10	259.0	4243	10	0.300	0.061	4.61	632
106	4800	10	259.0	4245	10	0.300	0.061	13.85	153
107	4870	13.2	248.0	3545	14	0.293	0.087	15.53	410
108	4871	25.1	247.6	3751	26	0.293	0.081	32.84	904
109	4871	25.3	248.2	3534	26	0.293	0.081	0.54	1421
110	4871	12.1	248.0	3547	14	0.293	0.072	3.51	432

Table A-4: Collected Data—cont.

#	Reservoir Pressure	Perforation Thickness	Flowing Temperature	Flowing Pressure	Reservoir Thickness	Water Saturation	Porosity	Permeability	Gas Rate
	psi	ft	°F	psi	ft	fraction	fraction	mD	MSCF
111	4872	6.2	247.5	3755	7	0.293	0.092	74.64	1532
112	4872	7.9	248.1	3538	10	0.293	0.079	8.15	3409
113	4873	10	247.9	3549	12	0.293	0.070	4.88	4399
114	4873	8	248.2	3540	10	0.293	0.066	16.20	8256
115	4873	10.1	247.6	3756	11	0.293	0.066	4.77	4441
116	4873	6.2	248.2	3550	9	0.293	0.074	1.91	4888
117	4874	4.8	249.1	3542	16	0.293	0.094	1.88	2335
118	4874	4.5	249.3	3552	15	0.293	0.095	0.45	1937
119	4874	4.6	248.6	3757	16	0.293	0.094	1.95	708
120	4880	13	250.5	3546	14	0.292	0.122	36.19	11449
121	4880	13	250.5	3556	14	0.292	0.122	0.58	6745
122	4880	13	250.6	3763	14	0.292	0.122	0.92	852
123	4881	30	253.6	4296	33	0.265	0.098	2.62	4404
124	4881	30	253.9	4308	33	0.265	0.098	6.25	2352
125	4881	30	254.5	4467	33	0.265	0.098	1.48	240
126	4916	34	242.1	3586	35	0.299	0.087	0.58	266
127	4916	34	241.5	3719	35	0.299	0.087	0.88	522
128	4922	5.4	242.2	4369	6	0.162	0.158	22.28	743
129	4923	12	241.7	3726	13	0.224	0.153	3.03	1133
130	4927	4.7	243.2	3596	6	0.423	0.114	2.92	256
131	4928	5.4	242.7	3731	6	0.303	0.169	7.88	3897
132	4928	9.7	243.1	4373	11	0.350	0.133	3.63	1550
133	4930	9.6	243.3	3598	14	0.176	0.090	3.58	359
134	4940	16.2	251.7	4477	17	0.169	0.115	9.44	4062
135	4944	10	255.4	4350	12	0.211	0.113	1.50	970
136	4944	10	255.5	4361	12	0.211	0.113	1.00	2096
137	4944	10	255.8	4521	12	0.211	0.113	5.67	1767
138	4944	33.8	251.7	4479	36	0.163	0.141	4.35	18495
139	4944	50	251.8	4554	52	0.166	0.131	1.78	10529
140	4947	20	285.5	3735	23	0.204	0.099	13.22	6992
141	4950	9.7	287.0	3739	14	0.247	0.139	3.22	10158
142	4950	15	252.2	4565	16	0.143	0.123	5.69	1743
143	4950	40	255.4	4352	43	0.182	0.143	20.34	25385
144	4950	40	255.5	4363	43	0.182	0.143	38.61	19602
145	4950	40	255.9	4522	43	0.182	0.143	3.20	9742
146	4969	12.4	252.6	4743	13	0.285	0.112	9.92	1364
147	4972	23.6	252.8	4745	27	0.282	0.074	9.67	371
148	5004	10	253.2	4585	11	0.271	0.109	14.91	2844

Table A-5: Collected Data—cont.

#	Reservoir Pressure	Perforation Thickness	Flowing Temperature	Flowing Pressure	Reservoir Thickness	Water Saturation	Porosity	Permeability	Gas Rate
	psi	ft	°F	psi	ft	fraction	fraction	mD	MSCF
149	5005	10.9	254.0	4587	13	0.253	0.109	3.40	679
150	5012	43.3	289.7	4129	44	0.374	0.066	13.11	352
151	5012	46.7	290.2	4479	48	0.374	0.092	4.73	137
152	5013	10.9	289.8	4135	12	0.373	0.081	6.38	3271
153	5014	60	289.5	3980	61	0.374	0.081	7.79	7116
154	5014	20.1	290.3	4485	21	0.373	0.066	3.43	1458
155	5022	11.8	291.1	4493	13	0.372	0.081	6.13	6049
156	5022	14.1	290.6	4143	15	0.372	0.092	13.96	12419
157	5022	14.7	290.3	3991	16	0.372	0.092	0.28	16976
158	5023	13.1	291.0	4495	14	0.372	0.092	2.56	1001
159	5024	9	256.4	4192	25	0.152	0.113	3.54	2045
160	5024	9	256.5	4235	25	0.152	0.128	14.68	1328
161	5024	8.2	291.1	4496	9	0.371	0.066	31.59	739
162	5024	18.8	290.4	3993	19	0.371	0.066	1.03	2180
163	5024	19.9	290.5	4145	21	0.371	0.066	0.85	1778
164	5025	7.3	291.7	4498	8	0.371	0.081	15.27	2887
165	5025	10.2	292.0	4148	11	0.371	0.081	0.36	7292
166	5025	10.9	291.1	3996	12	0.371	0.081	4.40	9277
167	5026	8.6	291.6	4001	10	0.371	0.092	32.65	573
168	5031	28.3	254.2	4803	29	0.296	0.110	29.26	1013
169	5032	15.9	246.7	3976	31	0.331	0.094	18.98	2068
170	5032	20	248.6	4029	30	0.298	0.081	4.86	960
171	5035	8	254.8	4810	13	0.419	0.079	1.63	1800
172	5046	9.5	255.8	4821	12	0.333	0.123	16.04	3230
173	5083	7.8	256.6	4301	11	0.145	0.135	1.99	1465
174	5083	8	256.4	4133	11	0.145	0.135	30.27	3254
175	5085	8.1	256.5	4134	10	0.126	0.138	6.50	2825
176	5085	12.2	256.7	4302	14	0.159	0.123	2.21	1799
177	5089	21.2	256.6	4136	25	0.141	0.127	46.70	10137
178	5089	21.8	256.9	4304	26	0.143	0.125	9.15	5286
179	5090	12	256.1	4631	13	0.171	0.107	5.91	701
180	5090	8.8	257.2	4139	10	0.159	0.132	16.03	1219
181	5090	8.2	257.5	4307	9	0.152	0.144	22.13	389
182	5092	9.9	256.8	4678	12	0.239	0.080	28.44	3983
183	5095	6.3	257.8	4143	10	0.157	0.123	0.51	2849
184	5095	7	258.0	4311	10	0.152	0.125	6.57	1367
185	5096	22.9	257.1	4679	24	0.244	0.096	29.14	1062
186	5101	10	262.2	4439	13	0.185	0.112	38.18	2692

Table A-6: Collected Data—cont.

#	Reservoir Pressure	Perforation Thickness	Flowing Temperature	Flowing Pressure	Reservoir Thickness	Water Saturation	Porosity	Permeability	Gas Rate
	psi	ft	°F	psi	ft	fraction	fraction	mD	MSCF
187	5104	10	262.2	4406	13	0.185	0.112	67.99	3727
188	5107	10	249.8	4069	13	0.242	0.131	20.11	2423
189	5111	20	262.9	4449	63	0.184	0.064	3.70	1332
190	5113	10	250.1	4072	11	0.139	0.163	1.98	6893
191	5114	20	262.8	4419	63	0.184	0.064	9.31	1786
192	5114	10	250.4	4073	12	0.178	0.122	6.61	1413
193	5119	15.9	250.0	4054	17	0.211	0.123	56.62	1057
194	5121	7	250.7	4076	12	0.232	0.111	31.87	9298
195	5125	10	250.1	4058	12	0.296	0.134	0.24	6827
196	5125	4	253.2	4080	14	0.320	0.060	11.41	1802
197	5126	6	253.3	4081	13	0.196	0.114	1.90	900
198	5130	9.9	251.7	4068	10	0.427	0.163	1.73	183
199	5163	20	264.2	4500	21	0.218	0.116	16.81	1408
200	5166	20	264.0	4477	21	0.218	0.116	5.23	2023
201	5171	27	264.2	4482	56	0.319	0.100	1.60	17525
202	5171	50	264.3	4504	56	0.319	0.100	29.23	11586
203	5249	21.9	264.3	4966	22	0.264	0.087	2.12	2268
204	5256	49.9	264.3	4969	51	0.420	0.048	22.69	175
205	5271	4.2	262.0	4658	8	0.252	0.065	3.76	110
206	5272	10	262.6	4752	15	0.237	0.089	34.16	2048
207	5272	10	262.4	4650	15	0.237	0.089	13.00	2106
208	5272	5.8	262.0	4658	8	0.228	0.113	1.17	2120
209	5272	11	262.4	4659	12	0.226	0.100	27.36	2385
210	5272	11	262.1	4630	15	0.237	0.089	8.45	2480
211	5275	5	262.8	4654	6	0.306	0.072	10.27	2547
212	5275	7.3	263.5	4757	12	0.289	0.081	5.88	798
213	5275	10	263.0	4663	15	0.305	0.078	2.35	2322
214	5275	10	262.5	4635	15	0.305	0.078	53.15	3569
215	5278	10	263.3	4665	12	0.225	0.065	18.00	153
216	5278	10	262.6	4638	12	0.225	0.065	1.08	165
217	5279	5	263.3	4667	8	0.289	0.050	16.42	210
218	5279	5	262.6	4640	8	0.289	0.050	2.93	962
219	5281	10	243.6	5007	25	0.152	0.105	5.52	267
220	5287	10	264.5	2949	11	0.302	0.105	24.85	473
221	5297	20	248.3	4538	35	0.251	0.118	8.31	7725
222	5297	20	248.6	4885	35	0.251	0.118	1.13	1705
223	5300	10	264.5	2955	10	0.328	0.097	3.33	18389
224	5300	30	252.9	4588	34	0.266	0.095	9.78	3023

Table A-7: Collected Data—cont.

#	Reservoir Pressure	Perforation Thickness	Flowing Temperature	Flowing Pressure	Reservoir Thickness	Water Saturation	Porosity	Permeability	Gas Rate
	psi	ft	°F	psi	ft	fraction	fraction	mD	MSCF
225	5313	8.6	266.3	5029	10	0.210	0.099	15.43	1268
226	5318	16.6	266.5	5033	18	0.187	0.088	0.75	3864
227	5325	20	250.2	4563	21	0.202	0.073	3.23	1382
228	5325	20	250.3	4907	21	0.202	0.073	8.44	404
229	5326	7	263.5	4709	8	0.221	0.119	2.12	3256
230	5326	7	263.5	4691	8	0.221	0.119	7.65	2511
231	5330	10.8	267.4	5046	12	0.338	0.079	17.32	2352
232	5333	29	264.2	4717	30	0.221	0.110	13.72	481
233	5333	29	263.2	4714	30	0.221	0.110	4.76	1331
234	5333	29	264.3	4722	30	0.221	0.110	5.86	650
235	5333	29	263.4	4696	30	0.221	0.110	2.10	2210
236	5337	2.6	264.4	4725	6	0.176	0.143	4.75	762
237	5337	7.5	263.4	4720	11	0.145	0.177	11.25	6908
238	5337	5	264.3	4726	7	0.109	0.216	6.15	5962
239	5338	9.9	264.9	4829	13	0.141	0.176	1.07	4851
240	5338	6.6	264.7	4727	8	0.109	0.184	4.14	404
241	5339	7.4	265.1	4831	9	0.119	0.163	4.05	1141
242	5339	4.7	264.7	4728	7	0.130	0.172	10.26	2464
243	5340	9.1	265.4	4729	28	0.170	0.110	3.39	834
244	5340	20.5	263.6	4722	39	0.156	0.127	2.41	3783
245	5340	28	264.6	4730	49	0.154	0.136	5.73	9880
246	5340	28	263.6	4704	49	0.154	0.136	17.02	13104
247	5346	20	244.5	5069	26	0.178	0.113	3.87	6560
248	5350	24.9	244.7	5073	28	0.148	0.128	4.99	7713
249	5374	16	252.2	4865	18	0.206	0.120	16.60	3784
250	5374	16	251.9	4714	18	0.206	0.120	32.74	5304
251	5374	16	251.9	4711	18	0.206	0.120	14.57	5593
252	5377	40	254.2	4645	44	0.232	0.112	2.51	11769
253	5381	30	251.1	4609	32	0.278	0.094	7.70	3311
254	5383	12	251.7	4875	15	0.203	0.082	4.32	756
255	5383	12	251.6	4725	15	0.203	0.082	43.46	203
256	5384	8	251.4	4727	10	0.396	0.052	6.28	298
257	5385	20	251.2	4614	21	0.187	0.107	3.33	2313
258	5390	10	255.4	4661	32	0.217	0.061	0.93	1560
259	5391	15	251.2	4620	16	0.148	0.126	28.29	10774
260	5391	15	251.4	4962	16	0.148	0.126	1.78	6451
261	5393	10	251.4	4623	13	0.265	0.084	2.44	6652
262	5393	10	251.2	4964	13	0.265	0.084	51.28	3226

Table A-8: Collected Data—cont.

#	Reservoir Pressure	Perforation Thickness	Flowing Temperature	Flowing Pressure	Reservoir Thickness	Water Saturation	Porosity	Permeability	Gas Rate
	psi	ft	°F	psi	ft	fraction	fraction	mD	MSCF
263	5400	40	252.8	4625	41	0.264	0.075	2.12	3534
264	5400	40	251.9	4966	41	0.264	0.075	5.41	140
265	5432	16	252.0	4781	23	0.171	0.121	22.32	920
266	5436	19.9	252.1	4939	21	0.121	0.128	2.04	8656
267	5436	20.8	252.0	4773	22	0.122	0.127	41.72	16688
268	5436	24.1	252.1	4785	25	0.128	0.130	6.34	12779
269	5439	22.2	252.8	4776	23	0.303	0.106	3.31	849
270	5443	13	244.6	4704	15	0.217	0.133	21.46	1565
271	5443	13	262.9	4928	15	0.217	0.133	3.54	726
272	5443	13	242.5	4571	15	0.217	0.133	24.79	1379
273	5444	12	254.2	4797	14	0.133	0.174	12.68	2585
274	5444	12	254.0	4782	14	0.133	0.174	0.96	3590
275	5448	20	244.8	4708	24	0.208	0.112	66.09	3623
276	5448	20	263.1	4932	24	0.208	0.112	1.26	1733
277	5448	20	242.6	4575	24	0.208	0.112	0.16	4777
278	5456	13.9	263.6	4940	15	0.368	0.066	2.59	1596
279	5457	18.6	243.5	4582	20	0.364	0.063	2.92	8484
280	5459	17.2	263.7	4942	19	0.383	0.044	36.43	4942
281	5459	14.7	243.4	4584	15	0.316	0.076	12.40	11825
282	5460	40	246.4	4716	41	0.324	0.075	94.94	13455
283	5463	20	259.4	4911	30	0.249	0.127	10.28	5208
284	5475	5.5	245.8	4557	6	0.357	0.149	2.65	2022
285	5476	7.4	246.5	4558	22	0.348	0.071	5.98	381
286	5510	6.3	264.6	4941	7	0.233	0.106	8.64	806
287	5511	11.6	264.5	4908	12	0.230	0.102	46.76	1214
288	5511	6.7	264.6	4943	7	0.242	0.102	16.62	538
289	5512	7	264.6	4943	9	0.273	0.130	15.79	2178
290	5512	8.4	264.5	4910	10	0.273	0.130	6.55	4247
291	5514	10	264.7	4945	12	0.274	0.137	1.07	4114
292	5514	10	264.6	4912	12	0.274	0.137	1.39	7075
293	5516	6	264.8	4948	7	0.226	0.122	2.13	3143
294	5516	7.7	264.7	4914	9	0.209	0.125	26.07	7312
295	5522	6.3	265.7	4920	7	0.343	0.121	21.80	2369
296	5523	7.4	265.7	4956	8	0.344	0.117	3.73	170
297	5547	28.7	253.5	5103	34	0.301	0.143	3.03	7784
298	5550	14	261.7	4973	14	0.200	0.215	2.69	1235
299	5560	10	261.9	4977	11	0.322	0.099	22.62	7248
300	5567	11.8	248.7	4633	12	0.272	0.096	17.25	2791

Table A-9: Collected Data—cont.

#	Reservoir Pressure	Perforation Thickness	Flowing Temperature	Flowing Pressure	Reservoir Thickness	Water Saturation	Porosity	Permeability	Gas Rate
	psi	ft	°F	psi	ft	fraction	fraction	mD	MSCF
301	5568	11.7	248.9	4634	12	0.205	0.128	1.01	947
302	5574	4.5	249.2	4640	6	0.314	0.102	21.96	4814
303	5575	5.5	249.3	4641	6	0.270	0.173	1.74	1119
304	5581	40	256.7	5136	62	0.331	0.074	5.31	126
305	5599	20	252.0	4806	21	0.165	0.154	1.09	2823
306	5631	14	257.7	5189	15	0.324	0.117	21.22	332
307	5638	20	257.8	5196	24	0.256	0.122	5.05	956
308	5644	9.7	258.1	5204	11	0.289	0.156	13.13	2923
309	5648	5.3	258.7	5209	8	0.416	0.134	9.89	2800
310	5684	8	254.7	4890	9	0.181	0.128	6.84	1009
311	5685	8	254.7	4891	9	0.232	0.086	54.03	1242
312	5687	7.1	254.8	4893	9	0.221	0.098	2.98	603
313	5689	12.6	254.9	4894	15	0.153	0.124	6.82	6350
314	5690	20.1	245.1	5291	24	0.296	0.139	25.87	4775
315	5691	14.7	245.4	5308	17	0.223	0.171	11.11	6735
316	5692	4.7	246.0	5311	13	0.284	0.106	25.83	563
317	5692	3.6	246.7	5296	12	0.295	0.097	6.29	270
318	5696	8.7	255.4	4902	10	0.119	0.151	4.11	2782
319	5700	6.4	255.9	4906	12	0.211	0.131	36.79	5099
320	5712	12	247.5	5329	13	0.130	0.121	3.02	301
321	5712	12	248.1	5315	13	0.130	0.121	8.99	104
322	5778	55	248.7	5387	58	0.194	0.123	28.10	9975
323	5778	55	249.3	5380	58	0.194	0.123	0.01	6316
324	5783	10	251.4	5399	13	0.206	0.099	8.18	873
325	5783	10	251.5	5392	13	0.206	0.099	14.46	949
326	5790	30	252.0	5404	31	0.300	0.082	18.54	1335
327	5790	30	252.1	5399	31	0.300	0.082	27.52	673
328	5932	4.8	251.0	4697	6	0.304	0.091	3.52	1368
329	5932	4.5	251.1	4698	6	0.221	0.143	8.22	3946
330	5932	5.1	250.5	5025	7	0.229	0.135	2.78	4313
331	5932	10.8	251.3	4524	12	0.267	0.107	32.22	4638
332	5933	7.5	252.0	4699	10	0.189	0.107	3.11	412
333	5934	4.8	251.8	5027	7	0.309	0.123	10.07	1270
334	5935	9.2	251.3	5028	12	0.332	0.110	1.89	295
335	5935	13.2	252.2	4700	16	0.323	0.115	9.97	1128
336	5993	7.6	249.9	5413	9	0.365	0.122	6.25	1211
337	5993	8.2	250.0	5402	9	0.365	0.122	5.89	1357
338	5994	8.4	250.1	5046	9	0.365	0.122	10.58	1786

Table A-10: Collected Data—cont.

#	Reservoir Pressure	Perforation Thickness	Flowing Temperature	Flowing Pressure	Reservoir Thickness	Water Saturation	Porosity	Permeability	Gas Rate
	psi	ft	°F	psi	ft	fraction	fraction	mD	MSCF
339	5995	10.5	250.3	5404	13	0.394	0.085	24.01	120
340	5996	14.7	250.2	5415	16	0.363	0.103	7.41	913
341	5997	12.8	250.4	5406	15	0.202	0.165	12.81	3579
342	5997	14.4	250.4	5050	16	0.212	0.159	28.15	4316
343	5997	10.4	250.3	5417	13	0.175	0.169	7.50	2802
344	6000	17.6	251.2	5053	22	0.383	0.063	1.91	414
345	6027	12	255.0	5121	13	0.171	0.107	9.51	169
346	6027	6.9	254.6	4784	8	0.162	0.115	20.39	1529
347	6027	6.8	254.3	4588	8	0.162	0.115	16.41	2271
348	6029	4.8	255.1	5124	6	0.291	0.100	2.42	138
349	6029	5.3	254.3	4590	7	0.327	0.092	66.85	2607
350	6030	15.5	254.7	4786	16	0.264	0.086	0.50	1573
351	6031	11.1	255.1	5125	12	0.182	0.106	10.76	1298
352	6033	17	254.3	4591	19	0.183	0.103	29.50	14711
353	6033	15.9	254.7	4788	18	0.195	0.104	12.01	6641
354	6040	7.9	256.0	5137	9	0.209	0.138	5.82	2424
355	6040	12	254.8	4796	13	0.205	0.128	18.91	4234
356	6040	12	253.9	4597	13	0.205	0.128	1.98	6909
357	6048	9	261.1	5693	13	0.432	0.068	1.21	3332
358	6069	20	256.0	5068	25	0.234	0.075	7.36	871
359	6069	20	255.7	4967	25	0.234	0.075	19.87	2770
360	6091	8.9	252.7	5134	11	0.445	0.072	32.01	7471
361	6091	10.6	252.7	5489	13	0.407	0.079	3.71	5091
362	6091	11.2	252.9	5507	13	0.407	0.079	1.53	3428
363	6093	15.1	252.9	5137	16	0.245	0.100	1.68	823
364	6097	6	250.4	5603	7	0.360	0.075	23.10	2250
365	6097	6	250.3	5646	7	0.360	0.075	26.37	3264
366	6100	10	253.0	5145	11	0.199	0.199	25.07	17989
367	6100	12	253.1	5498	13	0.214	0.191	5.23	10834
368	6100	12	253.3	5516	13	0.214	0.191	0.89	7315
369	6100	15	250.9	5605	16	0.196	0.105	0.14	328
370	6100	15	250.9	5648	16	0.196	0.105	0.48	1048
371	6110	40	254.2	5505	42	0.302	0.077	4.04	782
372	6110	40	254.3	5521	42	0.302	0.077	7.59	542
373	6111	15	251.3	5616	17	0.292	0.058	5.68	117
374	6111	15	251.2	5657	17	0.292	0.058	25.18	907
375	6131	20	262.3	4554	21	0.309	0.096	0.47	1671
376	6167	8	252.0	5707	9	0.467	0.061	1.03	491

Table A-11: Collected Data—cont.

#	Reservoir Pressure	Perforation Thickness	Flowing Temperature	Flowing Pressure	Reservoir Thickness	Water Saturation	Porosity	Permeability	Gas Rate
	psi	ft	°F	psi	ft	fraction	fraction	mD	MSCF
377	6173	35.8	252.1	5676	37	0.176	0.131	5.76	7471
378	6173	38.6	252.0	5708	41	0.188	0.128	2.12	14350
379	6187	8.1	254.1	5736	9	0.275	0.085	10.06	3439
380	6187	8.5	254.1	5706	9	0.275	0.085	9.89	2785
381	6221	10	265.0	5789	14	0.259	0.095	11.22	2397
382	6221	10	264.7	5733	14	0.259	0.095	3.69	5842
383	6298	10	267.3	5861	12	0.186	0.099	8.83	1306
384	6298	10	267.3	5793	12	0.186	0.099	22.86	1766
385	6304	23.5	267.5	5797	24	0.159	0.097	13.58	6237
386	6305	30	267.6	5865	30	0.157	0.102	16.09	4512
387	6316	7.9	268.7	5879	9	0.323	0.083	3.55	2135
388	6317	10.3	268.2	5810	11	0.290	0.077	4.00	6077
389	6326	6.4	261.3	5596	8	0.245	0.060	24.65	11011
390	6326	7	261.5	5538	8	0.241	0.067	4.83	11805
391	6326	8.2	261.1	5844	9	0.232	0.078	0.22	6009
392	6391	16	265.0	5907	18	0.168	0.125	60.14	736
393	6391	16	264.7	5657	18	0.168	0.125	5.17	1962
394	6391	16	264.7	5591	18	0.168	0.125	4.56	2954
395	6396	17.5	264.9	5596	18	0.094	0.114	2.91	5645
396	6396	19.5	264.9	5661	20	0.094	0.114	1.24	3693
397	6397	21.7	265.1	5912	23	0.098	0.111	16.30	1943
398	6406	5.2	265.8	5673	6	0.320	0.037	12.78	3188
399	6407	7.7	265.7	5606	9	0.214	0.070	24.93	5871
400	6407	8.6	265.9	5923	10	0.200	0.086	17.17	2014
401	6407	4.9	265.8	5674	6	0.136	0.122	18.74	287
402	6408	17	254.0	5021	19	0.261	0.126	40.28	1332
403	6410	21.4	265.9	5924	35	0.175	0.061	2.31	110
404	6410	22.3	265.7	5607	36	0.173	0.063	11.14	591
405	6415	5	254.2	5027	9	0.382	0.110	2.58	770
406	6422	4.6	254.3	5032	7	0.177	0.155	23.50	746
407	6423	7.4	254.3	5033	9	0.128	0.220	33.62	6554
408	6461	4.4	262.0	6106	11	0.212	0.070	5.35	444
409	6462	5.6	262.0	6107	11	0.275	0.101	0.83	206
410	6467	7.9	262.1	6111	9	0.213	0.131	0.80	947
411	6469	12	262.1	6113	13	0.205	0.123	89.51	1120
412	6473	14.5	262.1	6115	16	0.260	0.084	5.95	8772
413	6474	10.2	262.5	6119	12	0.253	0.129	2.49	4047
414	6475	5.3	263.0	6120	7	0.238	0.120	2.00	198

Table A-12: Collected Data—cont.

#	Reservoir Pressure	Perforation Thickness	Flowing Temperature	Flowing Pressure	Reservoir Thickness	Water Saturation	Porosity	Permeability	Gas Rate
	psi	ft	°F	psi	ft	fraction	fraction	mD	MSCF
415	6475	5	252.2	5860	7	0.194	0.104	2.01	3032
416	6476	4	252.5	5885	6	0.178	0.126	4.09	2675
417	6476	10	252.3	6004	13	0.185	0.112	26.47	2292
418	6476	5	252.7	5861	7	0.170	0.118	0.78	963
419	6489	12.7	253.6	5896	14	0.262	0.067	10.54	206
420	6490	4.6	253.5	5898	6	0.163	0.122	31.34	1871
421	6490	9	252.7	5874	10	0.196	0.100	5.06	2176
422	6490	10	253.2	6018	53	0.172	0.066	25.24	1264
423	6557	10	254.0	5934	11	0.203	0.129	0.50	1159
424	6558	20	254.6	6082	21	0.218	0.116	1.15	594
425	6558	20	254.7	5961	21	0.218	0.116	11.38	1199
426	6558	10	254.4	5936	11	0.228	0.093	23.70	387
427	6561	9	254.7	6086	10	0.293	0.083	5.14	2978
428	6561	10	254.3	5939	11	0.300	0.084	16.75	8604
429	6561	10.5	254.8	5965	12	0.290	0.086	2.61	6305
430	6564	15	254.8	6088	17	0.255	0.105	6.43	1746
431	6564	16	254.3	5941	18	0.246	0.116	15.83	7256
432	6564	16.2	255.0	5968	18	0.239	0.117	0.63	4730
433	6568	26	255.3	6091	33	0.355	0.108	0.35	186
434	6568	23.1	255.8	5970	30	0.370	0.096	2.39	107
435	6568	24	254.8	5944	31	0.364	0.099	16.98	404
436	6671	12.3	252.9	6122	18	0.247	0.178	7.52	10286
437	6672	20	251.2	6322	67	0.273	0.134	6.17	8192
438	6672	20	252.2	6179	67	0.273	0.134	5.68	9909
439	6672	7.7	253.5	6124	51	0.281	0.121	17.94	789
440	6679	13.5	244.8	6360	18	0.358	0.114	7.57	549
441	6679	14.6	245.1	6335	19	0.352	0.114	24.71	1595
442	6680	9	245.2	6337	11	0.128	0.230	5.49	8735
443	6681	6.4	245.8	6339	14	0.275	0.118	2.66	1794
444	6681	16.5	244.9	6362	24	0.219	0.158	35.72	10405
445	6703	12	246.3	6359	13	0.130	0.121	27.30	1106
446	6703	12	246.6	6387	13	0.130	0.121	19.41	147
447	6708	4	246.8	6393	6	0.231	0.055	54.56	121
448	6734	6	250.7	6487	21	0.208	0.126	3.36	6576
449	6734	6.9	250.6	6515	22	0.208	0.126	14.81	8299
450	6734	8.5	250.5	6525	23	0.208	0.126	45.63	3458
451	6736	14	251.7	6489	15	0.422	0.072	1.74	329
452	6736	13.1	251.8	6516	14	0.475	0.074	3.51	1699

Table A-13: Collected Data—cont.

#	Reservoir Pressure	Perforation Thickness	Flowing Temperature	Flowing Pressure	Reservoir Thickness	Water Saturation	Porosity	Permeability	Gas Rate
	psi	ft	°F	psi	ft	fraction	fraction	mD	MSCF
453	6766	10	255.2	6419	16	0.409	0.104	11.92	304
454	6766	10	255.3	6274	16	0.409	0.104	1.84	612
455	6766	10	255.3	6206	16	0.409	0.104	100.81	1321
456	6767	20	253.2	6516	21	0.202	0.073	3.08	283
457	6767	20	253.0	6541	21	0.202	0.073	6.07	873
458	6771	10	255.3	6424	12	0.268	0.142	20.69	389
459	6771	10	255.4	6279	12	0.268	0.142	3.67	1793
460	6771	10	255.3	6211	12	0.268	0.142	68.27	3408
461	6772	24.8	247.6	6457	29	0.180	0.137	5.20	1867
462	6775	43.9	247.3	6424	48	0.197	0.124	10.68	11768
463	6776	11.1	248.2	6430	12	0.171	0.115	29.24	1107
464	6776	30.2	247.8	6461	31	0.212	0.106	2.34	3435
465	6779	30	255.6	6429	36	0.264	0.114	11.74	742
466	6779	30	255.6	6284	36	0.264	0.114	8.66	3983
467	6779	30	255.6	6215	36	0.264	0.114	3.31	5265
468	6782	10	249.9	6436	13	0.206	0.099	10.06	741
469	6782	10	250.0	6470	13	0.206	0.099	9.98	407
470	6784	9	250.1	6438	10	0.247	0.068	1.65	360
471	6784	9	250.2	6473	10	0.247	0.068	6.35	258
472	6785	10	256.5	6293	12	0.240	0.110	7.82	944
473	6785	10	256.1	6223	12	0.240	0.110	26.57	3576
474	6790	30	250.5	6441	31	0.300	0.082	9.32	527
475	6790	30	250.4	6476	31	0.300	0.082	2.81	366
476	6828	30	254.2	6571	32	0.278	0.094	44.87	591
477	6828	30	254.0	6593	32	0.278	0.094	2.04	1713
478	6833	20	254.5	6617	21	0.187	0.107	33.83	501
479	6833	20	254.4	6577	21	0.187	0.107	3.66	1139
480	6833	20	254.3	6598	21	0.187	0.107	0.62	1647
481	6840	15	254.9	6625	16	0.148	0.126	12.44	3439
482	6840	15	254.8	6584	16	0.148	0.126	42.20	6126
483	6840	15	254.8	6605	16	0.148	0.126	3.04	6716
484	6843	10	254.8	6628	13	0.265	0.084	26.58	1213
485	6843	10	254.8	6587	13	0.265	0.084	0.38	2082
486	6843	10	254.7	6608	13	0.265	0.084	5.42	2422
487	6845	7.4	254.9	6630	8	0.230	0.120	30.54	125
488	6845	8.3	254.7	6610	9	0.223	0.121	3.72	1648
489	6880	10	252.1	6026	27	0.317	0.072	4.39	957
490	6960	10	253.4	6083	10	0.394	0.138	23.45	12023

APPENDIX B: DATA ANALYSIS:

B-1: STATISTICS

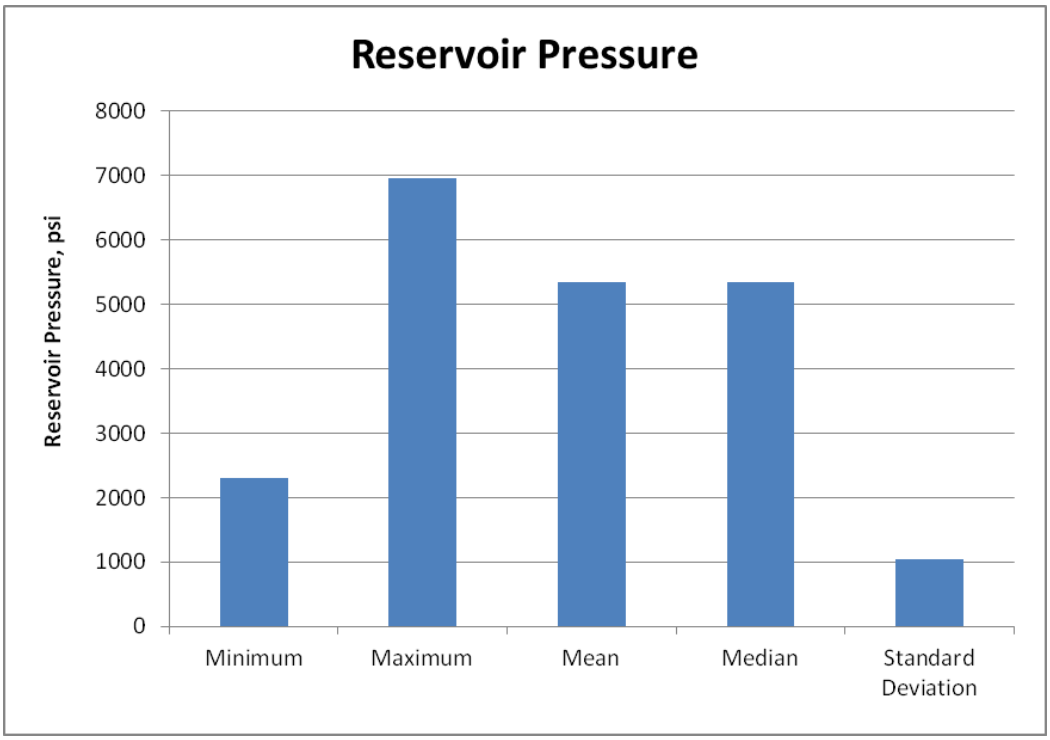

Figure B-1: Reservoir Pressure Statistical Analysis

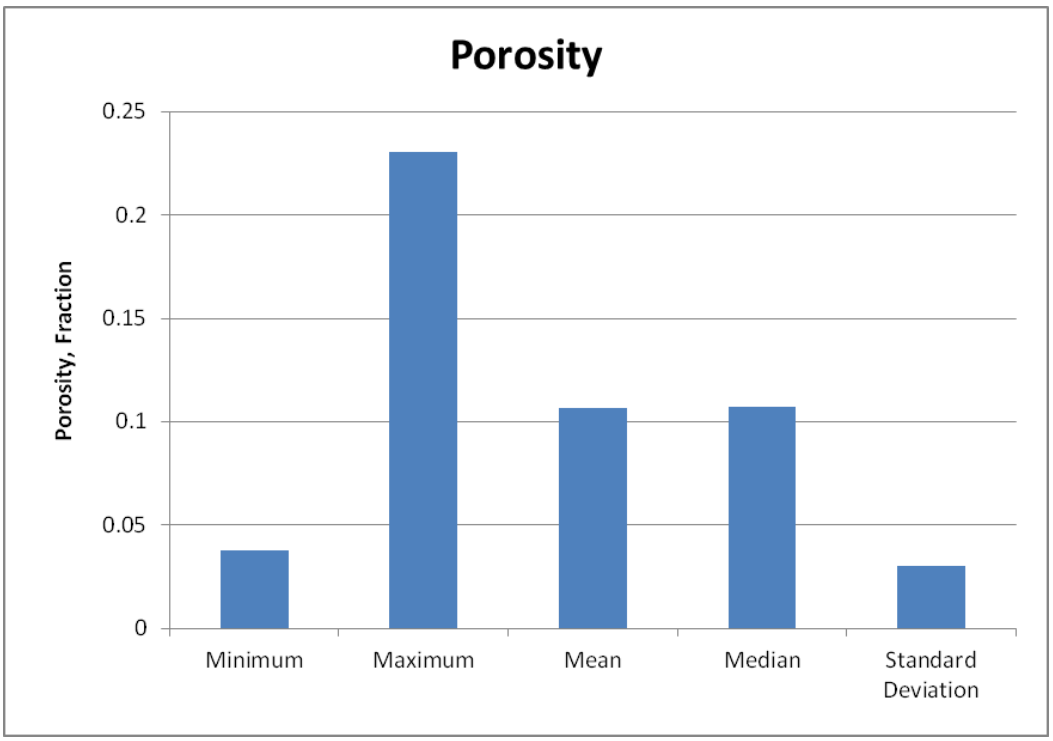

Figure B-2: Porosity Statistical Analysis

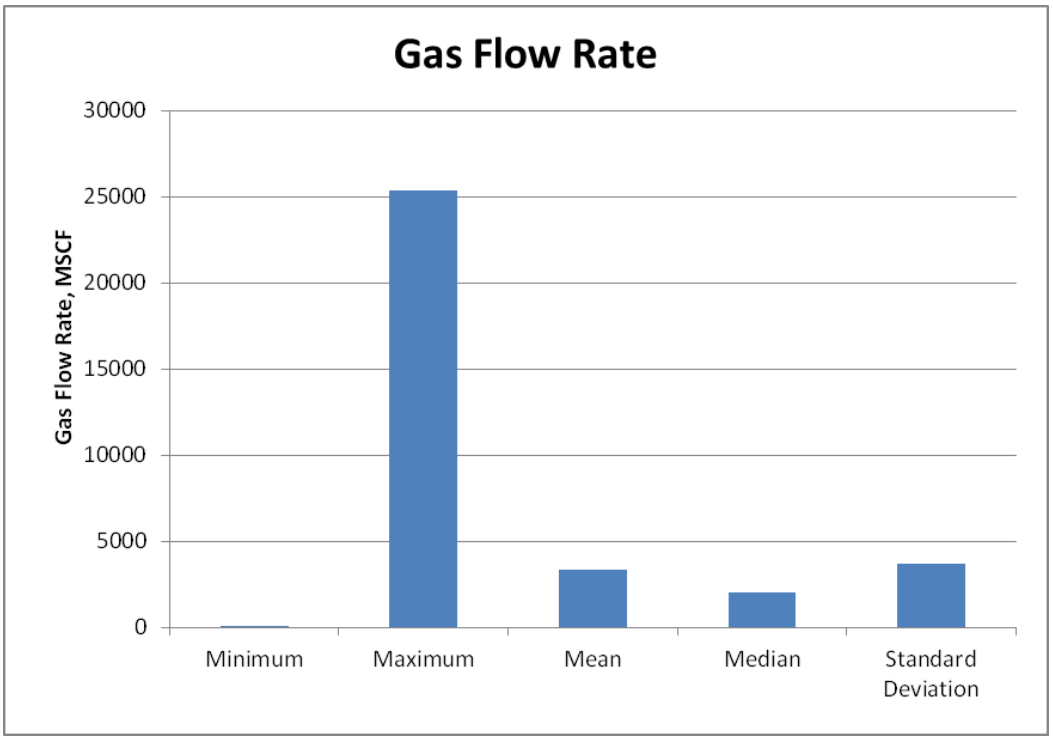

Figure B-3: Gas Flow Rate Statistical Analysis

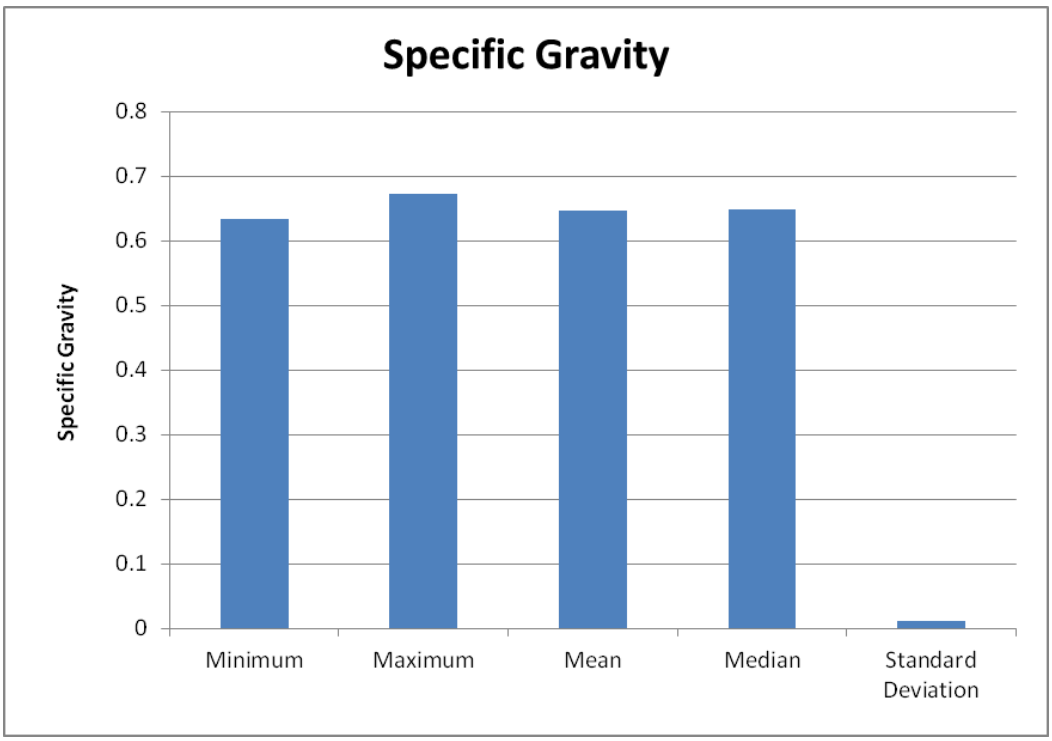

Figure B-4: Specific Gravity Statistical Analysis

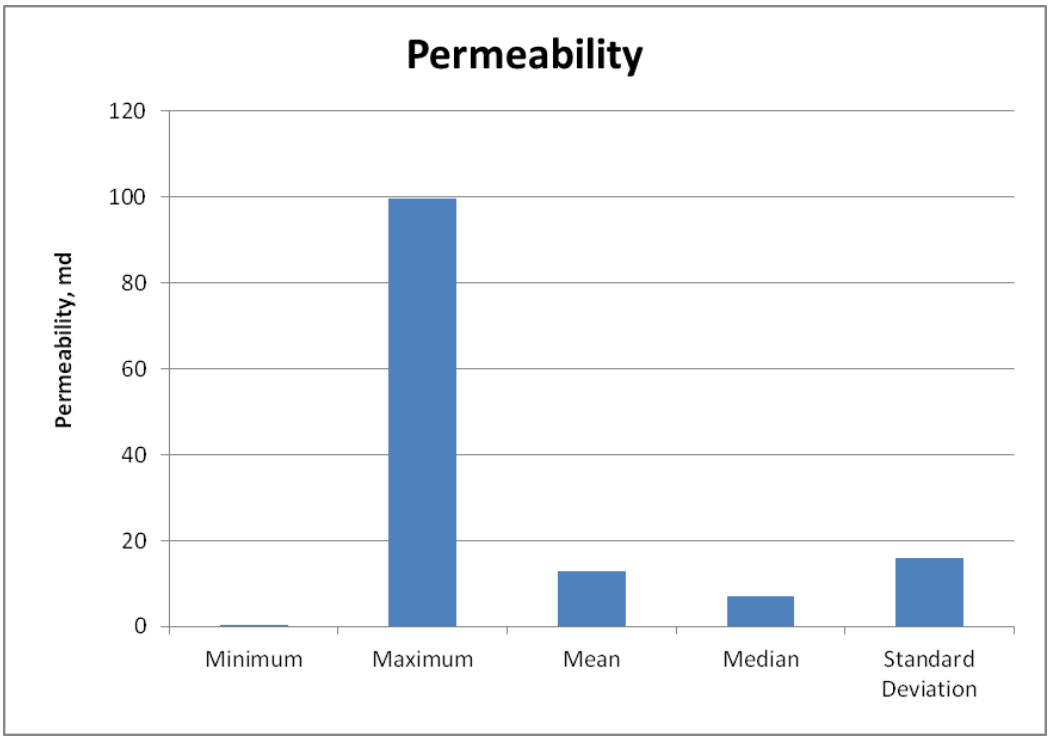

Figure B-5: Permeability Statistical Analysis

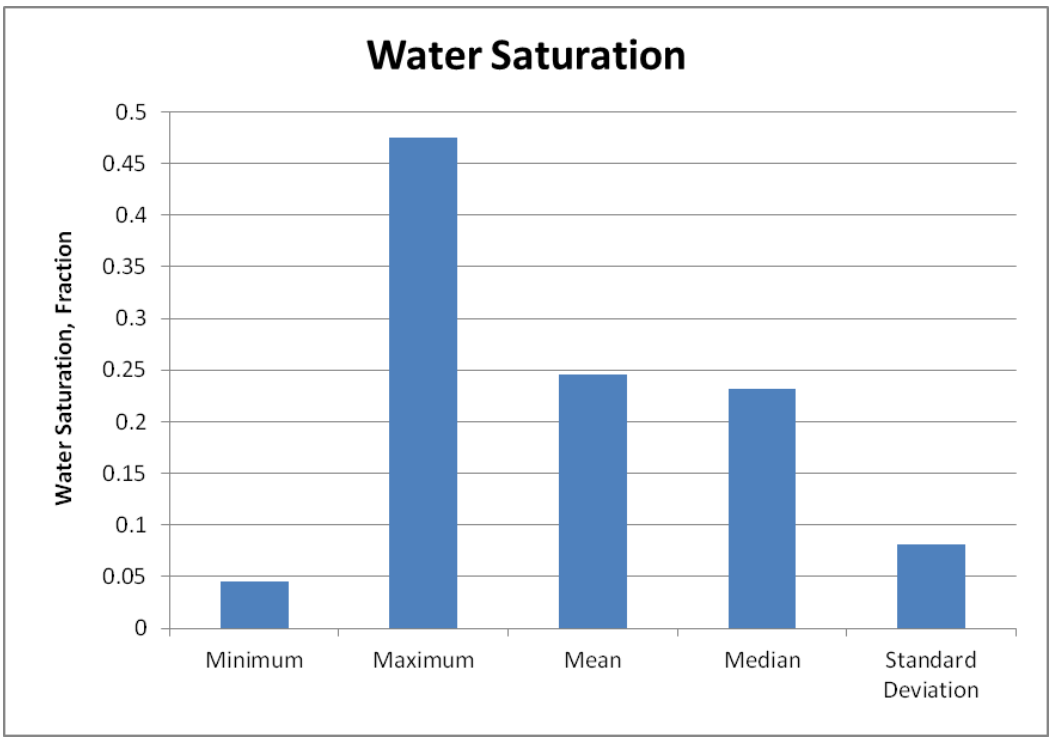

Figure B-6: Water Saturation Statistical Analysis

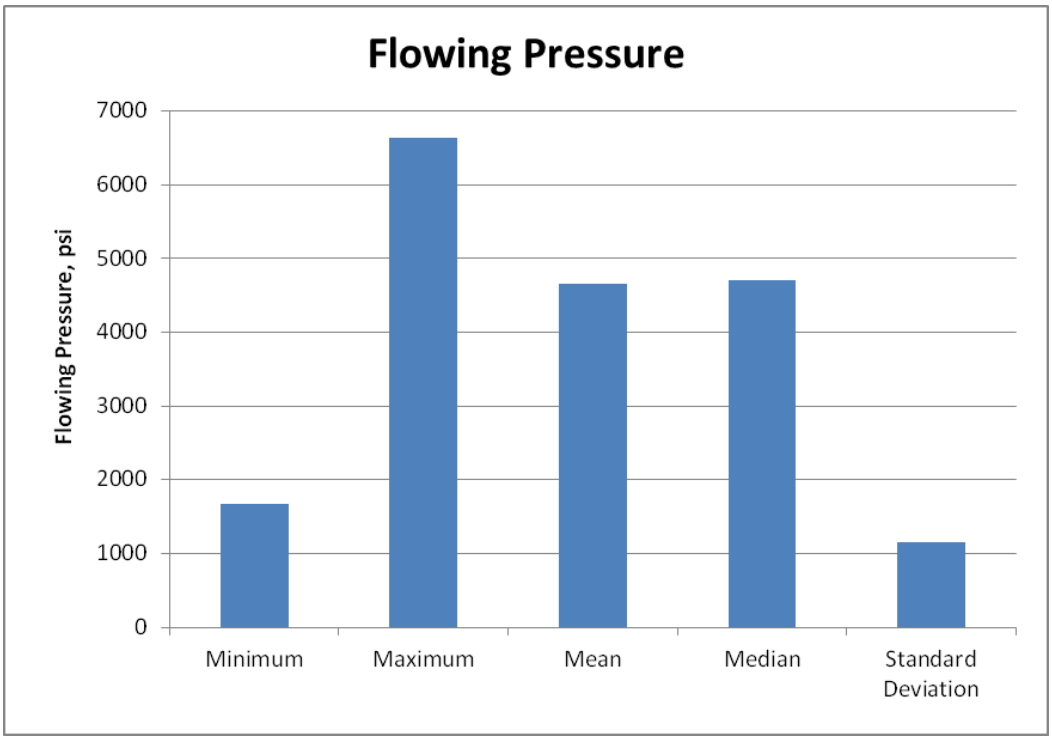

Figure B-7: Flowing Pressure Statistical Analysis

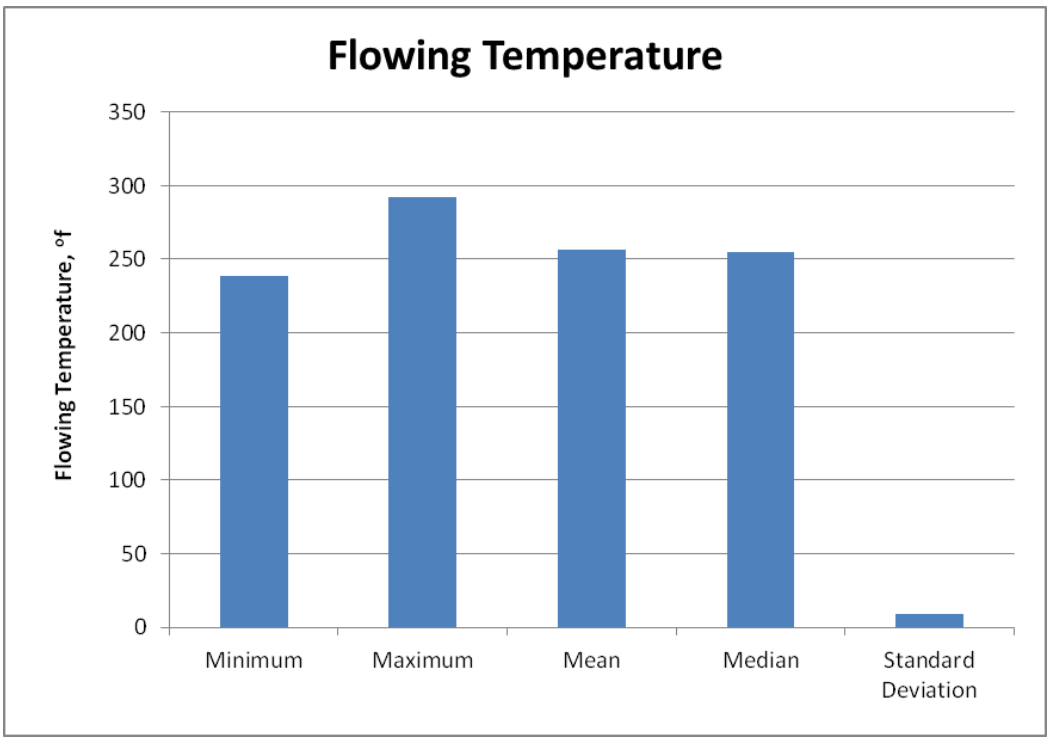

Figure B-8: Flowing Temperature Statistical Analysis

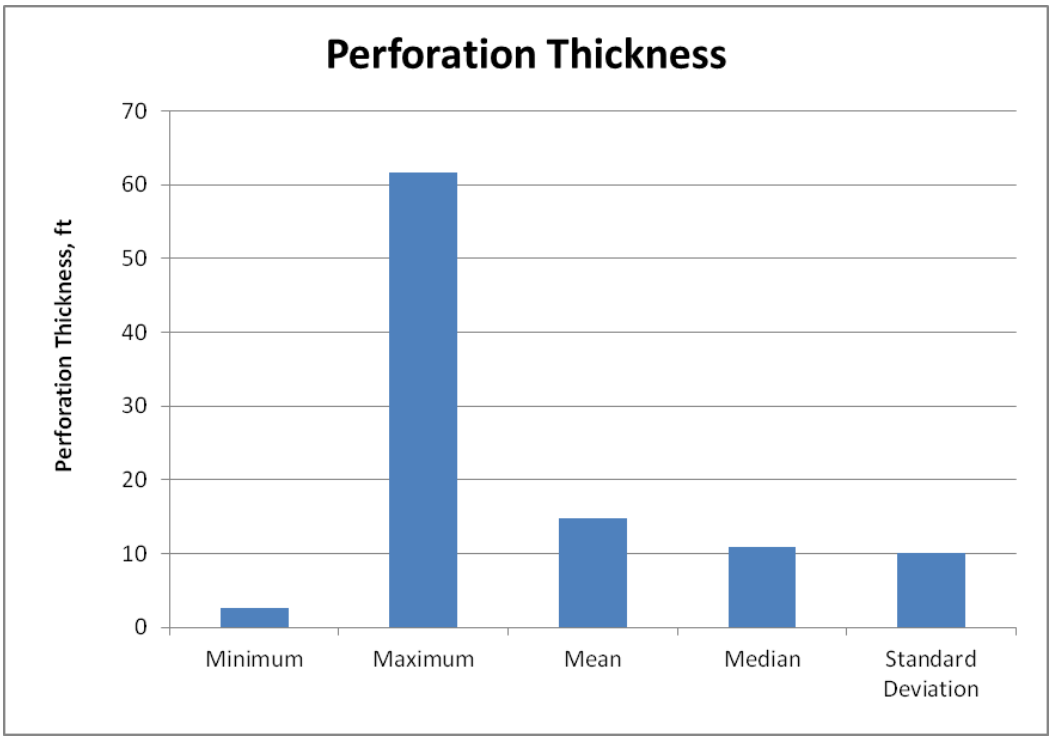

Figure B-9: Perforation Thickness Statistical Analysis

B-2: HISTOGRAMS

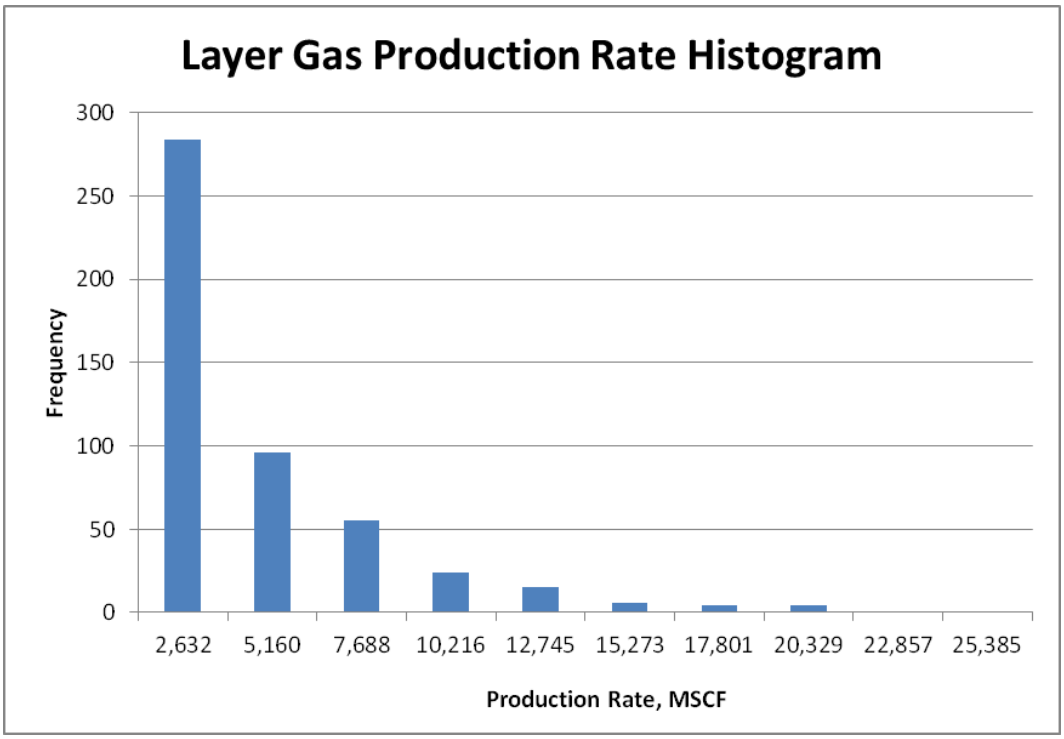

Figure B-10: Layer Gas Production Rate Histogram

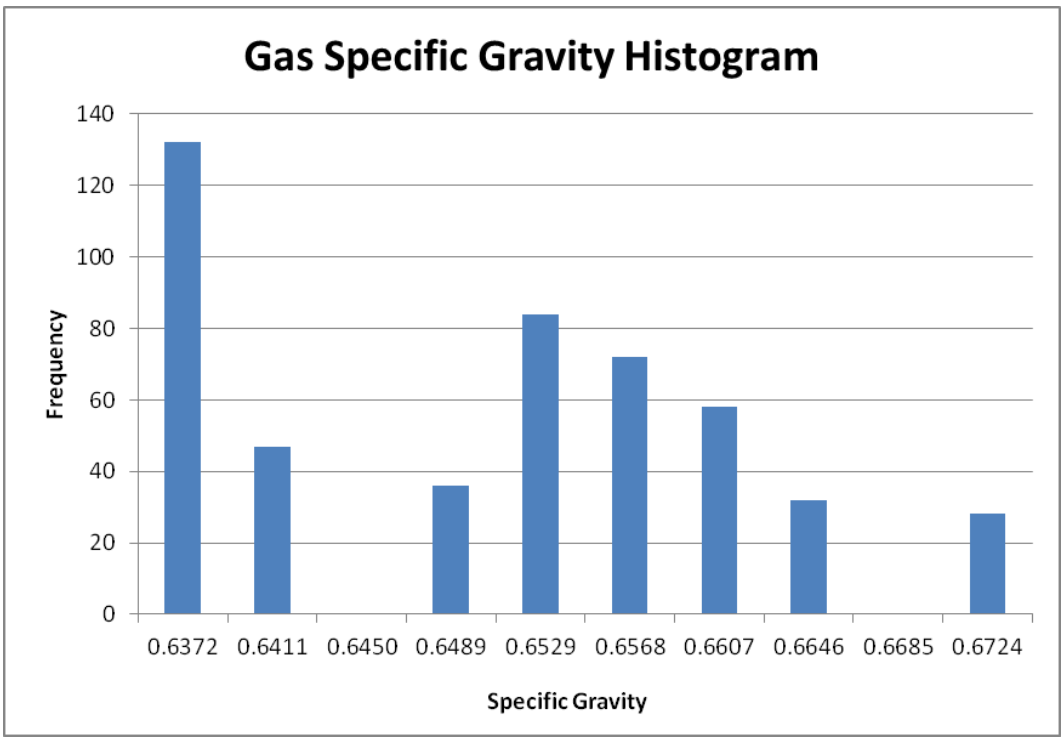

Figure B-11: Gas Specific Gravity Histogram

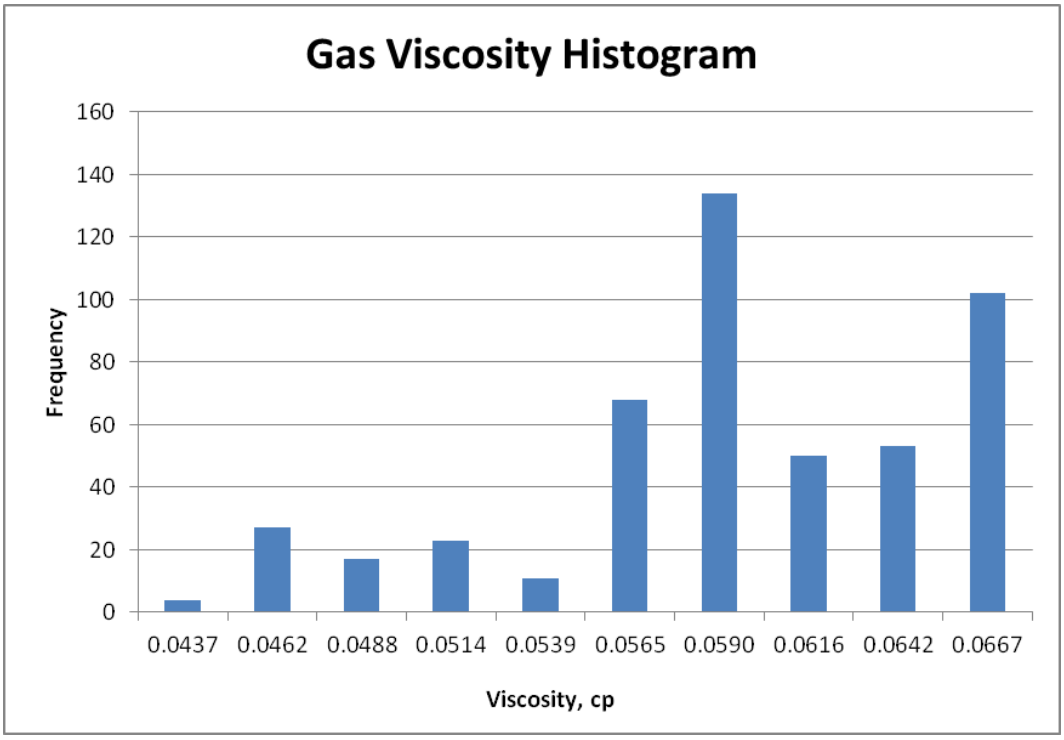

Figure B-12: Gas Viscosity Histogram

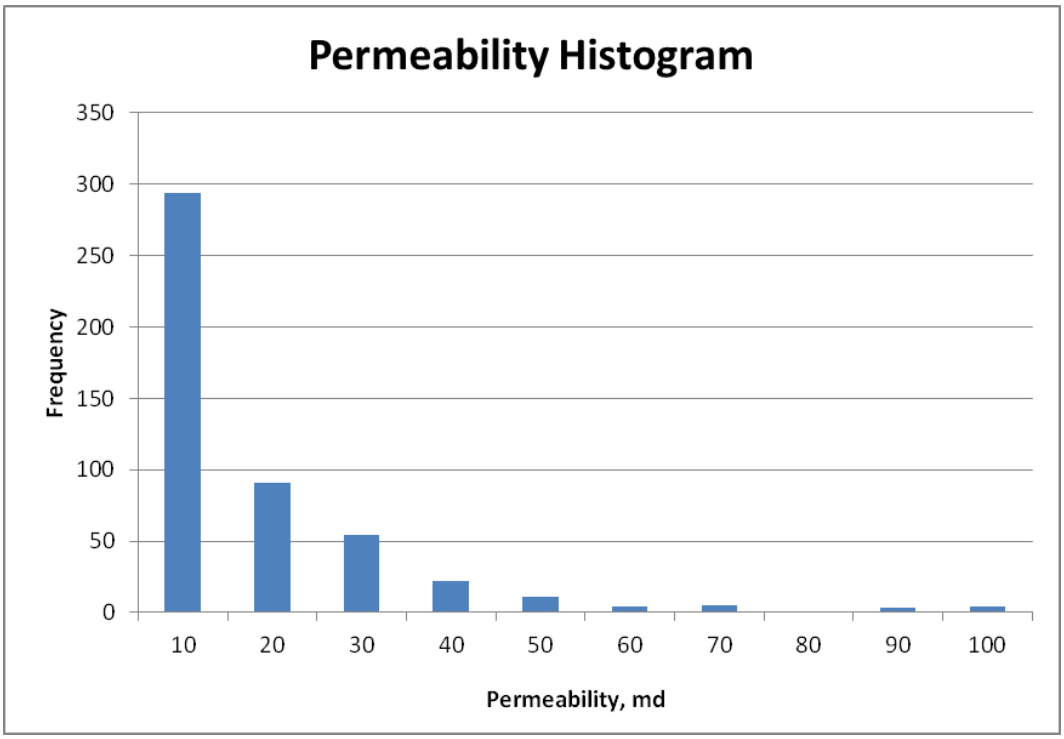

Figure B-13: Permeability Histogram

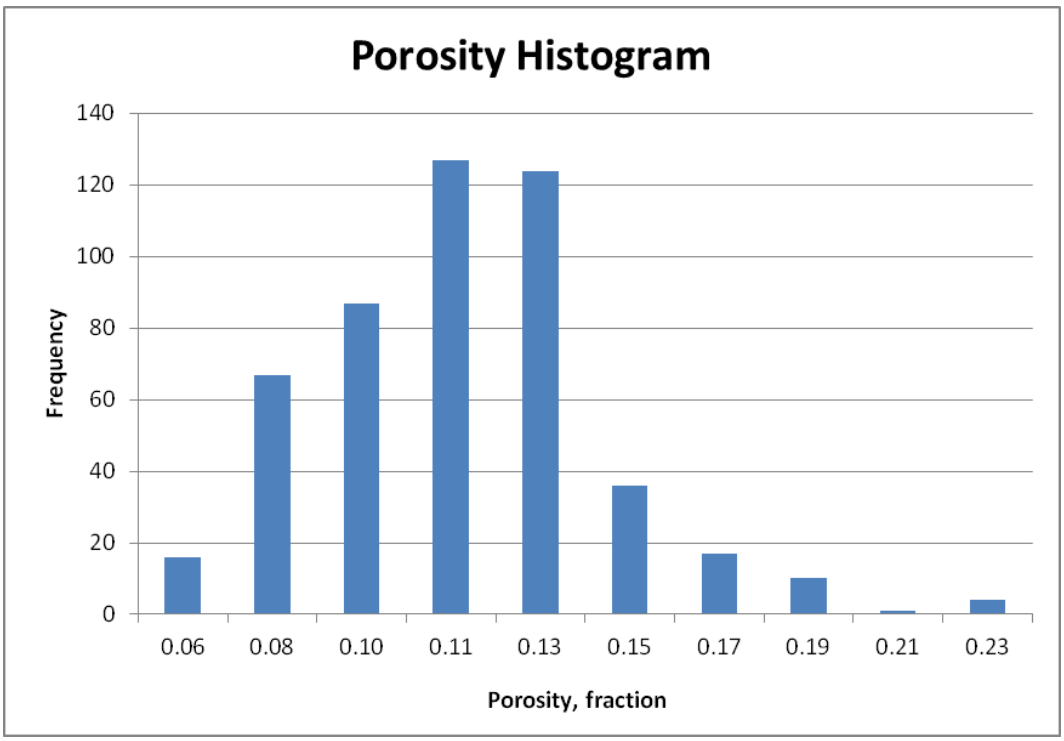

Figure B-14: Porosity Histogram

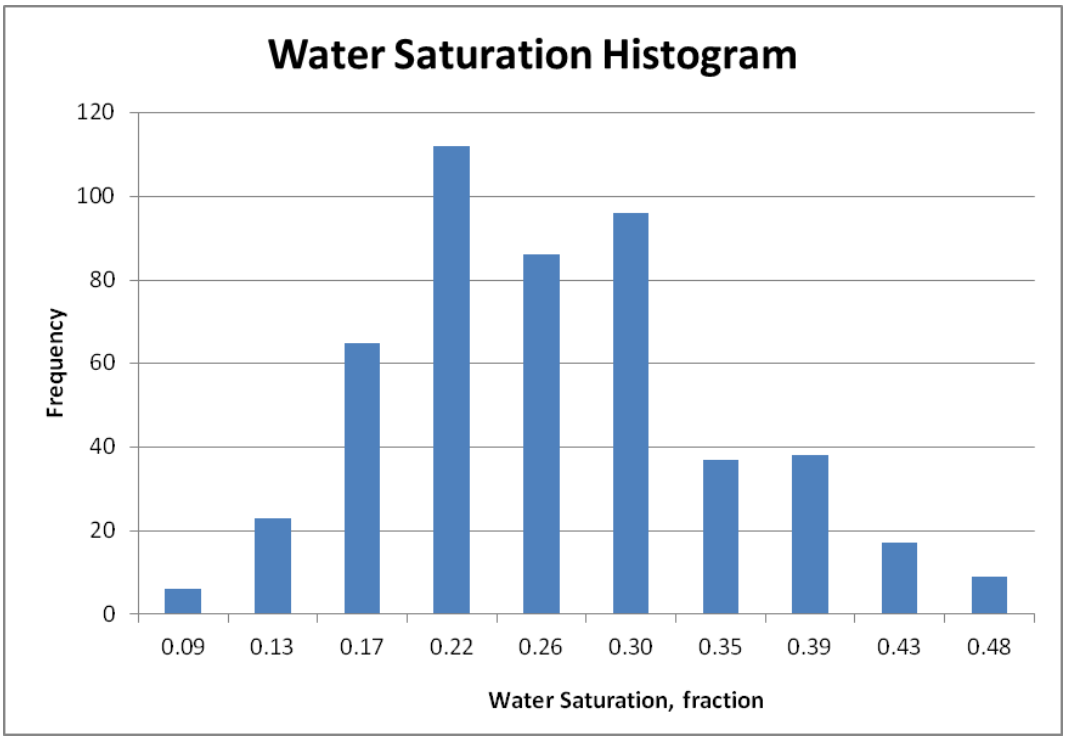

Figure B-15: Water Saturation Histogram

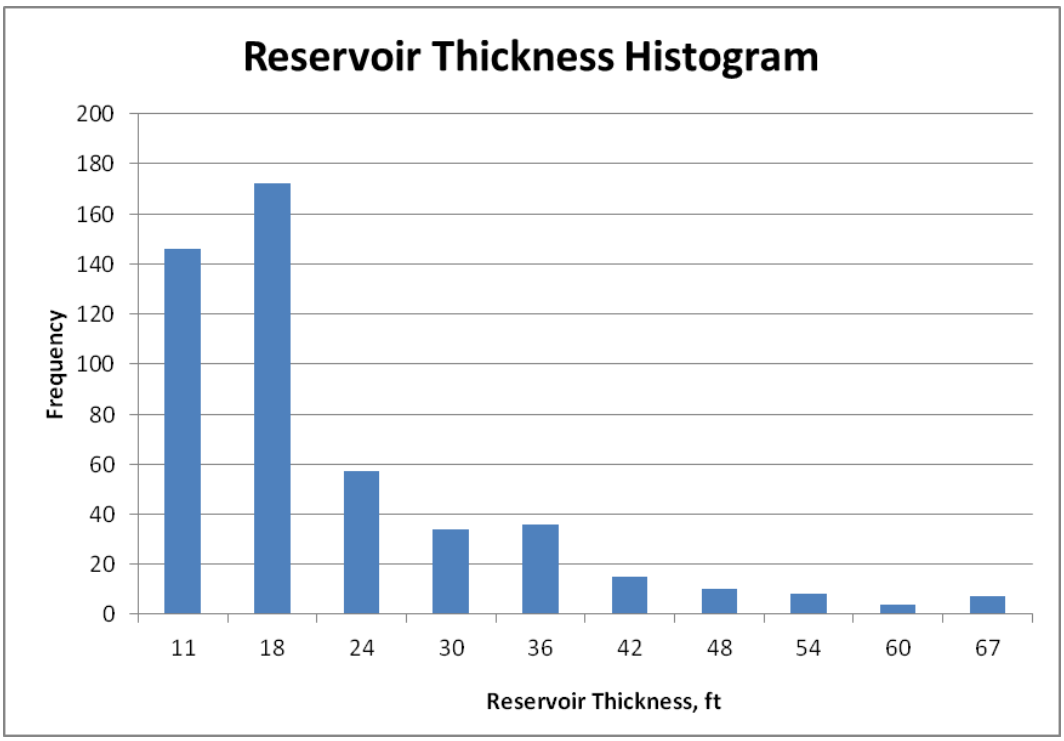

Figure B-16: Reservoir Thickness Histogram

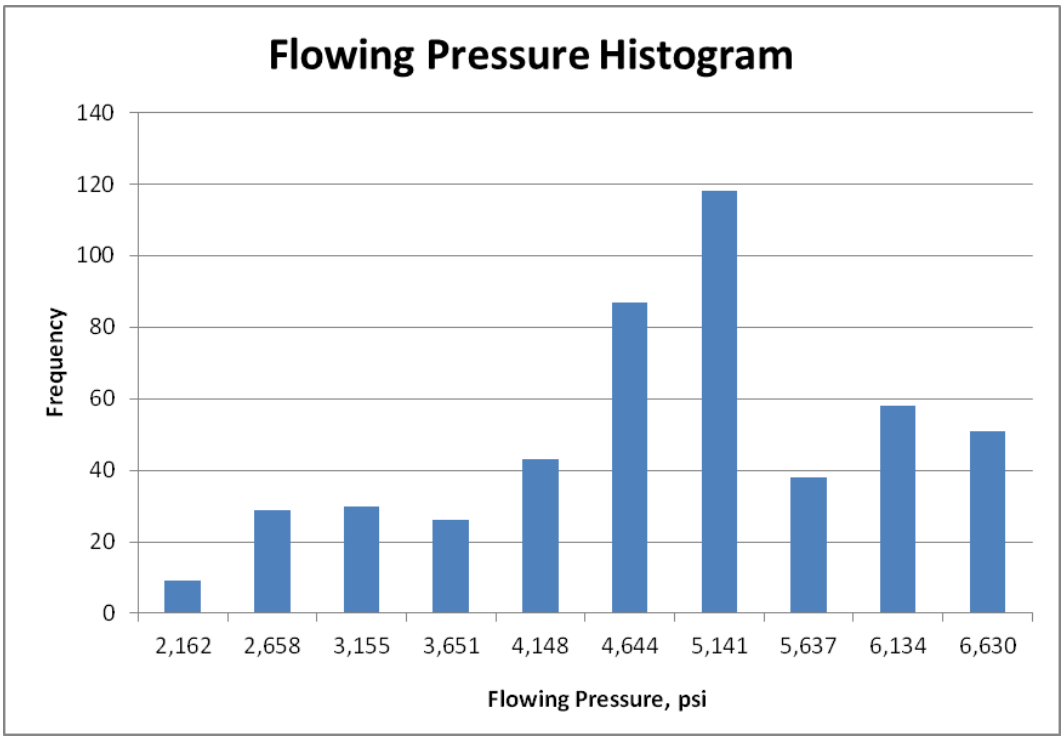

Figure B-17: Flowing Pressure Histogram

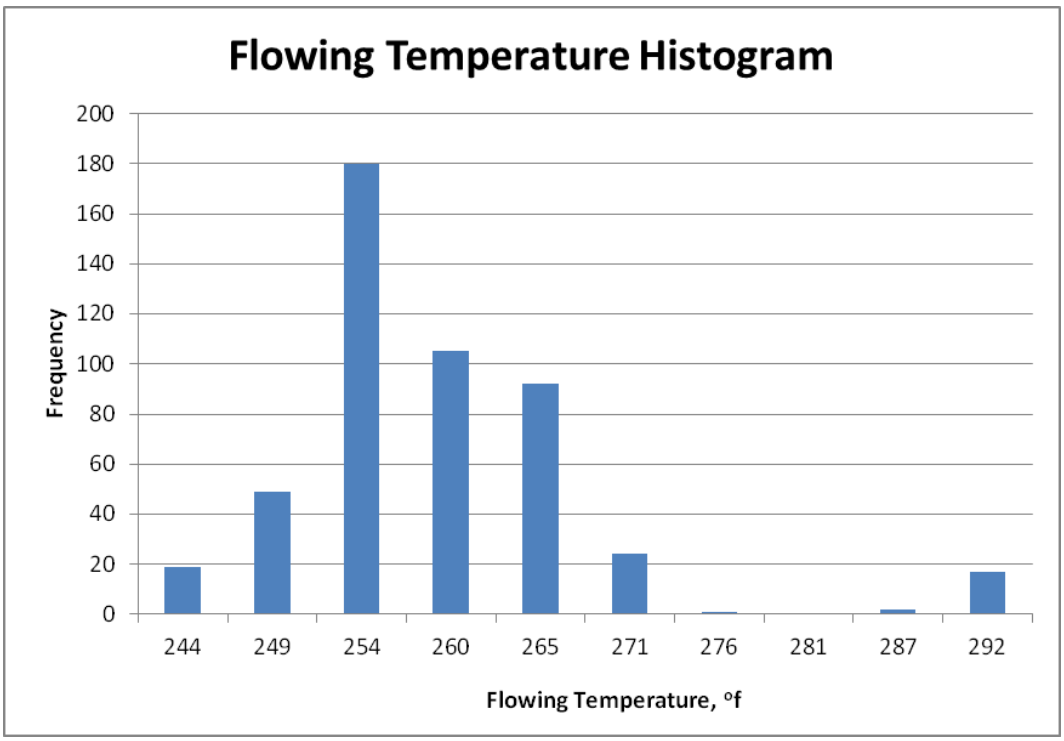

Figure B-18: Flowing Temperature Histogram

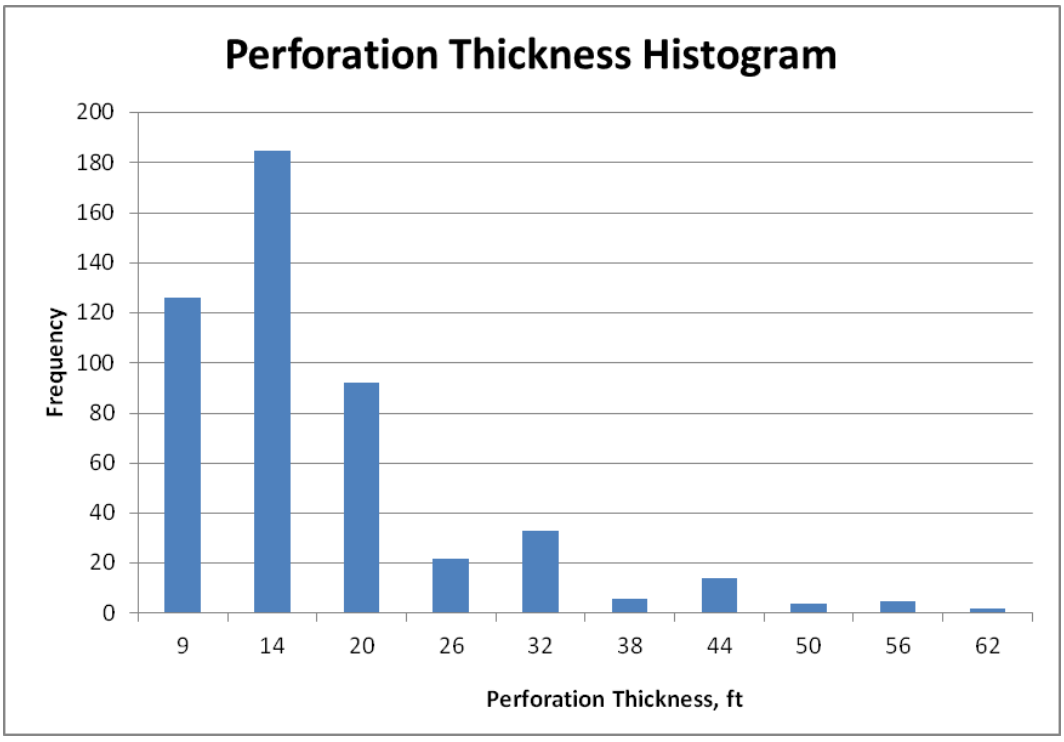

Figure B-19: Perforation Thickness Histogram

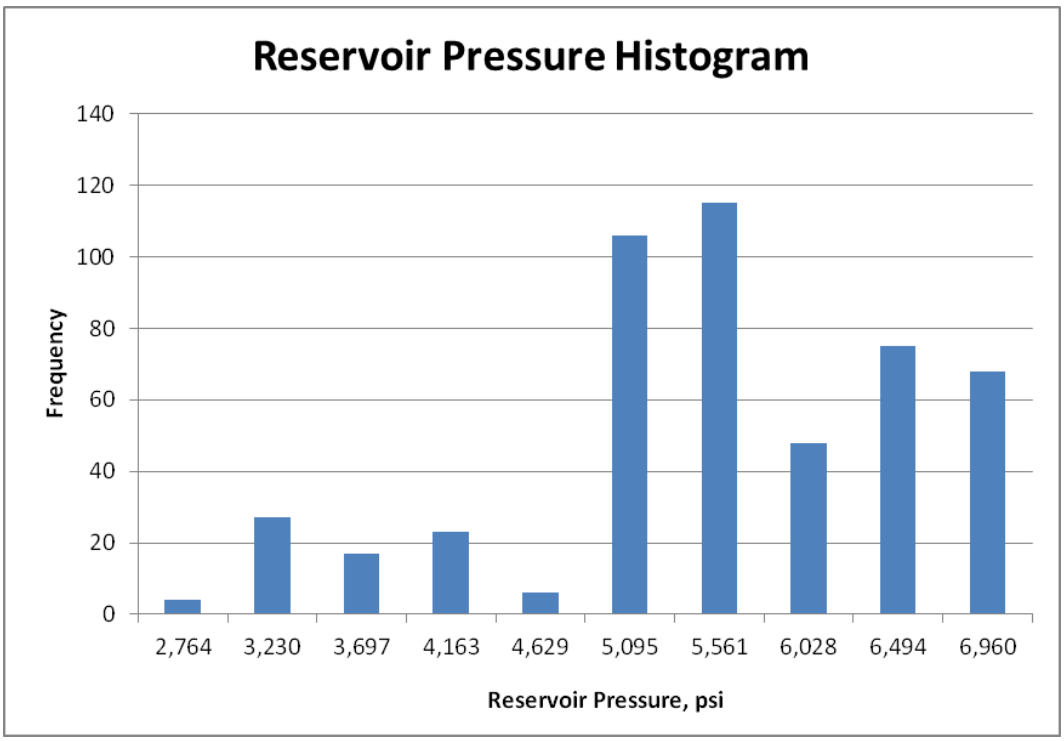

Figure B-20: Reservoir Pressure Histogram

APPENDIX C: SAMPLE PVT REPORT

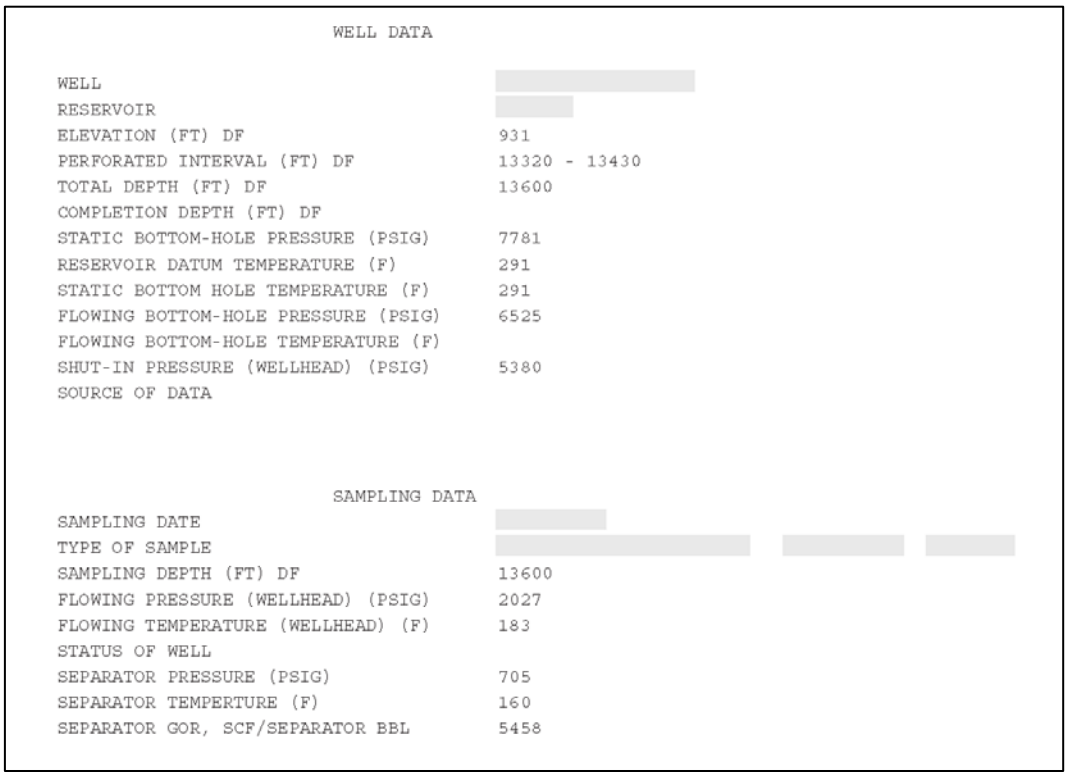

WELL DATA

WELL	
RESERVOIR	
ELEVATION (FT) DF	931
PERFORATED INTERVAL (FT) DF	13320 - 13430
TOTAL DEPTH (FT) DF	13600
COMPLETION DEPTH (FT) DF	
STATIC BOTTOM-HOLE PRESSURE (PSIG)	7781
RESERVOIR DATUM TEMPERATURE (F)	291
STATIC BOTTOM HOLE TEMPERATURE (F)	291
FLOWING BOTTOM-HOLE PRESSURE (PSIG)	6525
FLOWING BOTTOM-HOLE TEMPERATURE (F)	
SHUT-IN PRESSURE (WELLHEAD) (PSIG)	5380
SOURCE OF DATA	

SAMPLING DATA

SAMPLING DATE	
TYPE OF SAMPLE	
SAMPLING DEPTH (FT) DF	13600
FLOWING PRESSURE (WELLHEAD) (PSIG)	2027
FLOWING TEMPERATURE (WELLHEAD) (F)	183
STATUS OF WELL	
SEPARATOR PRESSURE (PSIG)	705
SEPARATOR TEMPERTURE (F)	160
SEPARATOR GOR, SCF/SEPARATOR BBL	5458

Figure C-1: PVT Report Sample – Page 1

	SEPARATOR LIQUID				
COMPONENT	LIQ MOL%	GAS MOL%	GPM	RSVR MOL%	GPM
HYDROGEN SULFIDE	0.00	0.20		0.17	
CARBON DIOXIDE	0.39	1.45		1.31	
NITROGEN	0.50	8.61		7.52	
METHANE	12.90	73.82		65.65	
ETHANE	4.82	8.71	2.329	8.19	2.190
PROPANE	5.32	3.96	1.089	4.14	1.139
ISO-BUTANE	1.60	0.62	0.203	0.75	0.245
N-BUTANE	4.65	1.36	0.429	1.80	0.567
ISO-PENTANE	2.42	0.37	0.135	0.65	0.238
N-PENTANE	3.25	0.40	0.145	0.78	0.283
HEXANE	5.56	0.29	0.118	1.00	0.408
HEPTANE	7.76	0.15	0.069	1.17	5.237*
OCTANE	8.64	0.05	0.026	1.20	
NONANES	10.23	0.01	0.006	1.38	
DECANES	7.84	0.00	0.000	1.05	
UNDECANES	4.59	0.00	0.000	0.62	
DODECANES PLUS	19.53	0.00	0.000	2.62	
	100.00	100.00	4.549	100.00	######

PROPERTIES OF HEPTANES PLUS

API GRAVITY @ 60 F.	42.6	43.0
DENSITY GM/CC @ 60 F.	0.8121	0.8102
MOLECULAR WEIGHT	168	167

CALCULATED SEPARATOR GAS GRAVITY (Air=1.000) = 0.7422
CALCULATED GROSS HEATING VALUE FOR SEPARATOR GAS = 1121 BTU
PER CUBIC FOOT OF DRY GAS @ 14.73 PSIA AND 60 F.

PRIMARY SEPARATOR GAS COLLECTED @ 705 PSIG AND 160F.
PRIMARY SEPARATOR LIQUID COLLECTED @ 705 PSIG AND 160F.

PRIMARY SEPARATOR GAS/SEPARATOR LIQUID RATIO = 5458 SCF/BBL @ 705 PSIG & 160F
PRIMARY SEPARATOR GAS/WELL STREAM RATIO = 865.80 MSCF/MMSCF
* GPM VALUE IS FOR HEPTANES PLUS FRACTION

Figure C-2: PVT Report Sample – Page 2

RSVR EXPANSION PRES. (PSIG)	RELATIVE VOLUME	DEVIATION FACTOR Z
8000	0.8711	1.405
7800	0.8786	1.382
7781 RESERVOIR PRESSURE	0.8794	1.380 (1)
7400	0.8949	1.335
7200	0.9037	1.312
7000	0.9129	1.289
6800	0.9228	1.265
6600	0.9334	1.242
6400	0.9448	1.219
6200	0.9571	1.197
6000	0.9706	1.174
5800	0.9854	1.153
5622 DEW POINT	1.0000	1.134 (2)
5600	1.0019	1.131
5400	1.0205	
5200	1.0415	
5000	1.0657	
4800	1.0933	
4600	1.1247	
4400	1.1596	
4200	1.1977	
4000	1.2388	
3800	1.2830	
3600	1.3315	
3400	1.3870	
3200	1.4550	

(1) GAS EXPANSION FACTOR = 1.4884
(2) GAS EXPANSION FACTOR = 1.308

Figure C-3: PVT Report Sample – Page 3

HYDROCARBON ANALYSIS OF PRODUCED WELL STREAM - MOL PERCENT

	RESERVOIR PRESSURE - PSIG							
COMPONENT	5622	4800	4000	3200	2400	1600	800	0*
HYDROGEN SULFIDE	0.17	0.17	0.17	0.17	0.17	0.17	0.18	0.20
CARBON DIOXIDE	1.31	1.32	1.33	1.34	1.35	1.36	1.36	1.36
NITROGEN	7.52	7.60	7.72	7.90	7.91	7.83	7.64	7.60
METHANE	65.65	66.88	67.74	68.33	68.95	68.35	67.38	65.53
ETHANE	8.19	8.40	8.42	8.44	8.45	8.45	8.44	8.43
PROPANE	4.14	4.10	4.00	3.98	4.03	4.25	4.44	4.77
ISO-BUTANE	1.80	1.76	1.74	1.71	1.70	1.72	1.90	2.29
N-BUTANE	0.75	0.74	0.73	0.71	0.71	0.73	0.81	0.92
ISO-PENTANE	0.78	0.70	0.68	0.67	0.66	0.71	0.83	1.10
N-PENTANE	0.65	0.61	0.58	0.57	0.56	0.57	0.66	0.76
HEXANE	1.00	0.95	0.90	0.88	0.85	0.90	1.01	1.25
HEPTANE	1.17	1.10	1.06	0.94	0.82	0.88	0.95	1.10
OCTANE	1.20	1.15	1.10	0.95	0.85	0.90	1.00	1.06
NONANES	1.38	1.21	1.11	1.02	0.87	0.92	1.02	1.10
DECANES	1.05	0.90	0.82	0.72	0.63	0.65	0.70	0.75
UNDECANES	0.62	0.51	0.40	0.32	0.24	0.26	0.28	0.33
DODECANES PLUS	2.62	1.90	1.50	1.35	1.25	1.35	1.40	1.45
	100.00	100.00	100.00	100.00	100.00	100.00	100.00	100.00
HEPTANES PLUS								
MOLECULAR WEIGHT	167	135	131	129	127	125	123	120
DENSITY	0.8102	0.7850	0.7815	0.7794	0.7777	0.7758	0.7736	0.7708
DEVIATION FACTOR - Z								
EQUILIBRIUM GAS	1.1340	1.0580	0.9860	0.9280	0.8940	0.8900	0.9230	1.0000
TWO-PHASE	1.1340	1.0480	0.9590	0.8960	0.8630	0.8660	0.9120	1.0000
WELL STREAM PRODUCED-								
CUMULATIVE % OF INITIAL		7.641	15.891	27.982	43.921	62.765	82.311	97.034

* COMPOSITION ASSUMED TO REPRESENT THE MID-POINT OF THE DEPLETION STUDY

Figure C-4: PVT Report Sample – Page 4

CUMULATIVE RECOVERY PER MMSCF OF ORIGINAL FLUID	INITIAL IN PLACE	RESERVOIR PRESSURE - PSIG							
		5622	4800	4000	3200	2400	1600	800	0
WELL STREAM - MSCF	1000.0		76.4	158.9	279.8	439.2	627.7	823.1	970.3
NORMAL TEMPERATURE SEPARATION *									
STOCK TANK LIQUID - BARRELS	142.36	0.00	8.48	17.19	27.39	38.47	51.61		
PRIMARY SEPARATOR GAS - MSCF	807.98	0.00	68.76	151.61	263.39	404.28	561.05		
SECOND STAGE GAS - MSCF	53.69	0.00	3.85	7.94	12.84	18.38	25.08		
STOCK TANK GAS - MSCF									
TOTAL <PLANT PRODUCTS> IN PRIMARY SEPARATOR GAS - GALLON									
ETHANE	1760.5	0.0	153.9	339.7	591.0	908.6	1261.5		
PROPANE	709.0	0.0	61.7	135.7	236.9	368.3	520.5		
BUTANES (TOTAL)	335.0	0.0	29.8	67.1	118.8	185.7	259.7		
PENTANES PLUS	206.7	0.0	18.8	42.0	75.0	118.2	165.7		
TOTAL <PLANT PRODUCTS> IN SECOND STAGE GAS - GALLON									
ETHANE	227.2		16.7	34.4	55.7	79.8	108.8		
PROPANE	114.6		8.4	17.3	28.1	40.7	56.6		
BUTANES (TOTAL)	53.3		4.0	8.5	13.9	20.3	27.9		
PENTANES PLUS	27.3		2.1	4.4	7.2	10.5	14.6		
TOTAL <PLANT PRODUCTS> IN WELL STREAM - GALLONS									
ETHANE	2190	0	172	357	630	990	1416	1857	2189
PROPANE	1139	0	86	177	309	486	706	945	1138
BUTANES (TOTAL)	812	0	61	126	219	341	488	657	808
PENTANES PLUS	6000	0	348	678	1113	1623	2256	2970	3564

* PRIMARY SEPARATOR AT 1000 PSIG AND 100 F., SECOND SEPARATOR AT 200 PSIG AND 100 F., STOCK TANK AT 0 PSIG AND 100 F.

Figure C-5: PVT Report Sample – Page 5

	RESERVOIR PRESSURE - PSIG							
	5622	4800	4000	3200	2400	1600	800	0
NORMAL TEMPERATURE SEPARATION*								
STOCK TANK LIQUID GRAVITY, API AT 60 F.	49.0	55.3	56.4	57.2	57.7	58.2		
SEPARATOR GAS/WELL STREAM RATIO, MSCF/MMSCF								
PRIMARY SEPARATOR GAS ONLY	807.98	834.46	851.49	865.86	878.91	870.00		
PRIMARY AND SECONDARY STAGE SEPARATOR GASES	861.67	881.20	893.46	903.87	913.43	907.18		
SEPARATOR GAS/STOCK TANK LIQUID, RATIO, SCF/STB								
PRIMARY SEPARATOR GAS ONLY	5676	8109	9513	10960	12715	11930		
PRIMARY AND SECONDARY STAGE SEPARATOR GASES	6053	8564	9982	11441	13215	12440		
GPM FROM SMOOTH WELL STREAM COMPOSITIONS								
ETHANE PLUS	10.320	8.723	8.147	7.713	7.336	7.573	7.989	
PROPANE PLUS	8.131	6.477	5.896	5.456	5.077	5.314	5.732	
BUTANES PLUS	6.992	5.349	4.795	4.361	3.968	4.144	4.511	
PENTANES PLUS	6.179	4.552	4.008	3.590	3.200	3.364	3.647	

* PRIMARY SEPARATOR AT 1000 PSIG AND 100 F., SECOND SEPARATOR AT 200 PSIG AND 100 F., STOCK TANK AT 0 PSIG AND 100 F.

Figure C-6: PVT Report Sample – Page 6

PRESSURE PSIG	RETROGRADE LIQUID VOLUME PERCENT OF HYDROCARBON PORE SPACE
5622 DEW POINT	
5600	0.17
5400	2.60
5200	5.59
5000	8.70
4800	11.47
4600	13.67
4400	15.27
4200	16.37
4000	17.10
3800	17.57
3600	17.87
3400	18.05
3200	18.14
3000	18.17
2600	18.06
2200	17.75
2000	17.53
1800	17.25
1600	16.92
1200	16.13
800	15.18
400	14.11
0	12.98

PROPERTIES OF ZERO PSIG RESIDUAL LIQUID

GRAVITY = 40.7 DEGREES API @ 60 F
DENSITY = 0.8208 GM/CC @ 60
MOLECULAR WEIGHT = 182

* DODECANES IN DEPLETION RECORD ARE DODECANE PLUS VALUES.

Figure C-7: PVT Report Sample – Page 7

NOMENCLATURE

D = non-Darcy flow constant, D/Mscf

h = reservoir/layer thickness, ft

h_{perf} = perforation thickness, ft

k = permeability, mD

k_s = permeability of the damaged/stimulated area, mD

MW = molecular weight

ρ_g = gas density, gm/cm^3

ρ_r = pseudo reduced density

$\bar{p}$ = average reservoir pressure, psi

p_{wf} = bottomhole flowing pressure, psi

$_pp_r$ = pseudo reduced pressure

q = gas flow rate, MSCF/D

q_l = layer gas flow rate, MSCF/D

r_e = drainage radius, ft

r_w = wellbore radius, ft

s = skin factor, dimensionless

T = temperature, ^{o}R

$_pT_r$ = pseudo reduced temperature

μ = viscosity, cp

$\bar{\mu}$ = gas viscosity evaluated at average reservoir pressure and temperature, cp

μ_g = gas viscosity, cp

V = volume, ft^3

V_{actual} = real gas volume, ft^3

V_{ideal} = ideal gas volume, ft^3

Z = gas deviation factor, dimensionless

$\bar{z}$ = gas deviation factor evaluated at average reservoir pressure and Temperature, dimensionless

REFERENCES

1. Akbari, M. K., Farahani, F. J. & Abdy, Y., 2007. *Using Artificial Neural Network's Capability for Estimation of Gas Condensate Reservoir's Dew point Pressure.* London, SPE 107032.

2. Al-Anazi, A. & Gates, I. D., 2010. Support-Vector Regression for Permeability Prediction in a Heterogeneous Reservoir: A Comparative Study. *SPE Reservoir Evaluation & Engineering,* Issue June, pp. 485-495.

3. Al-Dhufairi, M. A., 2011. *Prediction of Mobility Profile with Minimum Real Time Measurements using Artificial Intelligence,* Dhahran, Saudi Arabia: KFUPM.

4. Al-Fattah, S. M. & A., A.-N. H., 2009. *Artificial-Intelligence Technology Predicts Relative Permeability of Giant Carbonate Reservoirs.* Aberdeen, SPE 109018.

5. Alger, R. P., Raymer, L. L., Hoyle, W. R. & Tixier, M. P., March 1963. Formation Density Log Applications in Liquid-Filled Holes. *JPT,* pp. 321-32.

6. Alrumah, M., Startzman, R., Schechter, D. & Ibrahim, M., 2005. *Predicting Well Inflow Performance in Solution Gas Drive Reservoir by Neural Network.* Calgary, Petroleum Society.

7. Al-Shammari, A. T., 2012. *Prediction of Pressure Drop for Two-Phase Flow in Vertical Pipes Using Artificial Intelligence.* Dhahran, Saudi Arabia: KFUPM.

8. Al-Sirri, D. & Gharbi, R., 2011. *Predicting Lower Fars Heavy Oil Molar Compositions Using Artificial Neural Networks.* Kuwait, SPE 150365.

9. Anifowose, F. A., 2011. *Artificial Intelligence Application in Reservoir Characterization and Modeling: Whitening the Black Box.* Dhahran, SPE 155413.

10. Anifowose, F. & Abdulraheem, A., 2010. *Prediction of Porosity and Permeability of Oil and Gas Reservoirs using Hybrid Computational Intelligence Models.* Cairo, SPE 126649.

11. Anifowose, F., Ewenla, A. & Eludiora, S., 2011. *Prediction of Oil and Gas Reservoir Properties using Support Vector Machines.* Bangkok, IPTC 14514.

12. Anon., 2010. *Fuzzy Logic ToolboxTM 2 User's Guide.* Natick(MA): The MathWorks, Inc..

13. Bassiouni, Z., 1994. *Theory, Measurement, and Interpretation of Well Logs.* Richardson, TX: SPE.

14. Beale, M. H., Hagan, M. T. & Demuth, H. B., 2010. *Neural Network Toolbox 7 User's Guide..* Natick(MA): The MathWorks, Inc..

15. Bhuddharaju, P., Laskar, S. & Samuel, R., 2007. *Robust Well Cost Estimation Using Support Vector Machine Model.* Houston, SPE 106577.

16. Chang-kai, Z. & Wen-kai, L., 2010. *Seismic Attributes Selection Based On SVM For Hydrocarbon Reservoir Prediction.* Denver, SEG.

17. Chaudhry, A. U., 2003. *Gas Well Testing Handbook.* Amsterdam: Elsevier.

18. Craft, B. C. & Hawkins, M. F., 1991. *Applied Petroleum Engineering.* Englewood Cliffs, NJ: Prentice Hall PTR.

19. Danesh, A., 1998. *PVT and Phase Behaviour of Petroleum Reservoir Fluids.* Amsterdam: Elsevier.

20. Dranchuck, P. M. & Abou-Kassem, J. H., July-September, 1975. Calculation of Z-Factors for Natural Gases using Equation of State. *JCPT,* pp. 34-36.

21. Duda, R., 1981. Knowledge-Based Expert Systems Come of Age. *Byte,* pp. 238-281.

22. Economides, M., Hill, A. D. & Ehlig-Economides, C., 1994. *Petroleum Production Systems.* Cliffs(NJ): PTR Prentice Hall.

23. Elsharkawy, A. M. & Foda, S. G., 1998. *EOS Simulation and GRNN Modeling of the CVD Behavior of Retrograde-Gas Condensate Reservoirs.* Kuala Lumpur, SPE 39745.

24. Gharbi, R. B., 2003. *Neural Network Prediction Model of Miscible Displacements in Heterogeneous Reservoirs.* Manama, SPE 81469.

25. Gidh, Y., Purwanto, A. & Ibrahim, H., 2012. *Artificial Neural Network Drilling Parameter Optimization System Improves ROP by Predicting/Managing Bit Wear.* Utrecht, SPE 149801.

26. Hill, A. D., 1990. *Production Logging: Theoretical and Interpretive Elements.* Richardson(TX): Society of Petroleum Engineers.

27. Huang, K. Y., Shen, L. C. & Weng, L. S., 2011. *Well Log Data Inversion Using Radial Basis Function Network.* San Antonio, SEG.

28. Juell, A. & Whitson, C., 2011. Backpressure Equation for Layered Gas Reservoirs. *SPE 146066.*

29. Kaftan, I. & Salk, M., 2009. *Determination Of Structure Parameters On Gravity Method By Using Radial Basis Functions Networks Case Study Seferihisar : Geothermal Area (Western Turkey).* Houston, SEG.

30. Kanj, M. Y. & Abousleiman, Y., 1999. *Realistic Sanding Predictions A Neural Approach.* Houston, SPE 56631.

31. Lee, A., Gonzalez, M. H. & Eakin, B. E., August 1966. The Viscosity of Natural Gases. *JPT.*

32. Lee, J. & Wattenbarger, R. A., 1996. *Gas Reservoir Engineering.* Richardson, TX: SPE.

33. Lei, L., Wei, X., Shifan, Z. & Zhonghong, W., 2011. *Reservoir Property Prediction Using the Dynamic Radial Basis Function Network.* San Antonio, SEG.

34. Lyons, W. C. & Plisga, G. J., 2005. *Standard Handbook of Petroleum & Natural Gas Engineering.* Burlington, MA: Gulf Professional Publishing.

35. Mohaghegh, S., 2005. Recent Development in Application of Artificial Intelligence in Petroleum Engineering. *JPT,* pp. 86-91.

36. Mohamed, L., Christie, M. & Demyanov, V., 2009. *Comparison of Stochastic Sampling Algorithms for Uncertainty Quantification.* The Woodlands, SPE 119139.

37. Mohammadpoor, M., Firouz, Q. & Torabi, F., 2012. *Implementing Simulation and Artificial Intelligence Tools to Optimize the Performance of the CO2 Sequestration in Coalbed Methane Reservoirs.* Orlando, CMTC 151307.

38. N., K. M., 1989. *Introduction to Wireline Log Interpretation.* s.l.:OGTI.

39. Nazari, S., Kuzma, H. A. & Rector, J. W., 2011. *Predicting Permeability From Well Log Data And Core Measurements Using Support Vector Machines.* San Antonio, SEG.

40. Oladiipo, A., Bankole, A. & Taiwo, E., 2009. *Artificial Neural Network Modeling of Viscosity and Wax Deposition Potential of Nigerian Crude Oil and Gas Condensates.* Abuja, SPE 128600.

41. Russel, B. H., Hampson, D. P. & Lines, L. R., 2003. *Application of the Radial Basis Function Neural Network to the Prediction of Log Properties From Seismic Attributes - A Channel Sand Case Study.* Dallas, SEG.

42. Salehi, S., Hareland, G., Ganji, M. & Dehkordi, K. K., 2007. *Using Neural Network System for Casing Collapse Occurrence and Its Depth Prediction in a Middle-Eastern Carbonate Field.* Cairo, SPE 107453.

43. Saputelli, L., Malki, H., Canelon, J. & Nikolaou, M., 2002. A Critical Overview of Artificial Neural Network Application in the Context of Continuous Oil Field Optimization. *SPE 77703.*

44. Schlumberger, 1973. *Production Log Interpretation.* s.l.:Schlumberger.

45. Schlumberger, 1989. *Log Interpretation Principles/Applications.* Sugar Land(TX): Schlumberger.

46. Sherrod, P. H., 2008. *DTREG Predictive Modeling Software User Manual.* s.l.:www.dtreg.com.

47. Silva, P. C., Maschio, C. & Schiozer, D. J., 2008. Application of Neural Network and Global Optimization in History Matching. *JCPT,* 47(11), pp. 22-25.

48. Tiab, D. & Donaldson, E. C., 2011. *Petrophysics: Theory and Practice of Measuring Reservoir Rock and Fluid Transport Properties.* Burlington, MA: Gulf Professional Publishing.

CURRICULUM VITAE

Personal Information

Name: Malik Alarfaj

Phone Number: +966-3-873-5163

E-Mail: malik.arfaj@aramco.com

Education

Bachelor of Science in Petroleum Engineering, 2009, Texas A&M University, College Station, TX.

Master of Science in Petroleum Engineering, 2012, King Fahd University of Petroleum and Minerals, Dhahran, Kingdom of Saudi Arabia.

Professional Affiliations

Member of SPE (Society of Petroleum Engineers) since 2005.

Member of Al-Jabal Toastmasters since 2010.

Work Experience

Summer 2008, Summer Intern, Northern Area Simulation Division, Saudi Aramco:

Sep 2009- Sep 2010, Facilities Engineer, Southern Area Facilities Division, Saudi Aramco.

Oct 2010- Sep 2011, Reservoir Engineer, Gas Reservoir Management Division, Saudi Aramco.

Oct 2011- Aug 2011, Petroleum Engineer, Reserve Assessment & Production Planning Division, Saudi Aramco.